

1 **A Holocene history of climate, fire, landscape evolution, and human**  
2 **activity in Northeast Iceland**

3 Nicolò Ardenghi<sup>1</sup>, David J. Harning<sup>1</sup>, Jonathan H. Raberg<sup>1</sup>, Brooke R. Holman<sup>1</sup>, Thorvaldur Thordarson<sup>2</sup>,  
4 Áslaug Geirsdóttir<sup>2</sup>, Gifford H. Miller<sup>1,3</sup>, Julio Sepúlveda<sup>1,3</sup>

5 <sup>1</sup>Institute of Arctic and Alpine Research (INSTAAR), University of Colorado Boulder, CO, 80309, USA

6 <sup>2</sup>80309, Faculty of Earth Sciences, University of Iceland, Reykjavík, Iceland

7 <sup>3</sup>Department of Geological Sciences, University of Colorado Boulder, CO, USA

8 *Correspondence to:* Nicolò Ardenghi (nicolo.ardenghi@gmail.com)

9 **† Abstract**

10 Paleoclimate reconstructions across Iceland provide a template for past changes in climate across the northern North Atlantic,  
11 a crucial region due to its position relative to the global northward heat transport system and its vulnerability to climate change.  
12 The roles of orbitally driven summer cooling, volcanism, and human impact as triggers of local environmental changes in the  
13 Holocene of Iceland, remain debated. While there are indications that human impact may have reduced environmental  
14 resilience during Late Holocene summer cooling, it is still difficult to resolve to what extent human and natural factors affected  
15 Iceland's Late Holocene landscape instability. Here, we present a continuous Holocene fire record of northeastern Iceland  
16 from proxies archived in Stóra Viðarvatn sediment. We use pyrogenic polycyclic aromatic hydrocarbons (pyroPAHs) to trace  
17 shifts in fire regimes, paired with continuous biomarker and bulk geochemical records of soil erosion, lake productivity, and  
18 human presence. The molecular composition of pyroPAHs and a wind pattern reconstruction indicate a naturally driven fire  
19 signal that is mostly regional. Generally low fire frequency during most of the Holocene significantly increased at 3 ka and  
20 again after 1.5 ka BP, before known human settlement in Iceland. We propose that shifts in vegetation type caused by cooling  
21 summers over the past 3 kyr, in addition to changes in atmospheric circulation, such as shifts in North Atlantic Oscillation  
22 (NAO) regime, led to increased aridity and biomass flammability. Our results show no evidence of faecal biomarkers  
23 associated with human activity during or after human colonisation in the 9<sup>th</sup> century CE. Instead, faecal biomarkers follow the  
24 pattern described by erosional proxies, pointing toward a negligible human presence and/or a diluted signal in the lake's  
25 catchment. However, low post-colonisation levels of pyroPAHs, in contrast to an increasing flux of erosional bulk proxies,  
26 suggest that farming and animal husbandry may have suppressed fire frequency by reducing the spread and flammability of  
27 fire-prone vegetation (e.g., heathlands).

28 Overall, our results describe a fire frequency heavily influenced by long term changes in climate through the Holocene. They  
29 also suggest that human colonisation had contrasting effects on the local environment by lowering its resilience to soil erosion  
30 while increasing its resilience to fire.

## 31 [21 Introduction](#)

32 Iceland is highly sensitive to most mechanisms controlling the evolution of Holocene climate in the North Atlantic, from  
33 millennial (e.g., shifts in deep water formation and ocean current positions) to sub-decadal timescales (e.g., variability of the  
34 North Atlantic Oscillation) (Harning et al., 2021; Mjell et al., 2016; Moossen et al., 2015; Petit et al., 2020). Recent lake  
35 sedimentary records in Iceland (Alsos et al., 2021; Geirsdóttir et al., 2009a, 2013, 2019, 2020; Harning et al., 2016, 2020;  
36 Hiles et al., 2021; Larsen et al., 2011, 2012; Richter et al., 2021) draw a comprehensive picture of Icelandic environments  
37 during the Holocene (last 11.7 kyr). These Holocene paleoclimate reconstructions derived from lake sediments in Iceland show  
38 first-order millennial trends that reflect orbitally-driven changes in Northern Hemisphere summer insolation, and millennial to  
39 sub-millennial changes that are primarily impacted by northern North Atlantic ocean circulation and to a part by local  
40 volcanism (e.g., Flowers et al., 2008; Geirsdóttir et al., 2013, 2020; Harning et al., 2018b; Larsen et al., 2012). These Holocene  
41 climate reconstructions further indicate a major shift from occasional to increasingly severe landscape instability and soil  
42 erosion occurring at least 300 years before the acknowledged settlement of Iceland (ca 870 CE; The Book of Icelanders  
43 “Íslendigabók”, by Ari Thorgilsson, 12<sup>th</sup> century CE, e.g., Smith, 1995), suggesting that human impact had a secondary role  
44 to climate by lowering the resilience of the environment to an already ongoing naturally driven erosion (e.g., Bates et al., 2021;  
45 Geirsdóttir et al., 2009b, 2020). The ability to generate high-resolution Holocene terrestrial climate records, along with  
46 Iceland’s relatively short settlement history, makes Iceland an ideal location to attempt disentangling the impact of natural  
47 climate variability and human activities on the changes in the local landscape during the Late Holocene.

48 In this study, we use multiple organic proxies from a Holocene sediment core from the Stóra Viðarvatn lake in northeast  
49 Iceland to investigate the effects of natural and anthropogenic drivers on the local Icelandic environment. First, we focus on  
50 tracing the evolution of fire regimes using pyrogenic polycyclic aromatic hydrocarbons (pyroPAHs; Lima et al., 2005). Fires  
51 can have a significant impact on ecosystems, affecting vegetation patterns, nutrient cycling, and wildlife habitat (e.g.,  
52 Goldammer and Furyaev, 1996). The frequency, intensity, and spatial extent of fires can provide insights into past climate and  
53 environmental conditions (e.g., Marlon, 2009; Power et al., 2008) and, to our knowledge, there are no such records for the  
54 Holocene in Iceland, while limited data is available for the surrounding regions (Chen et al., 2023; Marlon et al., 2013; Segato  
55 et al., 2021; Zennaro et al., 2014). Second, as fire frequency can be influenced by human activities as well (e.g., Marlon et al.,  
56 2009, 2013; Zennaro et al., 2015), we also analyse faecal markers of human presence (Vázquez et al., 2021). By analysing  
57 these biomarkers from deglaciation to present, we can define their natural, pre-settlement background levels and thus  
58 potentially trace anthropogenic impact on the local environment, pinpointing human arrival in the lake catchment.

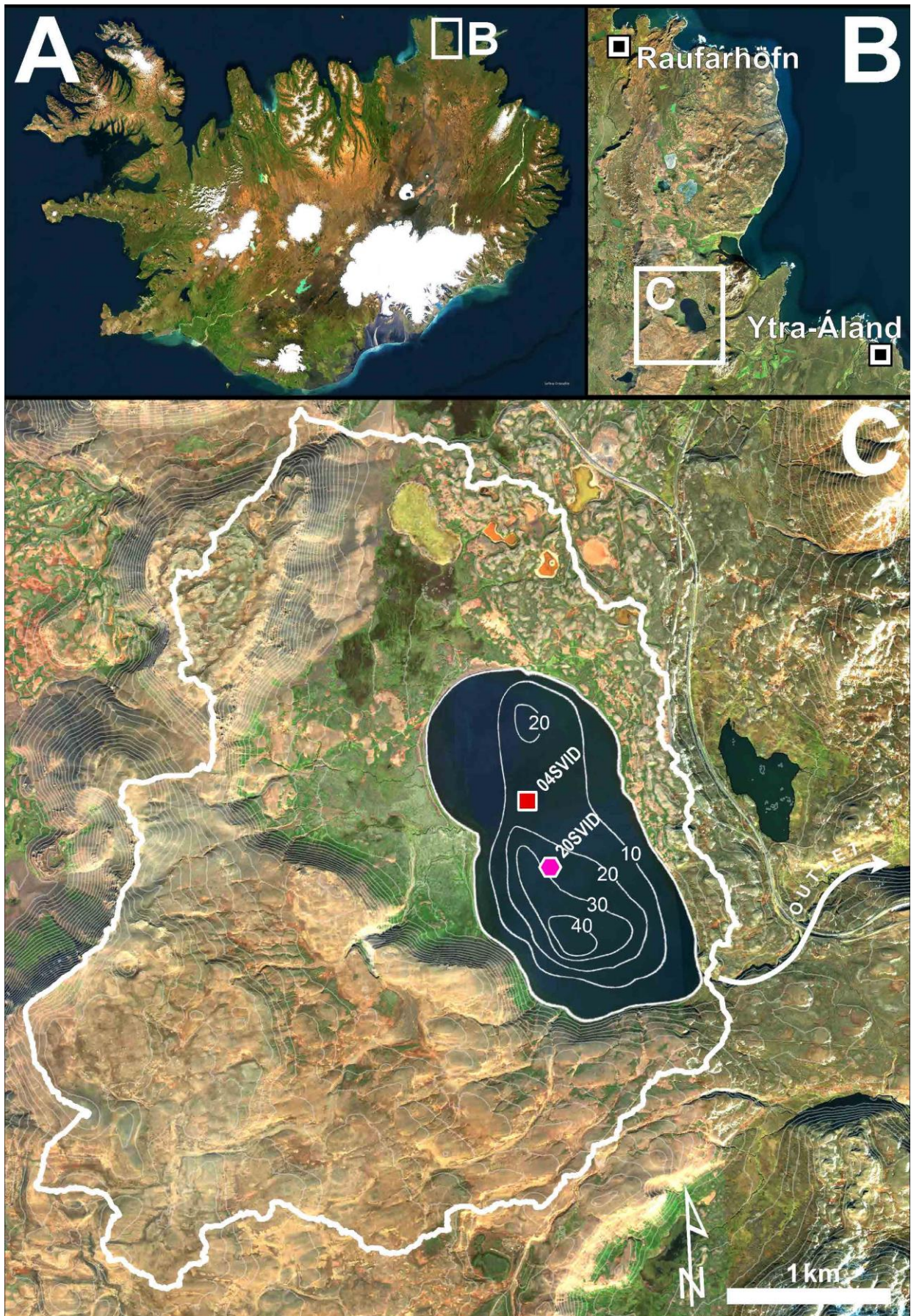
59 Finally, by coupling fire and human presence biomarker records with established proxies for environmental change (e.g., soil  
60 erosion and primary productivity, e.g., Argiriadis et al., 2018; Geirsdóttir et al., 2013; Gross, 2017), we test what control  
61 natural and/or human factors had on the evolution of the Holocene landscape in Iceland.

## 62 [3.2 Methods](#)

### 63 [3.12.1 Study site](#)

64 Stóra Viðarvatn (SVID) is a lake (2.6 km<sup>2</sup> surface area) located in NE Iceland (Fig. 1A-B) at an elevation of 151 m asl. SVID  
65 has a maximum depth of 48 m, a catchment area of 17 km<sup>2</sup> (including the lake surface), and a volume of ca 3.6×10<sup>7</sup> m<sup>3</sup> (this  
66 study, based on data from the National Land Survey of Iceland, Landmælingar Íslands, 2023; Axford et al., 2007). The lake is  
67 surrounded by Quaternary age basaltic lavas and glacial hyaloclastites formed by subglacial eruptions, as well as some  
68 Holocene soil with several mm-cm thick tephra layers (Hjartarson and Sæmundsson, 2014). The nearby Raufarhöfn station  
69 (Icelandic Meteorological Office, 2022) provides weather data for the 1961–1990 CE interval: mean annual temperature is  
70 2 °C with a maximum in July-August (8 °C), while the lake surface is usually frozen between November and March; mean  
71 annual precipitation is 733 mm a<sup>-1</sup> with lowest values occurring in May (28 mm) and the highest in October (ca 86 mm),  
72 suggesting a lake-water residence time between five and nine years.

73 In February 2020, we recovered a 8.93 m long core 20-SVID-02 (66.236867° N; -15.837837° E; 1C) from 17.4 m water depth  
74 near the centre of the lake (Harning et al., 2023). The sediment was retrieved in seven drives of ~150 cm each, using lake ice  
75 as a coring platform. The core was subsequently stored in a cool room (4 °C) at the Institute of Arctic and Alpine Research,  
76 University of Colorado Boulder, where it was subsampled. Previously, two studies have analysed an 8 m long core (04-SVID-  
77 03; 1C) retrieved in February 2004 to trace Holocene temperature (Axford et al., 2007) and δ<sup>18</sup>O from chironomid remains, as  
78 well as the δD, δ<sup>13</sup>C, δ<sup>15</sup>N of total organic matter (Wooller et al., 2008) at a 1–0.2 kyr resolution.



79

80 Figure 1: (A) Study area in NE Iceland; (B) Location of the Raufarhöfn climatological station and Ytra-Áland site (Karlisdóttir et  
 81 al., 2014), which are 20 km NNW and 13 km ESE from Stóra Viðarvatn (SVID), respectively; (C) Location and catchment area of  
 82 the Stóra Viðarvatn lake: 20-SVID-02 core is marked by a pink hexagon and an older 04-SVID-03 core by a red square (Axford et  
 83 al., 2007); SVID bathymetry (10 m isolines) is reported by Axford et al. (2007); watershed catchment and contour lines (10 m)  
 84 are calculated via ArcGIS (Esri, 2023) based on digital elevation models provided by the National Land Survey of Iceland; basemap  
 85 sourced from Esri.

## 86 3.22.2 Tephrochronology

87 Our sediment core chronology takes advantage of the geochemical fingerprints of visible Icelandic tephra layers and their  
88 correlation to marker tephra of known age. Thirteen tephra layers were sampled along the vertical axis, sieved to isolate glass  
89 fragments between 125 and 500  $\mu\text{m}$ , and embedded in epoxy plugs. At the University of Iceland, individual glass shards were  
90 analysed on a JEOL JXA-8230 electron microprobe using an acceleration voltage of 15 kV, beam current of 10 nA, and a  
91 beam diameter of 10  $\mu\text{m}$ . The international A99 standard was used to monitor for instrumental drift and maintain consistency  
92 between measurements. Tephra origin was then assessed using major oxide compositions, following the systematic procedures  
93 outlined in Jennings et al., 2014 and Harning et al., 2018a. Briefly, based on  $\text{SiO}_2$  wt% vs total alkali ( $\text{Na}_2\text{O} + \text{K}_2\text{O}$ ) wt%, we  
94 determined whether the tephra volcanic source is mafic (tholeiitic or alkalic), intermediate and/or rhyolitic. From here, we  
95 objectively discriminate the source volcanic system through a detailed series of bi-elemental plots produced from available  
96 compositional data on Icelandic tephra. Source eruption was then determined using the geochemical fingerprint and relevant  
97 stratigraphic information. See supplemental information for complete major oxide compositions and bi-elemental plots.

98 Using the 13 marker tephra layers of known age (Table 1), we generated a Bayesian age model using the R package rbacon  
99 2.5.7 (Blaauw and Christen, 2011; R Core Team, 2020) and default model functions (Fig. 2). We used the ‘slumps’ function  
100 for the thicker tephra layers (e.g., Hekla 3 and Hekla 4) to reflect their instantaneous deposition on geologic timescales.

## 101 3.32.3 Sample preparation and analysis

102 At the University of Colorado Boulder, we retrieved a total of 196 sediment core samples at an average spacing of 4.5 cm,  
103 providing a temporal resolution of decadal to centennial time scales. We freeze-dried samples for 24–48 hours, and ground  
104 and homogenised them (mean weight 1.5 g, range 0.6–6.6 g) using an agate mortar and pestle. Using 13–70 mg of sediment,  
105 we measured total carbon (TC), total nitrogen (TN), and  $\delta^{13}\text{C}$  (relative to VPDB) on an elemental analyser linked to a Thermo  
106 Delta V isotope ratio mass spectrometer (EA-IRMS) in the Earth Systems Stable Isotope Laboratory at the University of  
107 Colorado Boulder; samples were analysed against a suite of secondary laboratory standards that are extensively calibrated to  
108 international standard reference materials to correct for size, blank-mixing, linearity and drift effects (Harning et al., 2018b).

109 We did not decalcify samples as the contribution of inorganic carbon to TC in Icelandic lake sediment is considered to be  
110 negligible (see par. 5.1; Geirsdóttir et al., 2020). We analysed 9–11 mg of sediment for biogenic silica by Diffuse Reflectance  
111 Fourier Transform Infrared Spectrometry (FTIRS) on a Bruker Vertex 70 with a Praying Mantis diffuse reflectivity accessory  
112 (Harrick) and report values in FTIRS - Fourier Transform Infrared Spectroscopy absorbance units (e.g., Harning et al., 2018b).  
113 We processed 86 selected samples for organic biomarker analyses. We extracted 0.4–2 g of dry sediment with an accelerated  
114 solvent extractor (Dionex ASE350). Sample size, matrix, and richness in organic compounds greatly varied along the core  
115 and initial tests occasionally showed coloration in the sample extract even after 4-5 cycles, likely due to the persistence of  
116 organics. Thus, to maintain consistency in lipid yields throughout the core, we used ~~using~~ dichloromethane (DCM):methanol  
117 (MeOH) 9:1 for six cycles of five minutes (static time), 100 °C, and 1,500 psi. After extraction, we spiked the total lipid extract  
118 (TLE) with 1000 ng of 3-methyl-heneicosane (CAS#: 6418-47-9, Sigma-Aldrich), 20 ng of p-terphenyl (CAS#: 92-94-4, TCI),  
119 and 50 ng of pregnanol (5 $\beta$ -Pregnan-3 $\alpha$ -ol, CAS#: 4352-07-2, Steraloids) as internal standards for the quantification of *n*-  
120 alkanes, PAHs, and sterols, respectively. We concentrated the TLE under a gentle flow of nitrogen and then mixed it with  
121 HCl-activated copper shots to remove elemental sulphur as copper sulphide precipitates. We then filtered the samples through  
122 a  $\text{NaSO}_4$ -packed Pasteur column to remove any residual water and copper sulphide and concentrated them under  $\text{N}_2$ . We  
123 subsequently separated the TLE into six chromatographic fractions using a Pasteur pipette packed with silica gel (60–200  
124  $\mu\text{m}$  - 60 A) and solvents of increasing polarity. We calculated the column’s dead volume (DV) with *n*-hexane, and then eluted  
125 samples with 1.5 DV of *n*-hexane (F1), 2 DV of *n*-hexane:DCM 4:1 (F2), 1.5 DV of DCM (F3), 2 DV of DCM:acetonitrile  
126 (F4), 1.5 DV of acetonitrile (F5), and 3 DV of MeOH (F6). We derivatised fraction F4, containing the sterols/stanols, using  
127 TMS-BSTFA (Supelco) and pyridine (50:50) at 70 °C for 15 minutes, then dried under  $\text{N}_2$  and redissolved it in *n*-Hexane. We

128 added 1 ng of p-terphenyl D<sub>14</sub> (CAS: 1718-51-0, Sigma-Aldrich) and 50 ng of 5 $\alpha$ -cholestane (CAS: 481-21-0, Sigma-Aldrich)  
129 to fractions F2 (PAHs) and F4 (sterols), respectively, as injection standards to check the recovery and quantification  
130 consistency of analyses.

131 We analysed the *n*-alkanes, PAHs, and sterols using a Thermo Scientific Trace 1310 gas chromatograph (GC) equipped with  
132 a PTV inlet and a Restek glass liner interphase to a TSQ8000-Evo triple quadrupole mass spectrometer (MS). We used a 60  
133 m DB1 column (DB-1MS, 0.25 mm, 0.25  $\mu$ m film thickness, Agilent, USA) to separate *n*-alkanes and a DB-5 column (DB-  
134 5MS, 0.25 mm, 0.25  $\mu$ m film thickness, Agilent, USA) for PAHs and sterols, and He (1.2 ml min<sup>-1</sup>) as a carrier gas. For *n*-  
135 alkane analysis, we injected samples in splitless mode at 65 °C and the PTV was ramped to 400 °C at 3 °C s<sup>-1</sup> and held for 5  
136 min. The GC oven temperature was programmed from 60 °C to 220 °C (25 °C min<sup>-1</sup>) and then to 315 °C (2.5 °C min<sup>-1</sup>, held  
137 13 min). *n*-Alkanes were analysed in full scan (50–600 m/z) using the following MS conditions: 300 °C EI source at 70 eV  
138 electron energy, 50 uA emission current, and 15 V electron lens voltage, with a transfer line at 315 °C. For PAH analysis, all  
139 samples were injected in splitless mode at 45 °C and the PTV was ramped to 400 °C at 11.6 °C s<sup>-1</sup> and held for 2 min. The GC  
140 oven temperature was programmed from 60 °C (held 1 min), to 150 °C (40 °C min<sup>-1</sup>), to 320 °C (3 °C min<sup>-1</sup>, held 15 min). MS  
141 conditions were as follows: 250 °C EI source at 70 eV electron energy, 50 uA emission current, and 15 V electron lens voltage,  
142 with a transfer line at 320 °C. For sterol/stanol analysis, all samples were injected in splitless mode at 90 °C, evaporated at  
143 100 °C (0.1 min), and the PTV was ramped to 400 °C at 8 °C s<sup>-1</sup> and held for 1 min). The GC oven temperature was programmed  
144 from 80 °C (held 1 min), to 200 °C (20 °C min<sup>-1</sup>), to 320 °C (5 °C min<sup>-1</sup>, held 20 min). MS conditions were ~~as the~~ same as for  
145 *n*-alkanes. PAHs and sterols/stanols were analysed in selected reaction monitoring (SRM) using the collision energies and  
146 mass transitions reported in Table A1 and Table A2).

#### 147 **3.42.4 Analysis of air parcel back-trajectory patterns**

148 To define the potential regional extent of airborne PAHs arriving to SVID's catchment area, we traced the back-trajectory of  
149 air parcels using HYSPLIT (hybrid single particle lagrangian integrated trajectory; Draxler et al., 1998; Stein et al., 2015).  
150 Using a modified version of an R script originally developed to trace precipitation patterns (Caves Rugenstein and  
151 Chamberlain, 2018), we analyse data from the NOAA Global Data Assimilation System (GDAS; resolution 1° by 1°) at a six  
152 hours frequency tracing back trajectories for three days (72 h) and two weeks (336 h) during two years characterised by  
153 opposite North Atlantic Oscillation (NAO; Hurrell et al., 2003) configuration (2009-2010, NAO-; 2013-2014, NAO+; NOAA,  
154 2023). PAHs deposition, which is enhanced by low temperatures, occurs not only via precipitation but in dry conditions as  
155 well (Arellano et al., 2018; Feng et al., 2017; Golomb et al., 2001; Halsall et al., 2001). Thus, we present data for air parcel  
156 trajectories that did and did not produce precipitation within six hours from the endpoint (SVID), initialising the trajectories  
157 at four different altitudes: 1000, 1500, 2000 m asl (water vapour usually advects within an altitude of 2 km; Bershaw et al.,  
158 2012; Lechler and Galewsky, 2013; Wallace and Hobbs, 2006), and 150 m asl (SVID surface elevation).

### 159 **4.3 Background on proxies**

#### 160 **4.13.1 Polycyclic aromatic hydrocarbons (PAHs)**

161 We use pyrogenic PAHs (pyroPAHs) as tracers for the frequency/intensity of fire episodes, and the PAH perylene as a biogenic  
162 PAH related to terrestrial organic matter input. PAHs are semi-volatile compounds that can be of pyrogenic, petrogenic, or  
163 biogenic origin (Kozak et al., 2017; Lima et al., 2005). Low molecular weight (LMW; see Table A1 for group definition)  
164 PAHs in their non-alkylated form (Page et al., 1999; Yunker et al., 2002) constitute the majority of the PAHs produced by the  
165 combustion of plant biomass, while the relative amount of high molecular weight (HMW) PAHs increases along with higher  
166 fire temperatures (McGrath et al., 2003). LMW PAHs tend to be airborne and show high aqueous solubility and higher  
167 volatility, whereas HMW PAHs are usually in a solid phase (associated to either soot or char), show lower volatility, and are

likely sourced locally (Hoffmann and Wynder, 1977; Junk and Ford, 1980; Karp et al., 2020; Lammel et al., 2009; Lima et al., 2005; Purushothama et al., 1998). Thus, low contributions of HMW PAHs in environmental samples are often considered indicative of either low temperature fires (e.g., Denis et al., 2012) or a distal source, while high relative amounts generally point toward a more local signal. Finally, perylene is a 5-hexa-ring PAH often detected in aquatic sediments and considered to be mostly of in situ biogenic origin, probably from precursor compounds present in saprophagous and mycorrhizal fungi (e.g., Aizenshtat, 1973; Jiang et al., 2000; Slater et al., 2013; Wang and Huang, 2021), and thus likely linked to higher organic matter content and terrigenous input (Guo and Liao, 2020; Hanke et al., 2019).

#### 4.23.2 Sterols/stanols as markers of plant sources and animal digestion

Stanols are saturated isomers of sterols (e.g., Patterson, 1971). When the bacterially mediated reduction of sterol double bonds occurs in an open environment (e.g., soil), it leads almost exclusively to the production of 5 $\alpha$  stanol isomers. When the reduction of sterols occurs in the animal's digestive tract, their enteric bacterial flora maximises the production of 5 $\beta$  stanols (Hatcher and McGillivray, 1979; Murtaugh and Bunch, 1967). Humans (and partially other omnivores and carnivores) maximise the production of coprostanol (5 $\beta$ -cholestan-3 $\beta$ -ol) through the saturation of animal derived cholesterol (5-encholest-3 $\beta$ -ol). Ruminants such as sheep and cattle, on the other hand, maximise the production of 5 $\beta$ -stigmastanol and 5 $\beta$ -campestanol (Leeming et al., 1996, 1994) from plant derived sterols like stigmasterol, sitosterol, and campesterol (e.g., Goad, 1977; Goad and Goodwin, 1966; Pancost et al., 2002). Higher/lower ratios of coprostanol and its derived epimer epicoprostanol (5 $\beta$ -cholestan-3 $\alpha$ -ol; McCalley et al., 1981; Quirk et al., 1980; Wardroper et al., 1978) to 5 $\beta$ -stigmastanol or 5 $\beta$ -campestanol are considered to be a proxy for higher/lower faecal input from human sources relative to ruminant sources, and have been widely applied to samples from modern/ancient sewage material and manured soil (e.g., Birk et al., 2012; Bull et al., 2001, 2002; Cordeiro et al., 2008; Evershed et al., 1997; He et al., 2018; Lerch et al., 2021; Simpson et al., 1999; Tyagi et al., 2009).

#### 4.33.3 *n*-Alkanes

Plants synthesise *n*-alkanes and other *n*-alkyl lipids as part of their waxy coating with a characteristic strong odd-over-even chain length predominance (Eglinton and Hamilton, 1967), which is summarised by their higher carbon preference index (CPI; Bray and Evans, 1961; Marzi et al., 1993). In contrast, lower CPI values are usually indicative of petrogenic, algal, or bacterial sources (Grimalt and Albaigés, 1987; Han and Calvin, 1969). Aquatic sources such as macrophytes and mosses (e.g., *Sphagnum*) maximise their leaf wax *n*-alkane production at mid-length homologues (C<sub>21-25</sub>), while terrestrial plants (e.g., grasses, sedges, trees, shrubs) are generally skewed toward longer homologues (C<sub>27-31</sub>), allowing for use of source discriminating ratios and indices (e.g., such as the aquatic plant index<sub>7</sub> (P<sub>aq</sub>, Ficken et al., 2000) and average chain length (ACL, Gagosian and Peltzer, 1986).

#### 4.43.4 Bulk geochemistry proxies

Aquatic and terrestrial catchment productivity, flux of inorganic sediments, and organic matter preservation are the main factors determining the level of total organic carbon content in lacustrine sediments (Meyers and Ishiwatari, 1993). The molar carbon to nitrogen ratio (C/N) in plant tissue varies between aquatic plants and phytoplankton (<10) and terrestrial plants and bryophytes (>10; Meyers, 1994). Thus, increases in C/N are usually interpreted as an increased catchment erosion and input of terrestrial organic matter and/or as a relative decrease of aquatic plant productivity (Fernández-Martínez et al., 2021; Kaushal and Binford, 1999; Meyers, 1997; Meyers and Teranes, 2001; Rieger et al., 1979). Shifts in the abundance of diatom derived biogenic silica (BSi) can trace lake productivity (Colman et al., 1995; Conley, 1988; Conley and Schelske, 2002). The conservation potential of diatom frustules is strongly related to sedimentation rate, with higher rates leading to better preservation. When sedimentation rates are considered relatively constant, shifts in BSi can reflect qualitative changes in



208 spring/summer temperature in high-latitude lakes, such as Iceland (Geirsdóttir et al., 2009a; McKay et al., 2008). The stable  
 209 isotopic composition of carbon ( $\delta^{13}\text{C}$ ) can trace shifts in the relative contribution of organic matter sources, with terrestrial  
 210 plants (but also bryophytes) and associated soils showing more  $^{13}\text{C}$ -depleted values (ca -32‰ to -25‰), aquatic plants  
 211 exhibiting more  $^{13}\text{C}$ -enriched values (ca -20‰ to -10‰), and freshwater algae and phytoplankton showing a wider isotopic  
 212 range (Meyers, 1994; Prokopenko et al., 1993; Rundel et al., 1979; Smith and Epstein, 1971; Geirsdóttir et al., 2020 and refs  
 213 therein). The physical mixing or stratification of a lake water column can also influence the carbon isotopic signature of aquatic  
 214 sources (Hernández et al., 2011).

## 215 [5.4 Results](#)

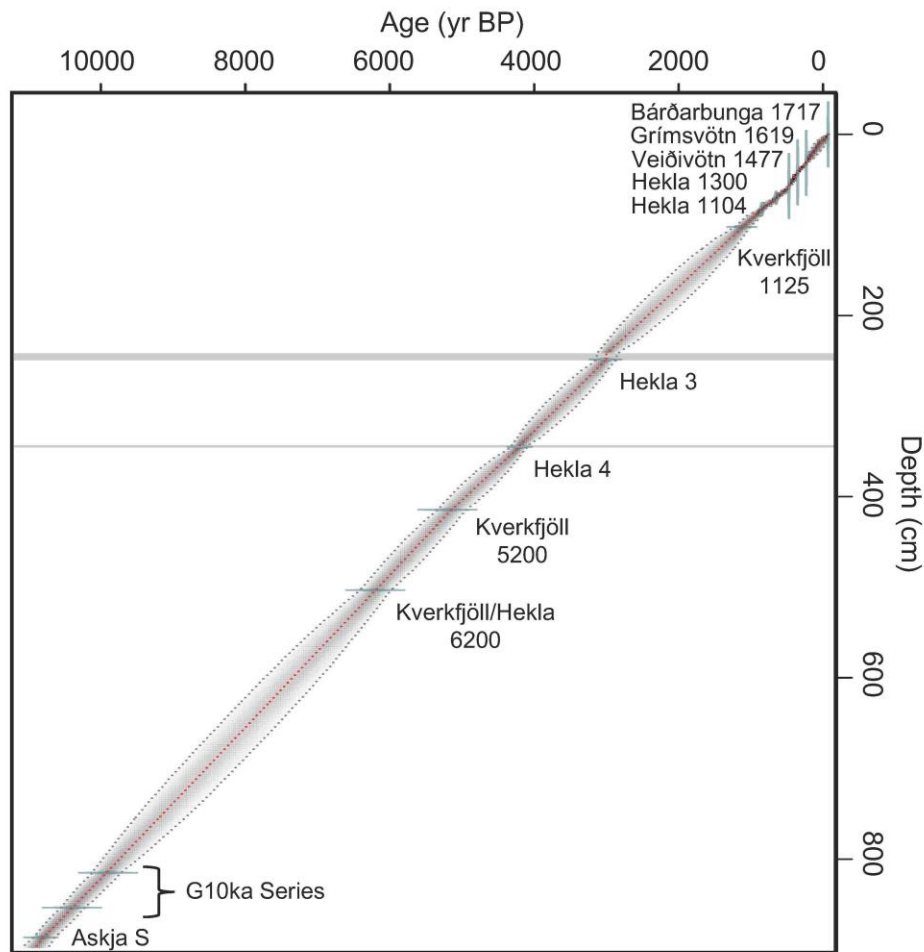
### 216 [5.14.1 Age model](#)

217 Based on major oxide composition and stratigraphical information, we identified 13 marker tephra layers of known age (Table  
 218 1). Our Bayesian tephra age model shows nearly constant sediment accumulation rates throughout the Holocene (Fig. 2).  
 219 There is increased uncertainty in age control between the G10ka tephra series and Kverkfjöll/Hekla 6200 due to fewer marker  
 220 tephra layers being present. However, the Late Holocene, particularly during the historical period of settlement, features  
 221 numerous tephra layers that result in substantially lower age estimate uncertainty.

222  
 223 **Table 1: Marker tephra layers of known age identified in 20-SVID-02 and used to develop the age model.**

Composite depth (cm)	Tephra layer ID	Layer age (a BP)	Reference
31.5	Bárðarbunga-Veiðivötn 1717	233 ± 2	Thorarinsson (1974)
42.0	Grímsvötn 1619?	352 ± 2	Thorarinsson (1974)
56.0 – 57.0	Veiðivötn 1477	473 ± 2	Larsen et al. (2002)
70.0	Hekla 1300	650 ± 10	Thorarinsson (1967)
82.5	Hekla 1104	846 ± 10	Thorarinsson (1967)
102.2	Kverkfjöll	1125 ± 50	Óladóttir et al. (2011)
242.5 – 248.5	Hekla 3	3010 ± 54	Dugmore et al. (1995)
344.0 – 345.0	Hekla 4	4200 ± 42	Dugmore et al. (1995)
414.0 – 414.5	Kverkfjöll	5200 ± 100	Óladóttir et al. (2011)
503.2	Kverkfjöll and Hekla	6200 ± 100	Óladóttir et al. (2011)
815.0	G10ka Series (top)	9900	Óladóttir et al. (2020)
853.5	G10ka Series (bottom)	10400	Óladóttir et al. (2020)
886.5	Askja S	10830 ± 57	Bronk Ramsey et al. (2015)

224



225

226

227

228

229

**Figure 2: Stóra Viðarvatn age model generated in Bacon (Blaauw and Christeny, 2011). Green horizontal lines denote the age and uncertainty of marker tephra layers, red line reflects mean values of model iterations, the grey lines denote the 95% confidence envelope, and darker shading reflects more likely ages. Gray vertical bars mark the ‘slumps’ used for the Hekla 3 and Hekla 4 tephra layers.**

230

231

232

233

234

235

236

237

238

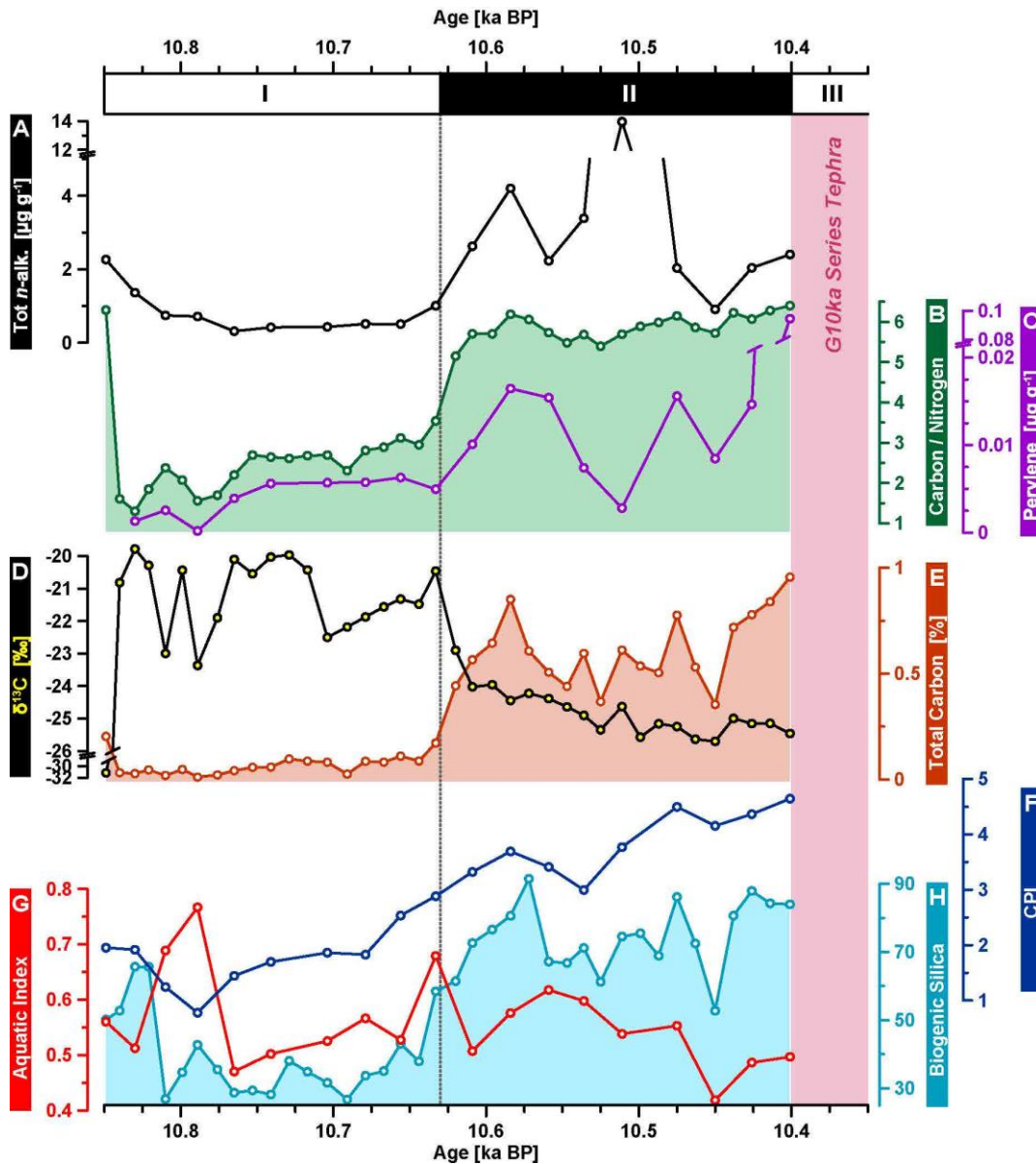
To facilitate the interpretation of downcore records, we present and discuss data (1) divided into nine time intervals (I–IX; Table 2) representing the most distinguishable periods of variability with respect to background values, and (2) separately for the sections preceding and following the G10ka tephra series (Óladóttir et al., 2020). We tried analysing some material from the G10ka series (a very thick tephra unit; Óladóttir et al., 2020) but the yields of organics were too low to be reliable (as expected; its contents are almost 100% inorganic). Thus, here we only included one sample at the bottom limit of the G10 ka tephra series and one at the upper limit.

**Table 2: Age intervals (approximate) and descriptions of the nine subdivisions of the 20-SVID-02 record used in this study.**

Interval	Age (ka BP)	Description
I	10.85–10.63	Potential Preboreal cooling
II	10.63–10.40	Pre-Boreal warming
III	10.4–9.9	G10 ka tephra series
IV	9.9–8.8	Early Holocene warming (rebound after G10 ka event)
V	8.8–7.5	Early Holocene instability (8.2 ka event?)
VI	7.5–3.0	Middle Holocene plateau and trend inversion
VII	3.0–1.3	Late Holocene cooling
VIII	1.3–0.25	Medieval period and Little Ice Age

240 **5.34.2 Bulk geochemistry**

241 The C/N ratio (Figs. 3-4B) ranged from ~1 to ~9.5, showing lowest values at the beginning of the record (I). At ca 10.63 ka BP, C/N increased sharply and reached mid-range values (5-6), remaining relatively stable throughout most of the remaining  
 242 Holocene (IV–VI), except for two drops, after the G10ka Series tephra and between 8.8 and 7.75 ka BP (V). In the last 2 kyr, C/N values steadily increased, leading to the highest values in the most recent portion of the record. The two periods with  
 243 C/N values steadily increased, leading to the highest values in the most recent portion of the record. The two periods with  
 244 decreased C/N values, as well as the initial increase (I to II), generally paralleled the behaviour of the total carbon (Figs. 3-  
 245 4E), biogenic silica (Figs. 3-4H), and  $\delta^{13}\text{C}$  (Figs. 3-4D) records. TC increased steadily throughout the Holocene from ~0%  
 246 while BSi rapidly increased at the beginning of the record (30 to 90) to then stabilise at 110–120 for more than 5 kyr (V–VI).  
 247 Both records peaked at ca 3.5 ka BP (2.8%, TC; ~160, BSi max) and temporarily dropped between ca 3 and 2.25 ka BP.  
 248 Subsequently, TC increased to its maximum value (3.6%, modern) while BSi decreased in a stepwise manner, reaching its  
 249 lowest value of the last 10 kyr (~50) at ca 0.2 ka BP. The  $\delta^{13}\text{C}$  record showed the most  $^{13}\text{C}$ -enriched values (-20‰) in the  
 250 oldest interval (I); it then decreased (to -26‰, modern) steadily throughout the Holocene, except for two major drops to its  
 251 most depleted values (ca -27‰) during periods II and V.  
 252

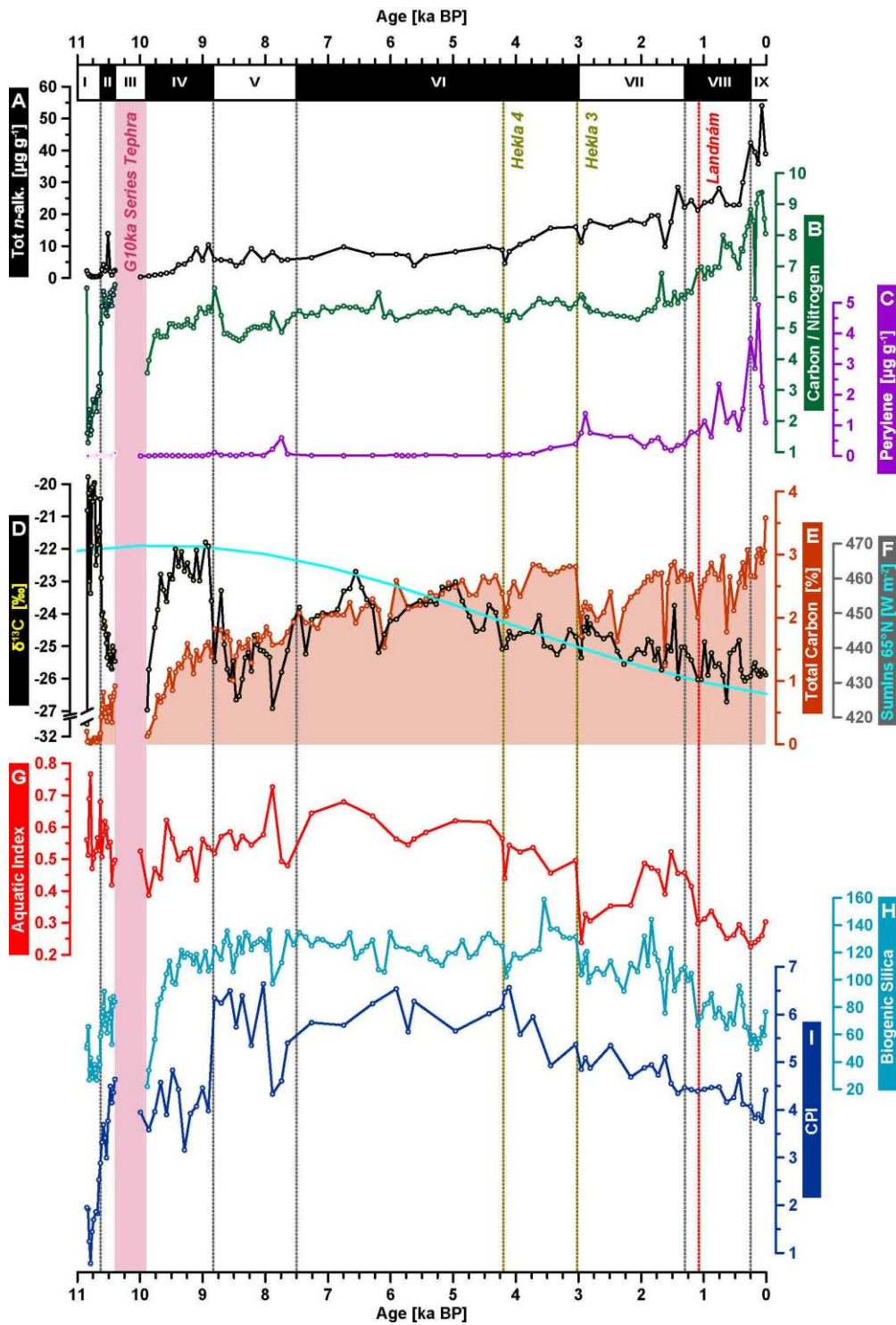


253

Figure

254  
255  
256  
257  
258

3: Erosional and primary productivity proxies from the pre-G10ka Series tephra interval (pink vertical band) of 20-SVID-02 core; all concentrations are on g of dry samples. (A, black) sum of C<sub>19-35</sub> *n*-alkanes concentration aquatic plant index derived from *n*-alkanes; (B, green) carbon to nitrogen ratio; (C, purple) perylene concentration; (D, black-yellow) stable isotopic composition of total carbon; (E, brick red) percentage of total carbon; (F, dark blue) *n*-alkanes carbon preference index (CPI<sub>19-31</sub>); (G, red) aquatic plant index derived from *n*-alkanes; (H, light blue) biogenic silica.



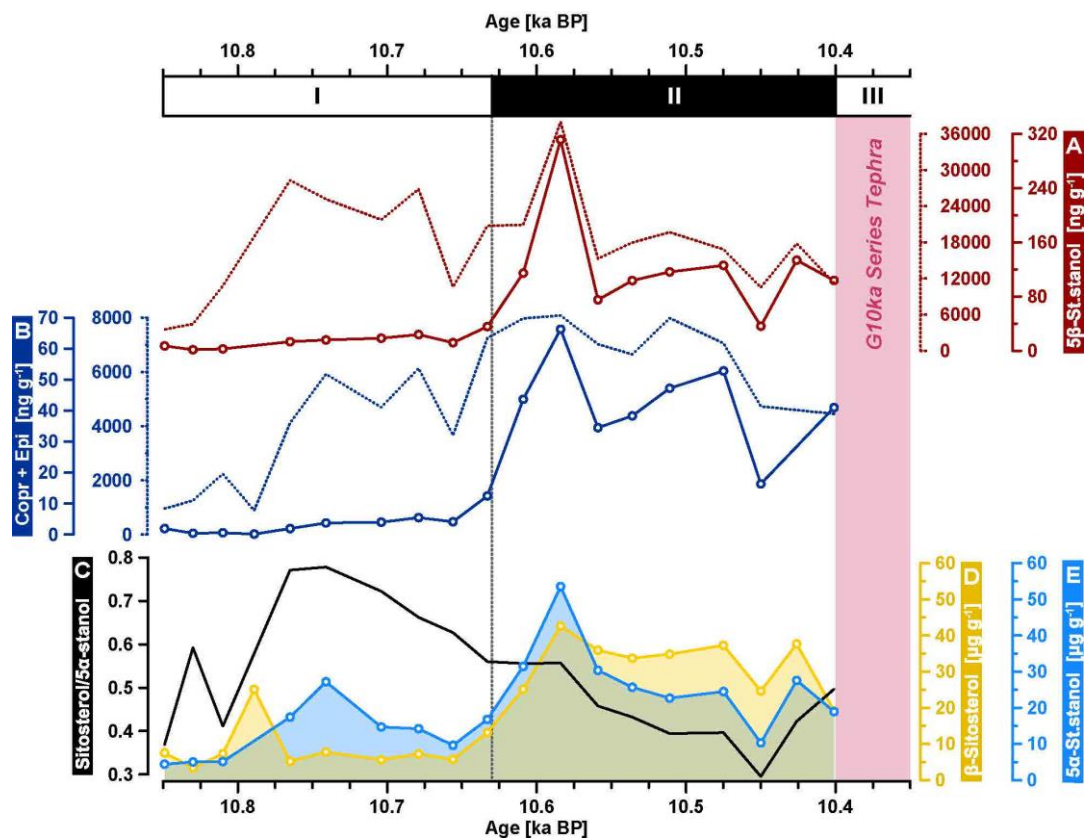
259

260 **Figure 4:** Erosional and primary productivity proxies of 20-SVID-02 core. (A, black) sum of C<sub>19-35</sub> *n*-alkanes concentration aquatic  
261 plant index derived from *n*-alkanes; (B, green) carbon to nitrogen ratio; (C, purple) perylene concentration; (D, black-yellow) stable  
262 isotopic composition of carbon; (E, brick red) percentage of total carbon; (F, cyan) northern hemisphere summer insolation at 65°  
263 N (Berger and Loutre, 1999); (G, red) aquatic plant index derived from *n*-alkanes; (H, light blue) biogenic silica; (I, dark blue)  
264 carbon preference index (CPI<sub>19-31</sub>). Red dotted line marks the conventional age (870 CE) of the settlement of Iceland (Landnám).  
265 Black vertical dashed lines mark the subdivision of the 20-SVID-02 record into nine intervals (Table 1).

267 We detected *n*-alkane homologues from C<sub>19</sub> to C<sub>33-35</sub> (Fig. A3) in most samples, with a total sum that ranged from 0.3 to 50  
 268  $\mu\text{g g}^{-1}$  (700–4000  $\mu\text{g g}^{-1}$  TC; Figs. 3-4A). The 10.8 to 4.2 ka BP interval showed relatively low and stable values ( $\sim 5 \mu\text{g g}^{-1}$ );  
 269 concentrations roughly doubled from 4 to 1.5 ka and then again after 0.5 ka BP, reaching its maximum value at the end of the  
 270 record. The CPI showed a stable odd-over-even predominance (3 to 6.5) through the whole record, except for low values (1 to  
 271 3) seen in the interval preceding the G10ka Series tephra (Figs. 3F-4I). The most abundant homologues were C<sub>23-27</sub> (45%) in  
 272 the 10.8 to 3 ka BP interval and C<sub>29-31</sub> (40%) in the last 3 kyr. This regime change was highlighted by a shift in P<sub>aq</sub> from  
 273 relatively high values (up to 0.8; avg. 0.6) through the early-mid Holocene to lower values (down to 0.2; avg. 0.3) after 3 ka  
 274 BP (Fig. 4G).

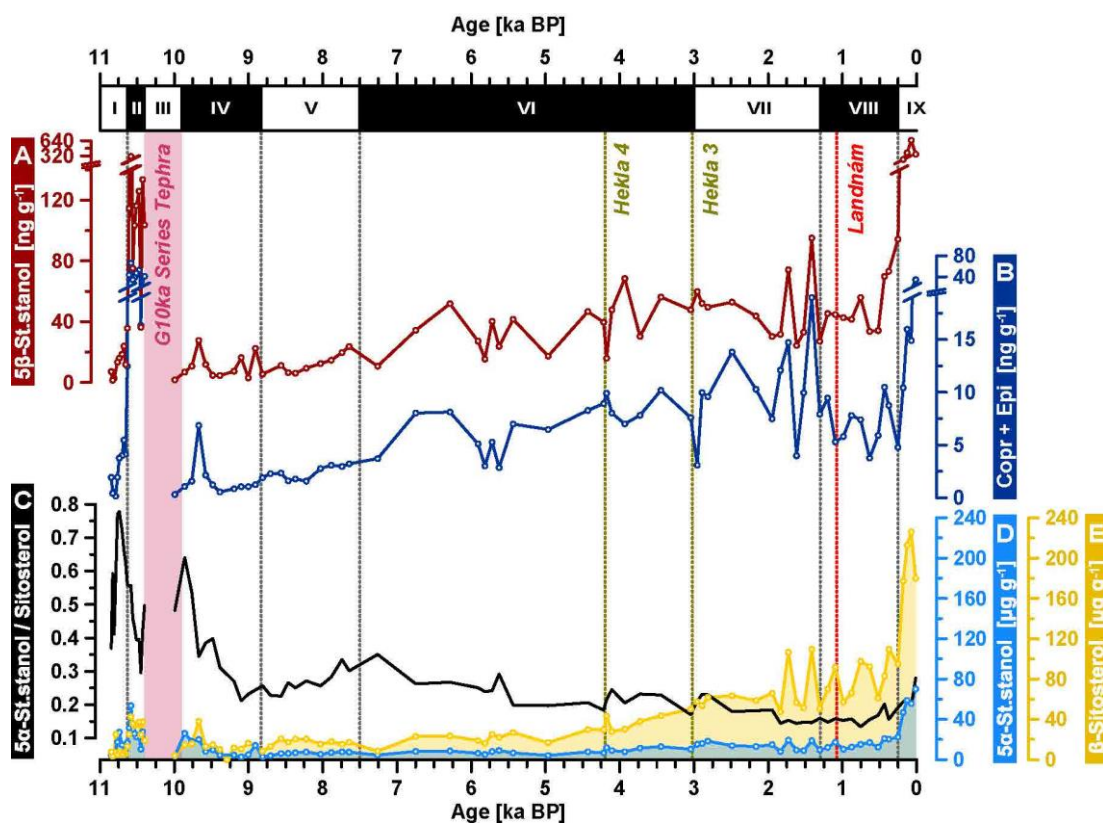
#### 275 5.54.4 Faecal sterol/stanols

276 We detected the three main faecal stanols: the plant derived 5 $\beta$ -stigmastanol was  $\sim 5$ –10 times more abundant (up to 3-500 ng  
 277  $\text{g}^{-1}$ ; Figs. 5-6A) than coprostanol + epi-coprostanol (10-30 ng  $\text{g}^{-1}$ ; Figs. 5-6B). The oldest interval (I) showed the lowest  
 278 concentrations for all three stanols, while the following interval (II) displayed high (highest for coprostanol and epi-  
 279 coprostanol) concentrations. All three stanols showed low and stable concentrations between  $\sim 9.5$  and 7.5 ka BP, gradually  
 280 increased from  $\sim 7.5$  ka BP before reaching a relative maximum around 1.5 ka BP (VII), dropping again during interval VIII,  
 281 and peaking during the last 200 to 300 years (IX). Parent sterols ( $\beta$ -sitosterol,  $\beta$ -stigmasterol, except cholesterol) and the  $\alpha$ -  
 282 stanol isomers, follow patterns similar to the  $\beta$ -stanols throughout the Holocene, but with 10 to 100 times higher concentrations  
 283 (Fig. A2).



284

285 **Figure 5: Sterols/stanols from the pre-G10ka Series tephra interval (pink vertical band) of 20-SVID-02 core. (A, red) 5 $\beta$ -stigmastanol**  
 286 **and (B, dark blue) sum of coprostanol and epi-coprostanol concentration on g of dry sample (full line) and on g of TC (dotted line);**  
 287 **(C, black)  $\beta$ -sitosterol to 5 $\alpha$ -stigmastanol ratio; (D, yellow)  $\beta$ -sitosterol concentration; (E, light blue) 5 $\alpha$ -stigmastanol concentration.**

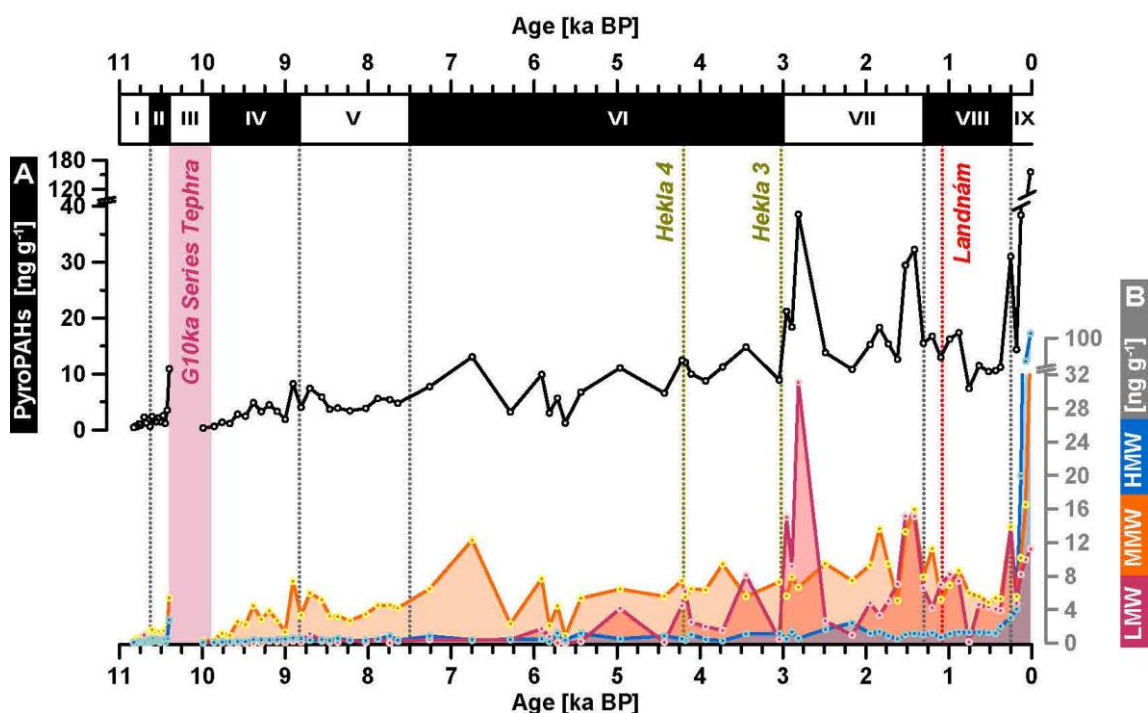


288

289 **Figure 6:** Sterols/stanols of the 20-SVID-02 core. (A, red) 5β-stigmastanol and (B, dark blue) sum of coprostanol and epi-coprostanol  
 290 concentration on g of dry sample (full line) and on g of TC (dotted line); (C, black) β-sitosterol to 5α-stigmastanol ratio; (D, yellow)  
 291 β-sitosterol concentration; (E, light blue) 5α-stigmastanol concentration. Red dotted line marks the conventional age (870 CE) of the  
 292 settlement of Iceland (Landnám). Black vertical dashed lines mark an arbitrary subdivision of 20-SVID-02 record into nine intervals  
 293 (Table 1).

#### 294 5.64.5 Polycyclic aromatic hydrocarbons (PAHs)

295 PAHs were present in all samples and generally in higher concentrations in more recent compared to older samples (Fig. A1).  
 296 Perylene (Figs. 3-4C), which accounts for more than 97% of detected PAHs, maintains low concentrations (0–20 ng g<sup>-1</sup>) from  
 297 10.5 to 4–3 ka BP. A first increase to 0.5–1.5 μg g<sup>-1</sup> occurred between 3.5 and 2.8 ka BP, followed by a decrease loosely coeval  
 298 to the decrease in TC and BSi (VII). After ca 1.5 ka BP, perylene increases to a maximum value (~6 μg g<sup>-1</sup>, ca 0.15 ka BP),  
 299 which generally matches the pattern of TC. The second most abundant compound was phenanthrene (0.01–31.1 ng g<sup>-1</sup>),  
 300 followed by pyrene (0.1–11.5 ng g<sup>-1</sup>) and fluoranthene (0.01–17.6 ng g<sup>-1</sup>). The least abundant PAHs were naphthalene,  
 301 acenaphthylene and acenaphthene. However, since the detection of these three low molecular weight compounds could have  
 302 been influenced by evaporation losses during sample preparation, their reported concentrations are likely to be underestimated.  
 303 Given the overwhelming dominance of perylene and its likely biogenic rather than pyrogenic origin, we removed it from total  
 304 PAHs abundance calculations to provide a record with features that were not apparent in perylene's trend. In terms of total  
 305 pyroPAHs abundance, we observe five distinguishable intervals (Fig. 7A). First, a 3 kyr-long interval (~80 years average  
 306 temporal resolution) starting at ca 10.5 ka BP displays a relatively stable low concentrations (< 5 ng g<sup>-1</sup>, SD σ = 2.3). The only  
 307 exception is a point taken within the G10ka Series tephra (up to 10 ng g<sup>-1</sup>) at ca 10 ka BP. Second, from ~7.5 to 2.9 ka BP  
 308 (~320 years average temporal resolution), the total PAHs concentration increases from ~5 to 10 ng g<sup>-1</sup>, although with enhanced  
 309 variability (σ = 3.7). Third, led by the increase of low molecular weight PAHs (LMW, Fig. 7B), during the 2.9 to 0.7 ka BP  
 310 interval, values fluctuate (σ = 7.5) between ~10 and 20 ng g<sup>-1</sup>, with two major peaks reaching 45 and 35 ng g<sup>-1</sup> at ~2.7 to 2.3  
 311 ka BP and 1.5 to 1.3 ka BP, respectively. Fourth, between 0.7 and 0.3 ka BP there is a relatively brief although clear drop (~10  
 312 ng g<sup>-1</sup>, σ = 1.5), led by both LMW and MMW PAHs. In the last 250 years we observe a sharp, 10-fold increase in PAHs  
 313 concentration leading to the highest recorded values (~200 ng g<sup>-1</sup>). When normalised for TC (Fig. A1), the absolute values  
 314 increase 10 to 100-fold, but the patterns do not substantially change.



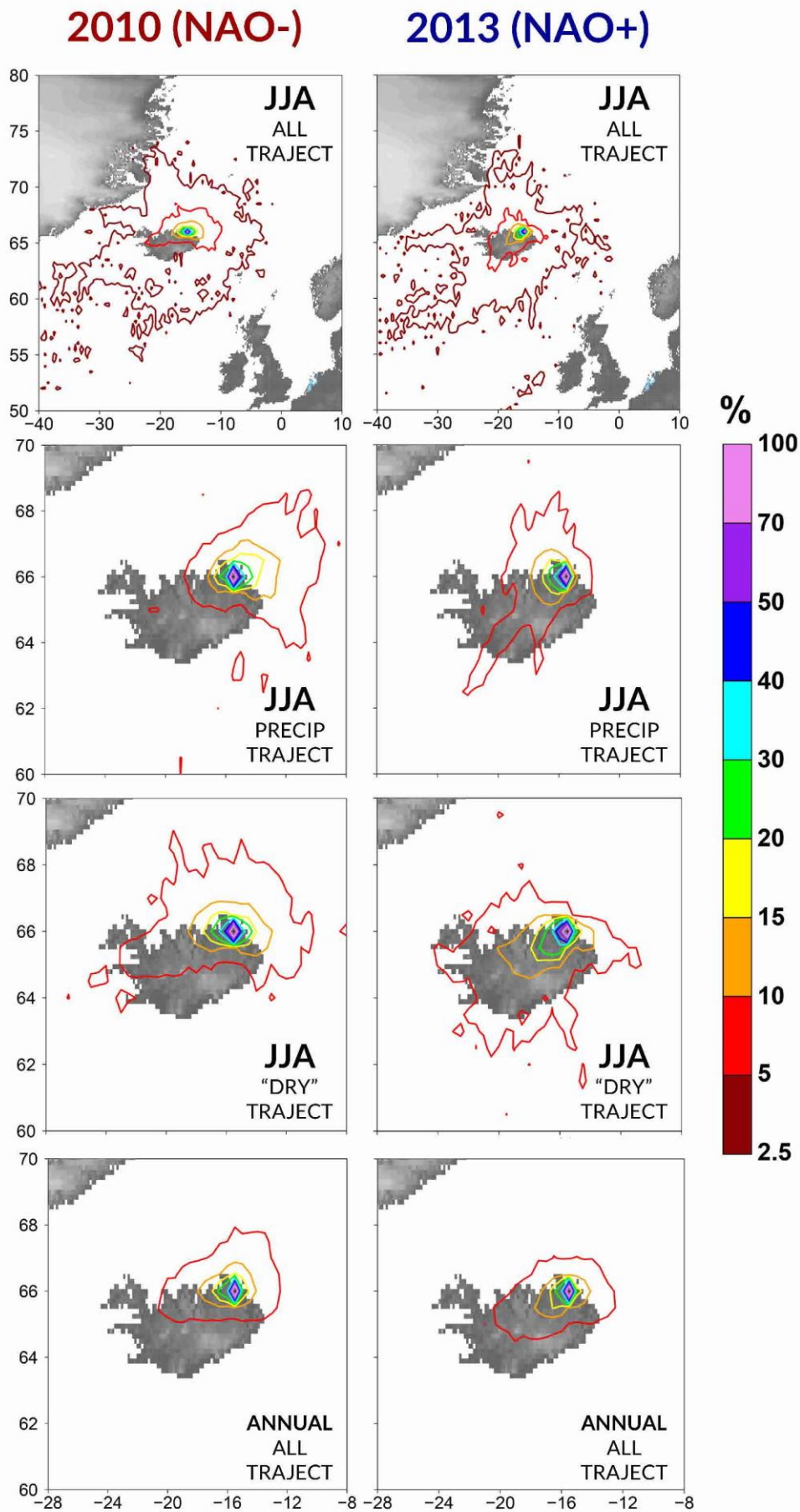
315

316 **Figure 7: PAHs record of the 20-SVID-02 core. (A, black) sum of pyrogenic PAHs concentrations; (B, fuchsia low, (orange) medium, and (blue) high molecular weight pyrogenic PAHs concentration. Red dotted line marks the conventional age (870 CE) of the settlement of Iceland (Landnám). Vertical pink band marks the G10ka Series Tephra. Black vertical dashed lines mark an arbitrary subdivision of 20-SVID-02 record into nine intervals (Table 1).**

#### 320 **5.74.6 HYSPLIT**

321 We calculated a total of 11,392 air trajectories, which we split by year, season, dry (i.e., not associated with precipitation), or precipitation bearing trajectories (Fig. A4). Most trajectories, even for two weeks intervals, show air parcels originating mostly from Iceland and surrounding areas of the North Atlantic, regardless of season or NAO configuration, while the contribution from nearby terrestrial regions (potential PAHs sources) such as Greenland, British Isles, or Scandinavia is negligible. As the marine environment is not conducive to combustion nor redeposition of particulates, this implies a dominantly Icelandic signal for PAH production.

327 Since wildfires are concentrated in the relatively dryer, snow-free summer season (Mccarty et al., 2021), we focus particularly on the JJA air trajectory data (Fig. 8). These results show that: (1) 95% of back-trajectories originate from Iceland and its nearby waters; (2) 90% of back-trajectories originate within 100–150 km radius from SVID; (3) dry trajectories more likely originate inland relative to precipitation carrying trajectories; (4) 95% of trajectories from a NAO- year tend to be confined to northern Iceland while during a NAO+ year trajectories more commonly originate from inland; (5) these patterns are consistent even when scaled from three days to two weeks intervals (Fig. A4).



333

334 **Figure 8:** HYSPLIT back trajectories of air parcels for 2010 (NAO-) and 2013 (NAO+), annual and summer (JJA). Trajectories are  
 335 calculated on a two-weeks (336 h) interval at a 6-hour frequency; "precip" indicates trajectories that produced precipitation within  
 336 6 h from the SVID endpoint, while "dry" trajectories did not. Contour colours indicate the frequency at which air parcels part of a  
 337 trajectory travel above a certain area.



339 **6.15.1 Primary aquatic production vs erosion/terrestrial input**

340 In Icelandic lacustrine environments,  $\delta^{13}\text{C}$  and C/N are generally considered proxies for the relative contribution of terrestrial  
 341 vs aquatic organic matter and shifts in primary productivity, as total carbon is virtually solely of organic origin (e.g., Geirsdóttir  
 342 et al., 2009a). Iceland's bedrock is dominantly comprised of basaltic bedrock, including the catchment of SVID (Hjartarson  
 343 and Sæmundsson, 2014), meaning there is negligible carbonate available. Although some dissolved inorganic carbon (DIC)  
 344 has been measured in Icelandic rivers, it is greatly outweighed by organic carbon (Kardjilov et al., 2006), whereas the amount  
 345 of inorganic carbon measured in soils is negligible (Mankasingh and Gísladóttir, 2019). This is important to consider as SVID  
 346 has no river inflow and water inflow is dominated by runoff from the catchment through soil. In addition, while there is some  
 347 evidence for the transport of Saharan dust to Iceland within the last decade (Varga et al., 2021), there is currently no evidence  
 348 of such transport during the Holocene. Additional pools of inorganic carbon from aquatic invertebrates, such as ostracods, are  
 349 also considered to be negligible (Alkalaj et al., 2019). Ostracods crystallise their shells in very close equilibrium to the carbon  
 350 isotopes of DIC (Decrouy, 2012), which for Iceland is notably enriched relative to bulk organic matter carbon isotopes  
 351 (Sveinbjörnsdóttir et al., 2020). If ostracods were a substantial contributor to the total carbon pool, we would expect lake  
 352 sediment carbon isotopes to deviate significantly from modern terrestrial and aquatic plant carbon isotope values. As Icelandic  
 353 lake sediment bulk geochemistry is consistent with the fields of modern plants (see Geirsdóttir et al., 2020), inorganic carbon  
 354 from aquatic invertebrates are not considered a significant contributor to the total carbon pool.  
 355 In addition, ~~†~~ in SVID, the similarity of the C/N record to the perylene curve reinforces its significance as a proxy for  
 356 terrigenous input.

357 **6.15.1.1 11-7.5 ka BP: Postglacial warming**

358 Deglaciation in the NE of Iceland set in between 15 and 13 ka BP and proceeded in a stepwise fashion, with two main glacier  
 359 re-advances at ca 12.7 (Younger Dryas) and 10.9 ka BP (Preboreal; Geirsdóttir et al., 2009b; Norðdahl and Pétursson, 2005).  
 360 Our record captures sediment below the Askja S tephra layer ( $10.83 \pm 0.57$  ka BP, Bronk Ramsey et al., 2015), showing ice-  
 361 free conditions and the start of organic sedimentation by 10.85 ka BP at SVID's location. Except for the oldest sample, high  
 362  $\delta^{13}\text{C}$  and low TC values indicate a primarily aquatic source of carbon during the oldest interval (I) (Fig. 3). This suggests an  
 363 absence of substantial terrestrial vegetation, consistent with a postglacial landscape and possibly a cooler climate associated  
 364 with the Preboreal period.

365 TC, BSi, and C/N increase suddenly at ca 10.65 ka BP, maintaining higher values for two-three centuries (vice versa for  $\delta^{13}\text{C}$ ),  
 366 indicating an enhanced terrestrial input likely resulting from a retreating glacier, development of soil and vascular plants, and  
 367 generally warming conditions (Fig. 3). After the G10ka Series tephra, all proxy values decrease, likely due to the destructive  
 368 impact of substantial volcanic ash fallout on both terrestrial and aquatic vegetation and related water chemistry alteration (e.g.,  
 369  $\delta^{13}\text{C}$  dropping due to acidification; Kilian et al., 2006) (Fig. 4). Following the volcanic event, all proxies increase at ca 9.75 ka  
 370 BP, whereas terrestrial- relative to aquatic-sourced carbon temporarily increase (ca 8.7–7.5 ka BP). The observed decrease in  
 371  $\delta^{13}\text{C}$  (and, partially, C/N) between 8.7 and 7.5 ka BP is identified in other Icelandic lake sediment records between 8.8 and 7.9  
 372 ka BP (e.g., Eddudóttir et al., 2018; Geirsdóttir et al., 2013; Harning et al., 2018b; Larsen et al., 2012) and has been attributed  
 373 to the likely impact of meltwater pulses into the northern North Atlantic due to the retreating Laurentide ice sheet and/or local  
 374 effusive volcanic eruptions (Geirsdóttir et al., 2013; Larsen et al., 2012).

375 The total sum of *n*-alkanes ( $\text{C}_{19-35}$ ; Fig. 4A), which is heavily controlled by  $\text{C}_{29}$  and  $\text{C}_{31}$  (Fig. A3), increases throughout the  
 376 Holocene similar to the pattern described by C/N and perylene as a result of an increased terrigenous input. As inferred by  
 377 high CPI values, most *n*-alkanes in SVID originate from plants (terrestrial and possibly also aquatic) through the Holocene

378 record (Fig. 4I). The relatively low CPI values in the oldest interval (I) indicate a negligible contribution from plant sources  
379 (relative to phytoplankton) to the carbon pool, which is consistent with a still cold, relatively barren, deglacial environment.  
380 The CPI curve shows a similar but opposite pattern to the  $\delta^{13}\text{C}$  record until ca 8 ka BP, reinforcing  $\delta^{13}\text{C}$  as a proxy mostly  
381 controlled by terrigenous input (*n*-alkanes from aquatics show lower CPI values than terrestrial plants; e.g., Bray and Evans,  
382 1961; Duan et al., 2014; Eglinton and Hamilton, 1967; Li et al., 2020). The reason for the change in the relationship between  
383 CPI and  $\delta^{13}\text{C}$  (which become positively correlated after 8 ka BP) is unclear. While it matches the timing of increasing  
384 temperatures (Axford et al., 2007; Fig. 10D) and *Betula* expansion in the region (Karlsdóttir et al., 2014; Fig. 10E), its  
385 interpretation is complicated by the fact that CPI can also be influenced by factors such as changes in mean annual precipitation,  
386 seasonality, plant community, and algal productivity (Li et al., 2020).

#### 387 **6.1.25.1.2 7.5-4.2 ka BP: Mid-Holocene Plateau and trend inversion**

388 Overall, all proxies suggest that the interval between ~7.5 and 4.2 ka BP, was characterised by relatively stable climatic  
389 conditions, generally warmer (Axford et al., 2007) and wetter (Moossen et al., 2015) than both the preceding and following  
390 periods. These conditions likely led to an enhanced primary productivity within the lake, as suggested by high values of BSi,  
391  $P_{\text{aq}}$ , CPI, and pollen inferred vegetation communities (Eddudóttir et al., 2016; Karlsdóttir et al., 2014). In fact, modelled  
392 reconstructions of Icelandic vegetation cover throughout the Holocene show the highest values during this interval (Ólafsdóttir  
393 et al., 2001). In particular, partly due to the retreat/disappearance of most glaciers, between 50% and 60% of Iceland was likely  
394 covered in vegetation, of which a quarter was birch forest, throughout the mid-Holocene, with two peaks, one at the Holocene  
395 Thermal Maximum (8–7 ka BP) and one at ~3.5 ka BP (Ólafsdóttir et al., 2001). The warm and moist climate, paired with the  
396 expansion of vegetation, may have stabilised the local environment, reducing erosion. Such stability is consistent with the low  
397 C/N, Perylene, and *n*-alkanes values throughout this interval.

398 Though this four thousand year period is broadly categorised by stability, a more detailed view reveals important inflection  
399 points in the long term trends of many proxies. For example, while some proxies keep increasing (e.g., TC, and summer  
400 temperature, Axford et al., 2007), some stop rising and remain relatively flat throughout this interval (e.g., C/N, Perylene),  
401 while others even invert their trends ( $\delta^{13}\text{C}$ ,  $P_{\text{aq}}$ , CPI). Another trend inversion occurred around 5 ka BP with the inception of  
402 neo-glaciation in Iceland when glaciers started to expand again (Geirsdóttir et al., 2019). This could be interpreted as a slow  
403 inertial response of the local environment to the decreasing NH summer insolation, likely reducing its resilience to short term  
404 events such as volcanic eruptions and NAO shifts, until some kind of threshold was finally reached around 4 ka BP (Geirsdóttir  
405 et al., 2013, 2019).

#### 406 **6.1.35.1.3 4.2 ka BP: Increased erosion in a cooling climate**

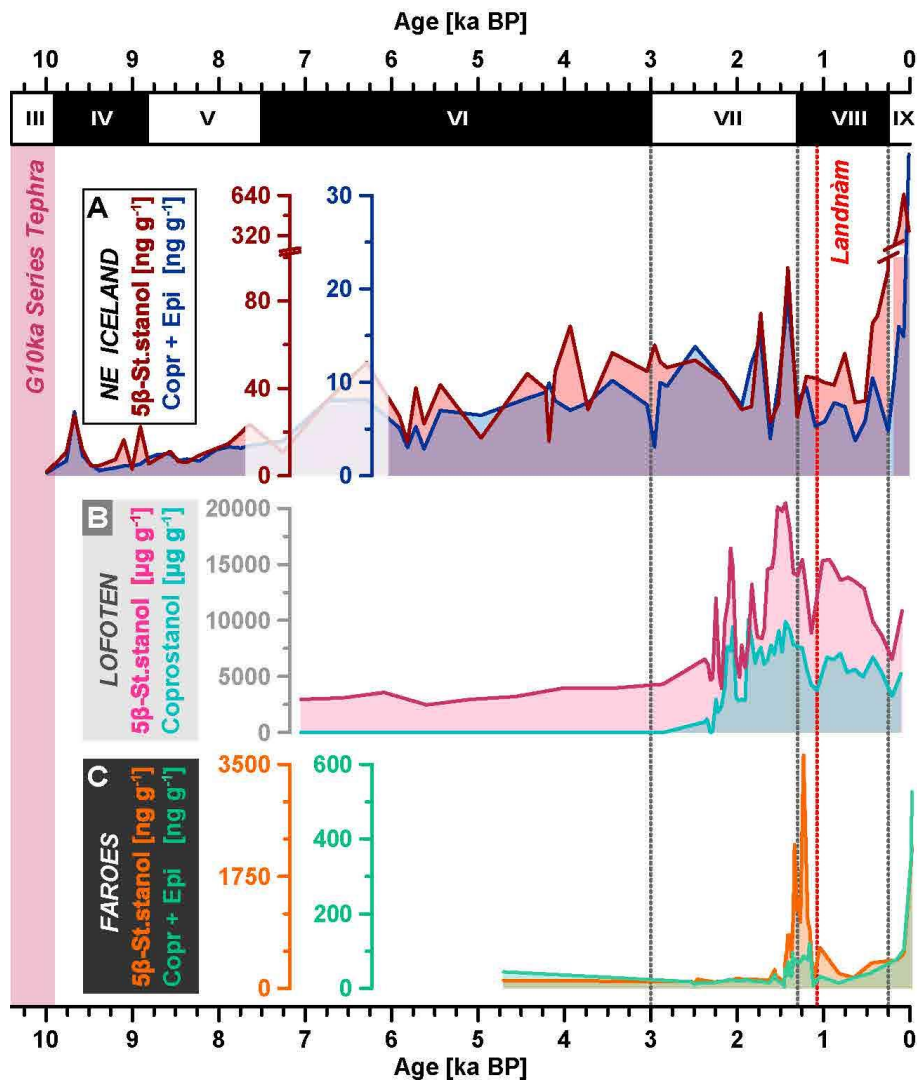
407 Our SVID proxy datasets generally agree with previous work using bulk geochemistry proxies in Icelandic lakes, which  
408 collectively point toward decreasing primary productivity and increasing landscape instability in response to declining  
409 Northern Hemisphere summer insolation (e.g., Geirsdóttir et al., 2013, 2019; Harning et al., 2018b, 2020; Larsen et al., 2012).  
410 The decreasing trend in  $\delta^{13}\text{C}$  is generally anticorrelated with the TC curve, indicating that TC is increasingly controlled by  
411 terrestrial input. BSi, TC, and C/N values drop or invert their trend after ca 4 ka BP, consistent with a general decrease in  
412 productivity. This is possibly related to a combination of decreasing moisture and/or summer temperatures (Axford et al.,  
413 2007), and the effect of the Hekla 4 volcanic event, pushing the local environment beyond a threshold (Eddudóttir et al., 2017).  
414 Absolute amounts of *n*-alkanes also increase starting at 4 ka (Fig. 4A), led by an increase in *n*-C<sub>29</sub> (Fig. A3), typical of terrestrial  
415 plants. The ratio between the mid- and long-chain homologues (aquatic plant index or  $P_{\text{aq}}$ ; Ficken et al., 2000) is often  
416 interpreted as a proxy for a wetter/drier environment. However, this is likely an oversimplification as questions remain about  
417 the relationship between *n*-alkane chain length and vegetation source, particularly for aquatic plants which are often a minor  
418 component of the leaf wax pool in Arctic lakes (Dion-Kirschner et al., 2020; Hollister et al., 2022). Nevertheless, when coupled

419 to the concentration data of *n*-alkanes (Fig. 4A; Fig. A3),  $P_{aq}$  can here be more safely interpreted as indicative of lower/higher  
420 terrigenous input. The SVID record (Fig. 4H; Sect. 3.3) shows higher  $P_{aq}$  values (mean 0.6) during the 10.8 to 4-3 ka BP  
421 interval, indicating an environment with significant aquatic plant production and likely limited erosion/in-wash. The record  
422 then switches abruptly to lower values (mean 0.3) at 3 ka BP, highlighting a shift toward greater in-wash of terrestrially derived  
423 material.

424 The massive Hekla 3 eruption (the most severe Hekla eruption of the Holocene; ~3,010 a BP; Larsen, 1977; Larsen and  
425 Eiríksson, 2008), was likely the cause, or at least the trigger, of this abrupt shift at 3 ka BP in most SVID proxy records,  
426 particularly the ones related to primary production and erosion (Larsen et al., 2011). In fact, the volcanic fallout likely killed  
427 terrestrial plants by burning, root suffocation, and reduced photosynthesis (e.g., Ifkirne et al., 2022; Mack, 1981; De Schutter  
428 et al., 2015), and had likely similar effects on aquatic flora as well, also through increased turbidity and acidity of lake waters  
429 (e.g., Ayris and Delmelle, 2012). The subsequent reduced coverage of terrestrial plants likely exposed the soil to increased  
430 erosion, resulting in more terrestrial in-wash (as reflected by a sudden perylene peak), skewed toward the inorganic components  
431 of soil (as reflected by a sudden drop in TC and *n*-alkanes lasting roughly a century). The increased terrestrial in-wash would  
432 have further reduced primary productivity within the lake, as suggested by the drop in BSi. At the same time, the short C/N  
433 peak and the major drop in  $P_{aq}$  seem to indicate that the productivity and contribution of terrestrial plants remained higher than  
434 aquatic sources (Larsen et al., 2011). The post-3 ka trend is temporarily interrupted by what appears to be a partial rebound in  
435 primary productivity (BSi increases too) and diminished in-wash of terrestrial material until ca 1.5 ka BP, whereafter it  
436 continues to decline.

#### 437 **6.25.2 Is there geochemical evidence for human settlement in the SVID catchment area?**

438 In paleoclimate studies, relative shifts to above natural background levels of  $\beta$ -stanols have been used as a proxy for human  
439 settlement, marking the appearance of humans and domesticated animals in specific areas of the world (Shillito et al., 2020;  
440 Sistiaga et al., 2014), often in lake catchments (Battistel et al., 2016; Callegaro et al., 2018; Raposeiro et al., 2021; Sear et al.,  
441 2020; Vachula et al., 2019, 2020). This method has detected the arrival of Viking settlers in other Nordic regions, such as in  
442 the Lofoten islands in northern Norway (D'Anjou et al., 2012, Fig. 9B) and in the Faeroe Islands (Curtin et al., 2021, Fig. 9C).  
443 However, SVID sterol/stanol records show no evident human signals at or around the time of colonisation (i.e., 9<sup>th</sup> century CE,  
444 ca 1.1 ka BP). While a relative maximum of sterol/stanol concentrations found at ca 1.4 ka BP resembles the timing of an  
445 earlier-than-colonisation stanol signal found in the Faeroes (Curtin et al., 2021), as well as an analogous signal in the Lofoten  
446 Islands (D'Anjou et al., 2012), we cannot confidently interpret this peak as indication of human presence as its amplitude is  
447 comparable in magnitude to the inherent variability in the record (i.e., low signal to noise ratio).



448

449 **Figure 9: Holocene sub-Arctic records of faecal stanols in North Atlantic Islands.** (A) 5β-stigmastanol (dark red) and sum of  
 450 coprostanol and epi-coprostanol (dark blue) from core 20-SVID-02, NE Iceland (this study); (B) 5β-stigmastanol (pink) and  
 451 coprostanol (light blue) from cores LILA09-LILC09 from Lilandsvatnet lake, Lofoten Islands (D’Anjou et al., 2012); (C) 5β-  
 452 stigmastanol (orange) and coprostanol + epi-coprostanol (green) from core EI-D-01-15 from Eiðisvatn lake, Faroe Islands (Curtin  
 453 et al., 2021).

454 The lack of a clear anthropogenic faecal biomarker signal could be explained by either (1) a scarce/null incidence of human  
 455 activities in the catchment (unlikely, given the archaeological evidence in nearby areas; Gísladóttir et al., 2012; Lebrun et al.,  
 456 2023) and/or by (2) dilution of the signal due to the relatively large size of the lake paired to a small catchment. The sterol/stanol  
 457 records show a general increase throughout the Holocene (Fig. A2) in a pattern that matches the C/N, *n*-alkanes and perylene  
 458 trends, suggesting that the primary driver of SVID’s sterol signal is likely landscape instability and soil erosion rather than  
 459 human/ruminant presence. Furthermore, ratios of sterols to their derived 5β-5α stanols can trace redox conditions in various  
 460 environments (e.g. Andersson and Meyers, 2012; Canuel and Martens, 1993; Jaffé et al., 1996; Routh et al., 2014) and thus,  
 461 potentially, human presence in a lake catchment, as anthropogenic activities tend to mobilise more soil and increase in-wash  
 462 of organic material, fostering reducing conditions (Argiriadis et al., 2018). In SVID, the stanol values (5β-5α) are consistently  
 463 lower than their respective sterol precursors, suggesting a generally oxidising environment throughout the Holocene (Fig. 6).  
 464 The only exception to this trend is in the earliest part of the record (ca 10.8–10.6 ka BP; Fig. 5), indicative of a more reducing  
 465 environment, though not linked to an increased organic input (low TC values), but more likely to lake stratification with  
 466 deglacial water sinking at the bottom of the lake (Sugiyama et al., 2021).

468 Pyrogenic PAHs are considered a reliable proxy for fire frequency on a local scale, within and around a catchment (Denis et  
469 al., 2012). Although other factors can influence the PAH signal in sedimentary archives (e.g., accumulation rates, degradation;  
470 Stogiannidis et al., 2015), we interpret SVID pyroPAHs data as a record of NE Iceland fire history through the Holocene.

471 The trend in pyroPAHs does not match the erosional signal described by bulk geochemical proxies and *n*-alkanes, suggesting  
472 that soil erosion is not a mechanism for Holocene pyroPAHs variability. We exclude chemical degradation as a source of the  
473 signal, as PAHs are relatively stable molecules on long time scales (e.g., Johnsen et al., 2005). In fact, the ratio between low  
474 molecular weight (more prone to chemical degradation and leeching) and high molecular weight PAHs (as defined in Fig. A5)  
475 remains above 1 in most samples. Similarly, the pyrene/coronene ratio shows high and stable values throughout the record,  
476 indicating good preservation, with no significant degradation or preferential removal of less recalcitrant PAHs such as pyrene  
477 (Fig. A5 and refs therein).

478 The pyroPAH record presents two peaks at ca 2.8 and 1.5 ka BP, both predating acknowledged human settlement. PyroPAH  
479 values subsequently drop (VIII) and increase again in the last two centuries reaching maximum values in the present (Fig. 7A).

480 Analysing PAH data subdivided in molecular weight classes (see 3.1; Table A1; Fig. 7B) can help explain these two features  
481 as well as the general trend. HMW pyroPAHs show low and stable relative contributions ( $12\pm 7\%$  of total pyroPAHs) through  
482 the whole record and rise to 70% in the last 200 years. This trend, paired with increased pyroPAH concentrations, is consistent  
483 with the burning of coal/oil, the use of internal combustion engines, and increased human presence (Abas and Mohamad, 2011;  
484 Kozak et al., 2017). MMW pyroPAHs show relatively stable concentrations through most of the record (until ca 0.2 ka BP).  
485 Their relative abundance ( $\sim 68\pm 35\%$ ) slowly decreases through the Holocene, proportionally to the increase of LMW  
486 pyroPAHs ( $\sim 20\pm 16\%$ ). The latter, which are predominantly present in the gaseous phase (Karp et al., 2020), peak at 3–2.8 and  
487 1.5 ka BP, and substantially control the shape of the pyroPAH record (Fig. 7A-B). Together, the (1) low and stable values of  
488 HMW pyroPAHs, the (2) stable MMW values, and the (3) increasing/peaking values of LMW pyroPAHs are consistent with  
489 a general increase in the frequency of low temperature fires (e.g., peat fires or crawling fires) at a regional level. While the  
490 Hekla 3 event (3.01 ka BP, the largest rhyolitic eruption during the Holocene; Larsen, 1977; Larsen and Eiríksson, 2008)  
491 occurs just before the first pyroPAH peak, it is unlikely to be its unique or even main cause. However, in an environment such  
492 as Iceland, is legitimate to ask if the several and frequent eruptions might have influenced the PAHs' natural background and  
493 if this is detectable in our records. As discussed below, we are confident that volcanic eruptions have had no significant direct  
494 impact on the amount and distribution of PAHs in the SVID archive.

495 Volcanic activity does produce PAHs (both in the gaseous and in the particulate phases) but generally their long term  
496 contribution is considered negligible, particularly in the modern world where the main PAHs source is the burning of fossil  
497 fuels (Guiñez et al., 2020; Kozak et al., 2017).

498 Overall, due to the high temperatures involved, volcanic eruptions tend to produce medium-high molecular weight PAHs in  
499 gases and particulates (Guiñez et al., 2020; Ilyinskaya et al., 2017). Volcanic layers can contain pyrogenic (unsubstituted but  
500 also alkylated) PAHs with a molecular weight distribution resembling modern fossil fuel combustion, dominated by  
501 unsubstituted forms (Murchison and Raymond, 1989) as well as traces of nitro- and oxy-PAHs (Guiñez et al., 2020). We do  
502 not see this distribution in any of our samples, not even when they include parts of tephra layers. This suggests that (1) either  
503 our sampling method does not capture volcanic layers (maybe due to its resolution) or that (2) there is no such signal in the  
504 SVID archive.

505 Regarding the first hypothesis (sampling method not capturing volcanic PAHs), Kozak et al. (2017) analysed the impact of  
506 2010 and 2011 Icelandic eruptions in Svalbard (Arctic Norway), finding high abundances of 4-5 ring PAHs in volcanic mud,  
507 great variations in the contribution of different eruptions to the total PAHs detected in sampled surface water, significant  
508 increases in the total abundance of PAHs during eruption years, but also that this increase in PAHs abundance as well as shifts  
509 in PAHs distribution do not seem to last beyond the eruption years. Considering the temporal resolution of our record (max

10-50 years), it is unlikely that any eruption would have impacted it significantly: from a geological point of view, eruptions tend to be short-living, and unless they relate to a massive event sustained over a long period of time, they are unlikely to have a strong impact on a sample that represents 10-50 years of sedimentation. No discernible correlation arose between the PAHs curve and the detected tephra, the only exceptions being the Hekla 3 and, to a lesser extent, the Hekla 4 tephra layers. However, these major volcanic events, besides marking the beginning of major shifts in most proxies, correlate to the initial phase of major shifts in low (and not high nor medium) molecular weight PAHs. This suggests that, if a connection between these two eruptions and PAH shifts exists, it must be indirect and, more likely, the two events acted as a general destabilising factor in an environment already subjected to increasing cooling and erosion.

The only possible example of an increased PAH concentration due to volcanic sources could come from the sample obtained from the lower limit of the G10ka series tephra (Fig. 7), which has a different composition (mostly inorganic) compared to the rest of the organic-rich samples in our record. In fact, HMW PAHs seem to spike here, even if they still exhibit an overall lower concentration than LMW PAHs; this could be due to its massive nature (Óladóttir et al., 2020).

Regarding the second hypothesis (missing signal of volcanic PAHs), it is possible that no detectable volcanic PAHs were present in the SVID archive due to (1) its geographical location, relatively far from volcanic sources and formations (Hjartarson and Sæmundsson, 2014), and (2) the same nature of Icelandic volcanic eruptions, which are characterised by relatively low-viscosity basaltic lava rather than highly explosive pyroclastic flows (Thordarson and Höskuldsson, 2008), thus reducing the chance of ash production and deposition, particularly in distal locations such as SVID.

The effects of tephra fallout on vegetation and related PAH deposition, seem to be quite short lived, with fires events likely coeval to the eruption and vegetation recovering within a few decades (Eddudóttir et al., 2017; Pickarski et al., 2023). The deposition of volcanic sourced PAHs also tends to be temporally confined to the eruption year and consist mainly of MMW PAHs (Kozak et al., 2017), while SVID pyroPAH peaks are clearly led by increases in LMW PAHs on a longer timescale.

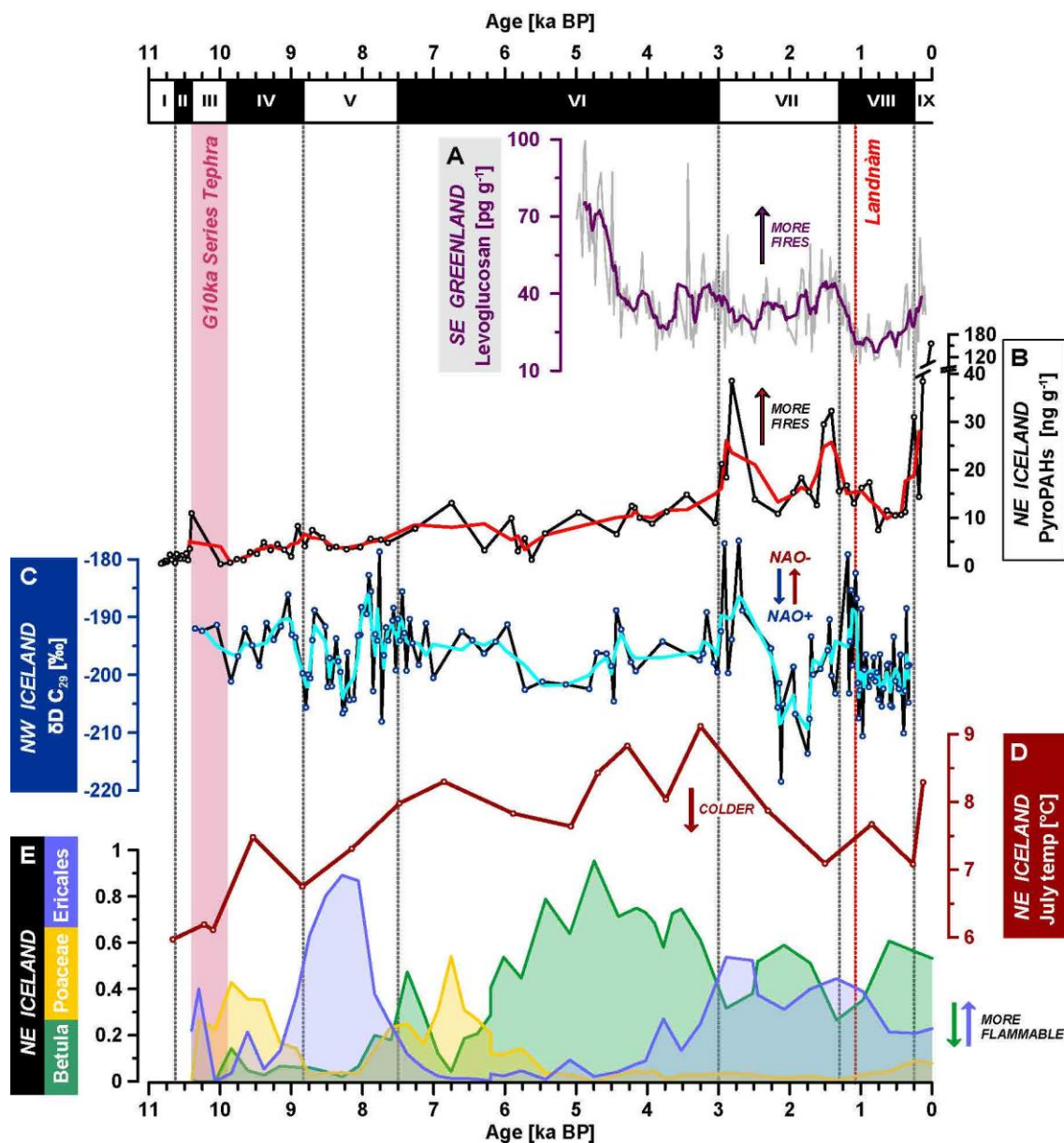
Notably, this shift in fire regime at ca 3 ka BP in Iceland falls within a wider pattern of increasing fire frequency emerging from the analysis of several Holocene fire records throughout Europe (Marlon et al., 2013). This is linked to either an increase of cultivated land (fire was used to clear land for agriculture) and/or, particularly in Europe, to increasing aridity (Marlon et al., 2013). We hypothesize that the latter is the most probable explanation for the shifts in NE Icelandic fire regimes as discussed in Section 5.4.

#### **6.45.4 Regional drivers of precipitation and their role on fire frequency**

Fuel moisture content and, more generally, environmental moisture, are the main variables controlling flammability in vegetational communities typical of temperate/sub-arctic regions (Marino et al., 2010; Plucinski et al., 2010; Santana and Marrs, 2014). The North Atlantic Oscillation (NAO; Hurrell et al., 2003) modulates the intensity of the westerly storm track and thus the amount and source of precipitation in Iceland. Its positive mode (NAO+) brings intervals of higher precipitation resulting in a wetter (and often warmer) climate than NAO- intervals, which are characterised by weaker westerlies, stronger northerly winds, and drier (and often colder) conditions (Hurrell, 1995; Trouet et al., 2009). Major changes in precipitation regimes usually lead to changes in the hydrogen stable isotopic value of environmental water ( $\delta D$ ; Dansgaard, 1964) which translate into shifts in the  $\delta D$  of plant waxes (e.g., *n*-alkanes; Sachse et al., 2012). This relationship has been calibrated in various environments, including the Arctic (e.g., Berke et al., 2019; Bush et al., 2017; McFarlin et al., 2019; Thomas et al., 2016) and applied for paleo-precipitation reconstructions (e.g., Ardenghi et al., 2019; Niedermeyer et al., 2016; Tierney et al., 2017; Wilkie et al., 2013). A  $C_{29}$  *n*-alkane  $\delta D$  record from a fjord core in NW Iceland (Fig. 10C; Moossen et al., 2015) describes a relatively stable NAO+ configuration (wetter - more D-depleted) throughout the Holocene, and two major shifts toward NAO- (drier - less D-depleted) conditions at ca 3–2.5 and 1.5–1.0 ka BP, matching the timing of first SVID pyroPAH peak and at least partially overlapping to the second one. A similar correlation of fire frequency shifts to NAO- configurations has recently been suggested for other Arctic sites, particularly in Svalbard (Chen et al., 2023).

552 Biomass typology (i.e., the kind of vegetation on site) also influences fuel flammability (Chandler et al., 1983; Fernandes and  
553 Cruz, 2012; Santana et al., 2011; Scarff and Westoby, 2006). In Iceland, many plant taxa appeared shortly after deglaciation  
554 (e.g., Alsos et al., 2021; Harning et al., 2023). Increasing summer temperatures led to the expansion of thermophilic woody  
555 plant taxa (e.g., birch) during/after the Holocene Thermal Maximum (e.g., Eddudóttir et al., 2016; Geirsdóttir et al., 2022;  
556 Karlsdóttir et al., 2014). Since ~6 ka BP, the birch woodland in the NE region has evolved into more open heathland and  
557 peatland, until the birch population decreased around 3 ka BP (Roy et al., 2018), along with a general temperature decrease  
558 (Axford et al., 2007). In this context, at Ytra-Áland (Fig. 1B), two major drops in *Betula* pollen coeval to two increases in  
559 Ericales (heather's order) pollen closely follow the NAO- shifts at 3 and 1.5 ka BP (Fig. 10E; Karlsdóttir et al., 2014).  
560 Heathlands, especially in low moisture conditions, are associated with higher flammability, particularly high sustainability  
561 (i.e., how well the combustion proceeds). Thus, heathlands are prone to longer, more stable fires, and with an increased  
562 potential for igniting higher canopy elements and underlying peat layers (Plucinski et al., 2010; Rein et al., 2008; Santana and  
563 Marrs, 2014). More frequent, more stable, slow crawling fires involving dense bushes and peat would increase the amount of  
564 pyroPAHs produced and deposited in the region while skewing their distribution toward LMW components (George et al.,  
565 2016; Iinuma et al., 2007; Siao et al., 2007), as observed in the SVID pyroPAH signal (Fig. 7). Lastly, the observed shifts in  
566 pyroPAHs are unlikely to be the result of a change in their source area. Our back-trajectory analysis reveals that more air  
567 parcels originate over Iceland or in the surrounding North Atlantic (Fig. 8). The analysis further reveals that trajectories with  
568 terrestrial origins are more likely in NAO+ than NAO- regimes. As such terrestrial trajectories would be the ones responsible  
569 for bringing combustion products to SVID, we might therefore expect a stronger pyroPAH signal during NAO+ intervals.  
570 However, our results display the opposite trend, with the initial increase in pyroPAH abundances at ~3 ka occurring during an  
571 NAO- mode and their subsequent drop occurring during a strong NAO+ interval. Thus, the late Holocene increase in pyroPAHs  
572 in SVID is likely to record a substantial increase in local fires (driven by vegetation change and NAO-modulated aridity) rather  
573 than a shift in the compounds' sources.

574 Overall, SVID pyroPAH signal describes a major shift from a relatively stable (i.e., low fire frequency) early and mid-Holocene  
575 environment to a dryer late-Holocene environment at ca 3 ka BP, naturally more prone to long term persistence of low  
576 temperature wildfires. This is likely the result of the combination of (1) recorded cooling and related shifts in vegetational  
577 communities, (2) NAO- shifts and associated dryer conditions.



578

579 **Figure 10: Regional comparison of climatic, fire, and vegetation records.** (A, purple) levoglucosan concentrations from the RECAP  
 580 ice core, south-eastern Greenland (Segato et al., 2021); (B, black) sum of pyrogenic PAHs concentrations – red line indicates a 3  
 581 points running average; (C, blue) stable isotopic composition of hydrogen of sedimentary *n*-alkanes from marine core MD99-2266  
 582 off the coast of NW Iceland (Moossen et al., 2015) – cyan line indicates a 3 points running average; (D, red) chironomid derived  
 583 temperatures from core 04-SVID-03 (Axford et al., 2007); (E) pollen percentages of *Betula* (green), *Poaceae* (yellow), and *Ericales*  
 584 (blue) in a peat section from the Ytra-Åland site, NE Iceland (Karlisdóttir et al., 2014).

585 **6.55.5 Evidence for a human influence on fire frequency?**

586 Unlike other proxies, pyroPAHs return to background levels after reaching high values at 1.5 ka BP, and then remain low  
 587 through the Medieval Warm Period (ca 900–1200 CE) and most of the Little Ice Age (1300–1900 CE), before peaking again  
 588 in the last 150–200 years. A similar drop in fire markers (anhydrosugars) is also observed in eastern Greenland (Segato et al.,  
 589 2021; Fig. 10A). Low pyroPAHs levels during an interval of known human presence in Iceland suggests that human activities  
 590 might have curbed regional fire frequency, thus modulating the natural signal, which would have otherwise remained relatively  
 591 high due to the persistence of colder conditions and more flammable plant communities (regardless of NAO shifts). In fact,  
 592 while increased pressure from grazing lowered environmental resilience to soil erosion (e.g., Bates et al., 2021; Eddudóttir et  
 593 al., 2016; McGovern et al., 2007), it likely also decreased fuel flammability (which is dependent on the amount of dead  
 594 biomass; Davies and Legg, 2011; Santana and Marrs, 2014) in the predominant heathland environment (Lake et al., 2001).  
 595 Additionally, the creation of farmland and pastureland at the expenses of areas with woody vegetation and heathland likely  
 596 reduced the extent of the biomes naturally prone to fires. This reduction of local wood availability is reflected in changes of



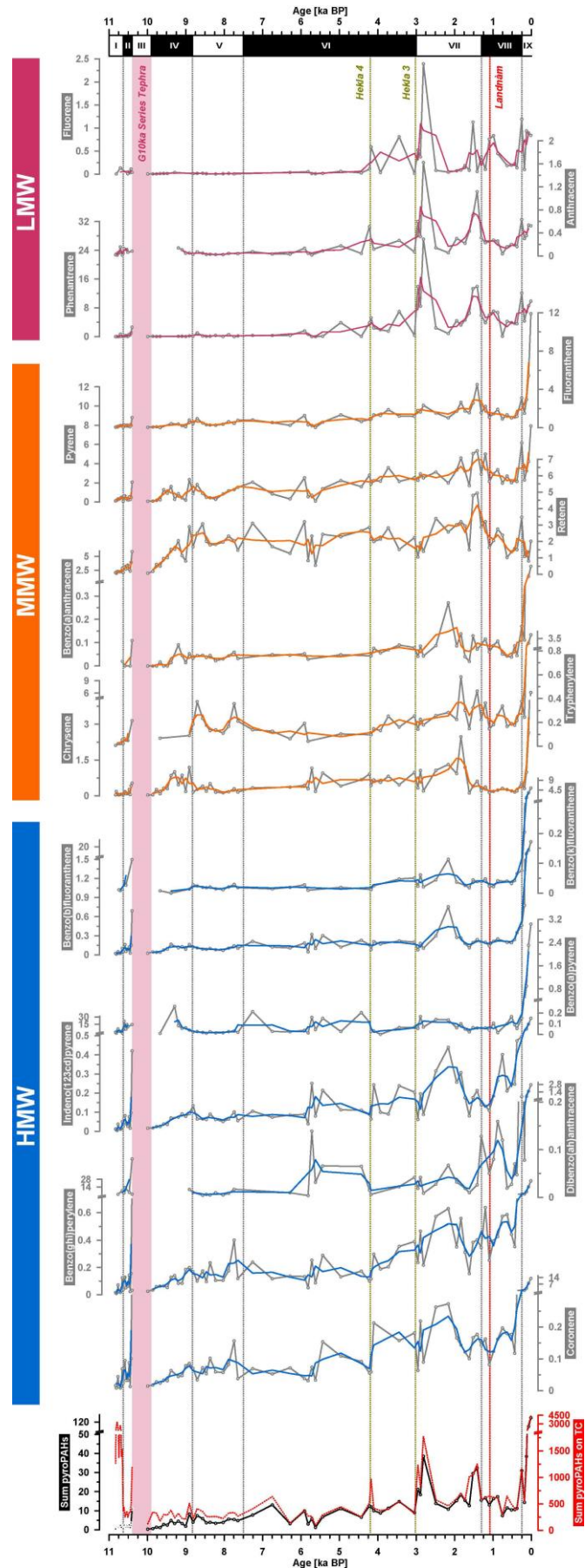
597 foraging habits, as settlers shifted to relying more heavily on more abundant fuel sources such as peat and turf, as well as other  
598 marine derived substances (e.g., seal oil, seaweed; Bold, 2012), while driftwood and imported wood (from Europe or North  
599 America, often with ad hoc expeditions) satisfied most of the need for timber (e.g., Bold, 2012; Edvardsson, 2010; Mooney,  
600 2016; Pinta, 2021; Sveinbjarnardóttir et al., 2007). A general mechanism for fire suppression due to the expansion of cultivated  
601 land has already been proposed for global data (Marlon et al., 2013), but assumed to be likely asynchronous in different regions  
602 and strongly influenced by local climatic, environmental, and social conditions.

603 We speculate that the drop in fire markers in Iceland from the reduction in wildfire risk due to husbandry and farming exceeded  
604 the production of fire markers due to human necessities (e.g., warming), resulting in an overall suppressed fire signal. This  
605 would also be consistent with the low population density, which started to increase only in the 1800s CE (Iceland Statistical  
606 Service, 2023; Jónsson and Magnússon, 1997), matching the coldest interval of the Little Ice Age and the sharp rise in HMW  
607 pyroPAHs. From this perspective, the pressure of human activities would have fostered erosion through decreased  
608 environmental resilience while, at the same time, suppressing natural fire frequency.

## 609 **7.6 Conclusions**

610 Our multiproxy analysis of Holocene sediments from Stóra Viðarvatn provides new insight into the coupled vegetation, fire,  
611 erosion, and climate regimes of NE Iceland:

- 612 • Bulk geochemistry proxies show that the general climatic evolution of NE Iceland is primarily driven by summer  
613 insolation: an initial deglacial warming followed by a relatively warm and stable climate until ca 4–3 ka BP, after which  
614 declining summer temperatures result in accelerating catchment erosion.
- 615 • Faecal biomarkers, traditionally linked to human activities, do not show an elevated signal at or around colonisation (9<sup>th</sup>  
616 century CE). Instead, faecal biomarkers roughly trace the erosional signal described by bulk geochemical proxies. This  
617 may result from a combination of (1) low local anthropogenic pressure (although sparse settlements existed a few km  
618 from the study area), and (2) signal dilution, due to the large lake size and its relatively small watershed. Therefore, we  
619 urge caution when interpreting faecal biomarkers as unequivocal proxies of human presence, particularly when highly  
620 sensitive analytical tools like the one used in this study are involved.
- 621 • PyroPAHs carry a regional (mostly confined to northern and north-eastern Iceland) and predominantly natural signal  
622 (i.e., controlled by parameters such as precipitation and moisture availability, vegetation typology and flammability).  
623 After generally low fire frequency throughout most of the Holocene, we observe major regime changes at 3 ka and 1.5  
624 ka BP, before known human colonisation in Iceland. During this interval, the distribution of pyroPAHs point toward a  
625 regional increase in low temperature fire frequency. This can be linked to a change in vegetation typology driven by the  
626 cooling of the last 4 to 3 kyr, coupled to major shifts in atmospheric circulation (i.e., NAO regimes) that led to increased  
627 aridity and thus flammability. Finally, low levels of pyroPAHs characterise the time following known human  
628 colonisation, before rising again (but with a molecular composition more distinctive of fossil fuels) in the last ~200 years.  
629 This suggests that human activities, particularly husbandry and farming, may have suppressed fire frequency by reducing  
630 the range and flammability of environments more prone to fire, effectively modulating the natural signal while decreasing  
631 the resilience of the local environment to soil erosion.



633

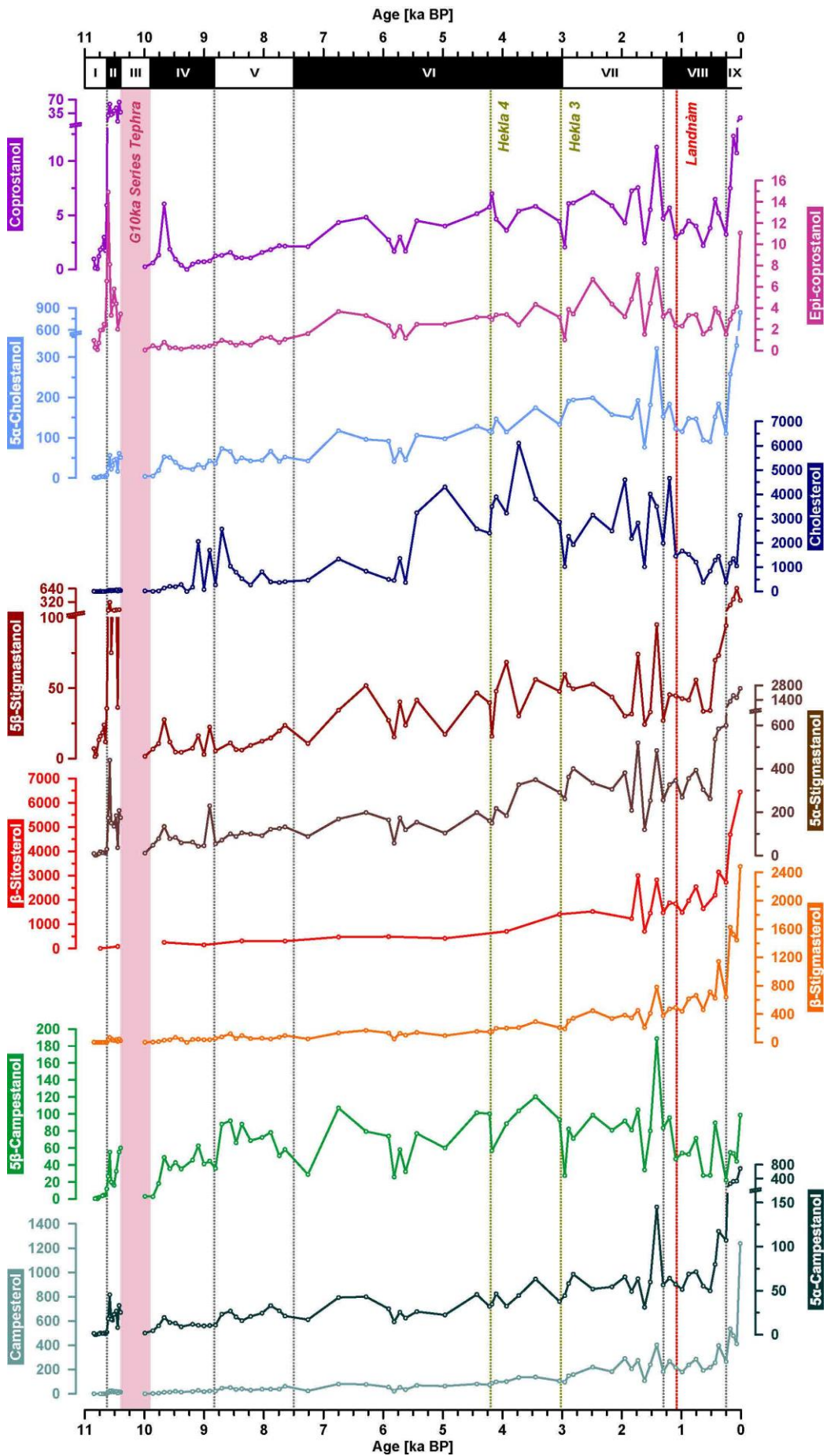
634

635

636

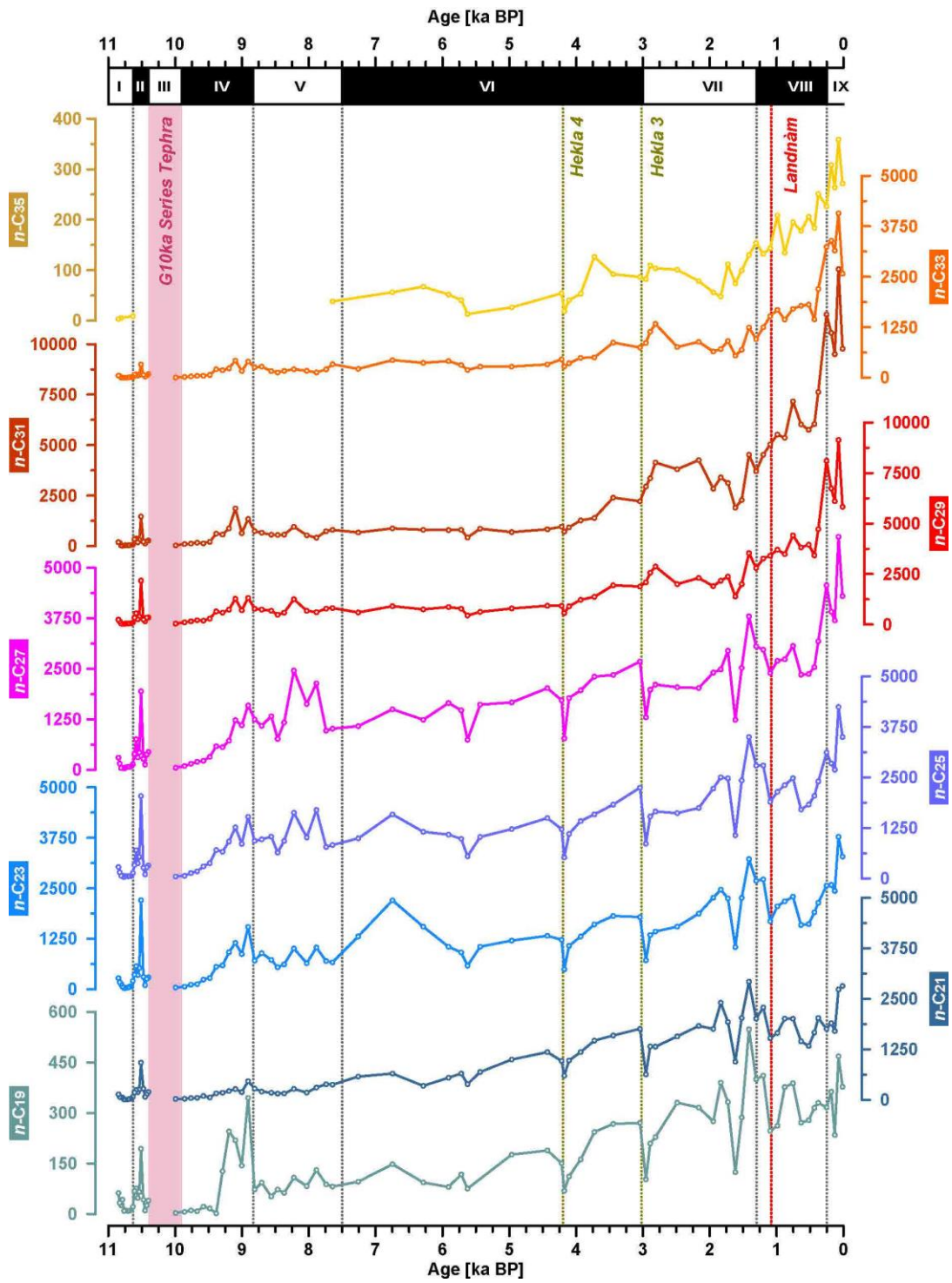
637

Figure A1: Concentration curves of all 20-SVID-02 pyrogenic PAHs recovered in this study. All concentrations are expressed as ng per g of dry sample, except for the last curve (red-dotted) which is in ng per g of TC. Note that several vertical axes have been adjusted to minimise the rise in the last 2–3 centuries. Compounds are listed in chromatographic order and grouped by molecular weight through colour shading (LMW in red-purple-magenta; MMW in yellow-orange; HMW in blue).



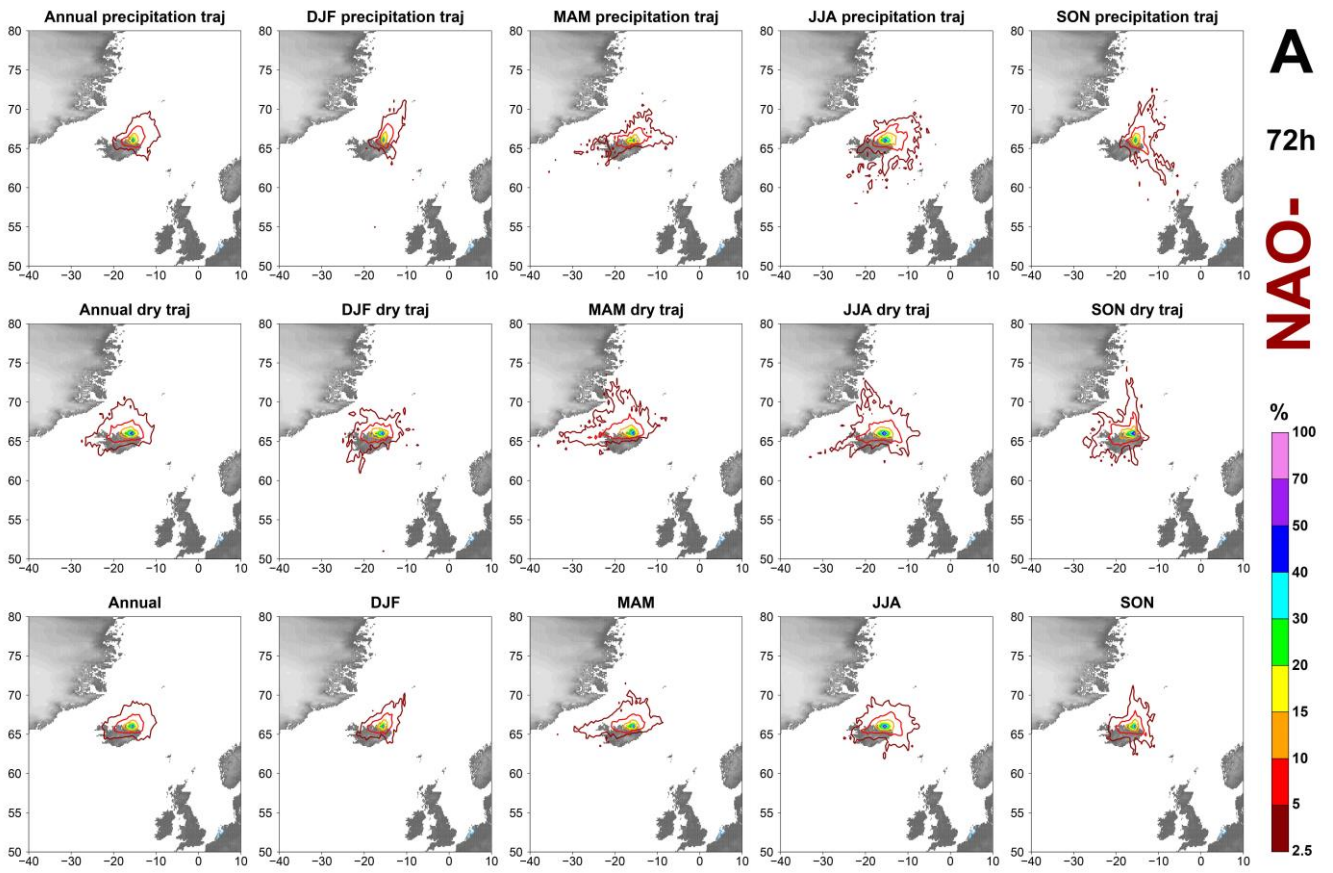
638

639 **Figure A2:** Concentration curves of all 20-SVID-02 faecal sterol/stanols of interest recovered in this study. All concentrations are  
 640 expressed as ng per g of dry sample. Note that several vertical axes have been adjusted to minimise the rise in the last 2–3 centuries.  
 641 Compounds are grouped and colour shaded by structure (cholesterol and stanol derivatives in blue purple; sito-stigma-  
 642 sterols and stanols in red orange; campesterol and campestanol in green).

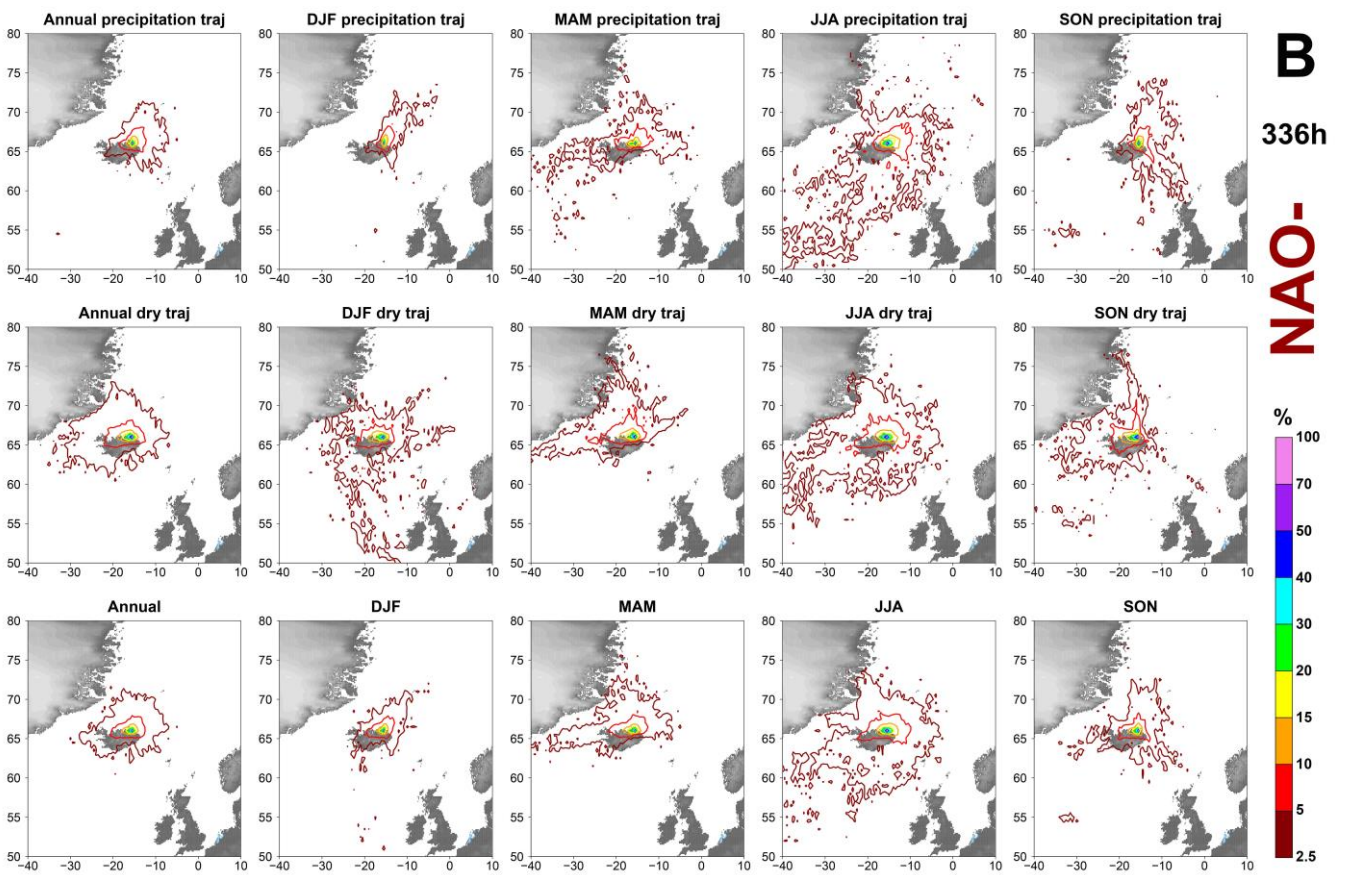


643

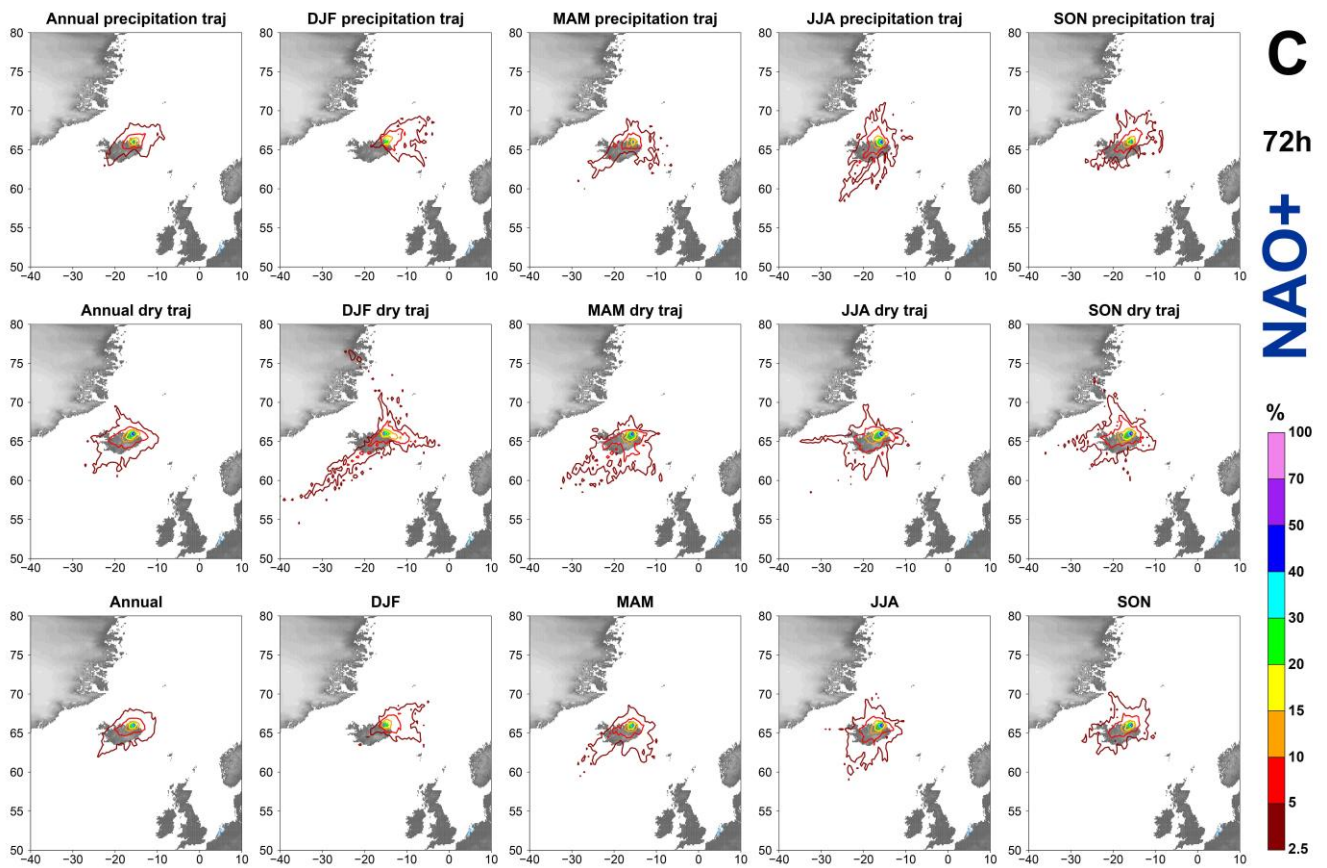
644 Figure A3: Concentration curves of all 20-SVID odd-numbered *n*-alkane homologues from *n*-C<sub>19</sub> to *n*-C<sub>35</sub> recovered in this study.  
 645 All concentrations are expressed as ng per g of dry sample.



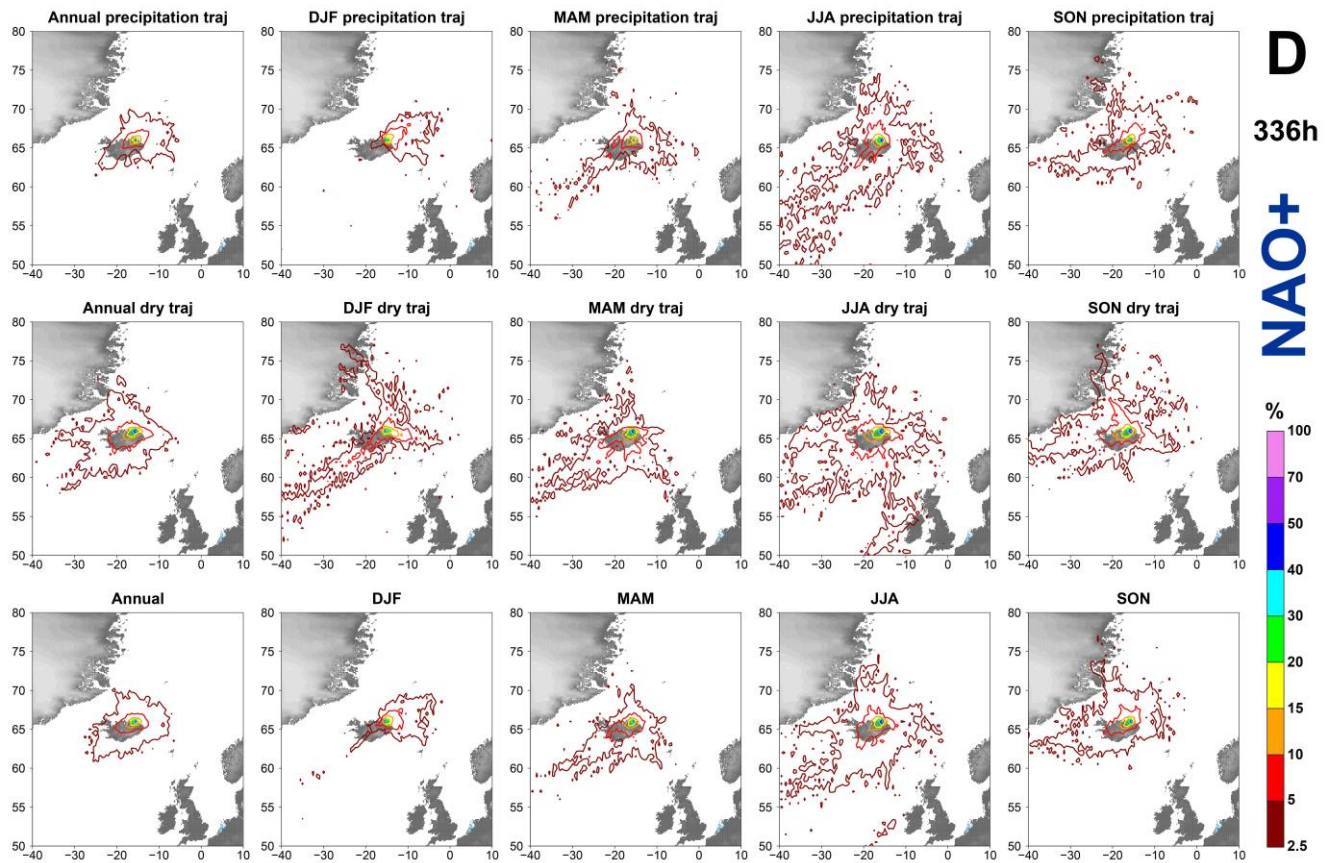
646



647

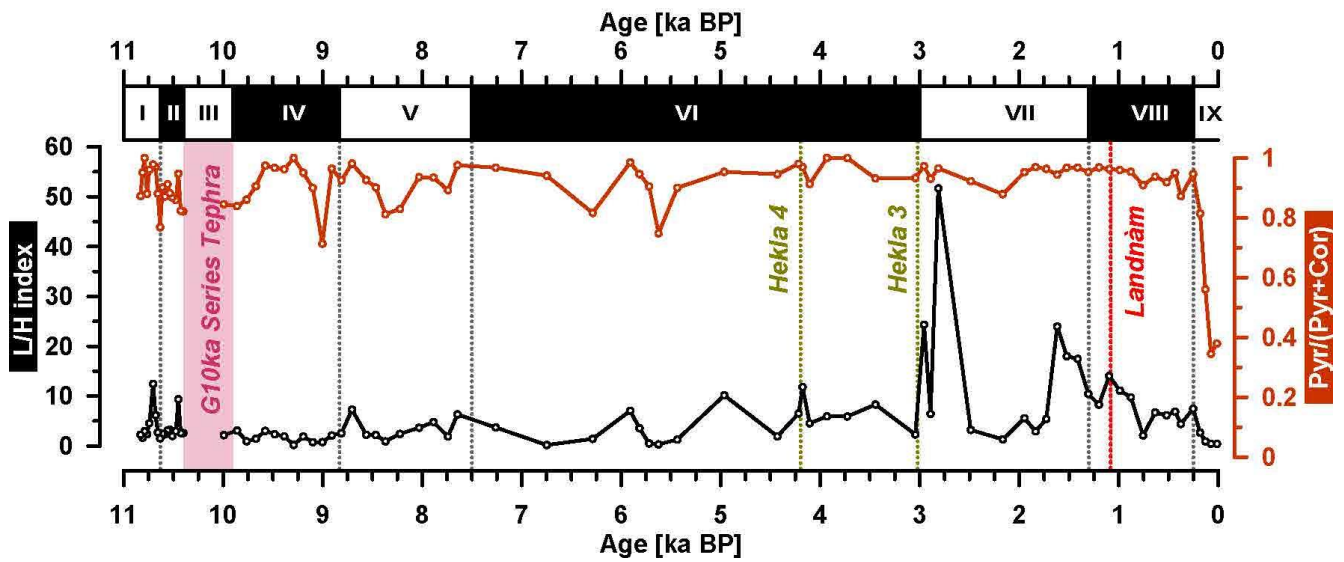


648



649

650 **Figure A4:** HYSPLIT back trajectories of air parcels for December 2009 to November 2010 (NAO-) and May 2013 to April 2014  
 651 (NAO+, except for October 2014). Trajectories are calculated on a three days (72 h, A-C) and a two weeks (336 h, B-D)  
 652 intervals at a 6 hours frequency; “precipitation” (top) indicates trajectories that produced precipitation within 6 h from the SVID  
 653 endpoint, “dry” (middle) vice versa; bottom plots are the sum of “precipitation” and “dry” trajectories. Contour colours  
 654 indicate the frequency at which air parcels part of a trajectory travel above a certain area.



655

656

Figure A5: PAH indices used as an indication of PAH preservation.

657

The L/H index (black) is a ratio between low and high molecular weight unsubstituted PAHs, defined as  $L/H = (\text{Phenanthrene} + \text{Anthracene} + \text{Fluoranthene} + \text{Pyrene}) / (\text{Benzo[a]anthracene} + \text{Chrysene} + \text{Benzo[k]fluoranthene} + \text{Benzo[a]pyrene} + \text{Indeno[1,2,3,c,d]pyrene} + \text{Dibenzo[a,h]anthracene} + \text{Benzo[g,h,i]perylene})$  (Magi et al., 2002; Stogiannidis et al., 2015 and refs. therein).

660

661

The Pyrene-Coronene index (orange) defined as  $\text{pyrene} / (\text{pyrene} + \text{coronene})$  is based on the assumption of an higher preservation potential of the HMW coronene over the lighter, more soluble pyrene (Denis, 2016; Denis et al., 2017; May et al., 1978); higher, more stable values point toward good preservation for both HMW and LMW PAHs.

663

664  
665  
666

**Table A1: Polycyclic aromatic hydrocarbons (PAHs) analysed in this study. Pyrogenic PAHs are grouped into low, medium, and high molecular weight. Elution order and SRM transitions are reported for each compound.**

Elution order	Group	Compound name	Mass	Product mass a/b	Collision energy
1		Naphthalene*	128	128/102	8
2		Acenaphthylene*	152	152	8
3	LMW	Acenaphthene*	154	153/154	8
4		Fluorene	166	166	8
5		Phenanthrene	178	178	8
6		Anthracene	178	178	8
7		Fluoranthene	202	202	8
8		Pyrene	202	202	8
11	MMW	Retene	234	234/219	8
12		Benzo[a]anthracene	228	228	8
13		Triphenylene	228	228	8
14		Chrysene	228	228	8
15	HMW	Benzo[k]fluoranthene	252	252	8
16		Benzo[j]fluoranthene	252	252	8
17		Benzo[a]pyrene	252	252	8
19		Indeno[1,2,3-C,D]pyrene	276	276	8
20		Dibenzo[a,h]anthracene	278	278	8
21		Benzo[g,h,i]perylene	276	276	8
22		Coronene	300	300	8
18		Perylene**	252	252	8
9		p-Terphenyl D14 (IS)	244	244	8
10		p-Terphenyl (IS)	230	230	8

\* Compound(s) difficult to quantify correctly and thus excluded from final sums.

\*\* Non-pyrogenic PAH.

667



**Table A2: Faecal sterols and stanols analysed in this study. Elution order and SRM transitions are reported for each compound.**

Elution order	Name	Detailed name	CAS #	Quantitative qualitative	Mass	Product Mass	Collision Energy
1	Pregnanol (IS)	5 $\beta$ -pregnan-3 $\alpha$ -ol	4352-07-2	Q q	361 361	215 191	10 10
2	5 $\alpha$ -Cholestane (IS)	5 $\alpha$ -cholestane	481-21-0		372	217	10
3	Coprostanol	5 $\beta$ -cholestan-3 $\beta$ -ol	360-68-9	Q q	370 460	215 215	10 10
4	Epi-Coprostanol	5 $\beta$ -cholestan-3 $\alpha$ -ol	516-92-7	Q q	370 460	215 215	10 10
5	Cholesterol	5-en-cholest-3 $\beta$ -ol	57-88-5	Q q	368 458	145 129	20 50
6	Cholestanol	5 $\alpha$ -cholestan-3 $\beta$ -ol	80-97-7	Q q	370 460	215 215	10 10
7	5 $\beta$ -Campestanol	24R-methyl-5 $\beta$ -cholestan-3 $\beta$ -ol	33947-18-1	Q q	384 474	215 215	10 10
8	5 $\beta$ -Stigma(sito)stanol	24R-ethyl-5 $\beta$ -cholestan-3 $\beta$ -ol	4736-91-8	Q q	383 488	147 215	20 10
9	Campesterol	24R-methyl-5-en-cholest-3 $\beta$ -ol	474-62-4	Q q	382 472	255 129	5 50
10	5 $\alpha$ -Campestanol	24R-methyl-5 $\alpha$ -cholestan-3 $\beta$ -ol	474-60-2	Q q	384 474	215 215	10 10
11	$\beta$ -Stigmasterol	24S-ethyl-5,22E-dien-cholest-3 $\beta$ -ol	83-48-7	Q q	394 484	255 211	5 20
12	$\beta$ -Sitosterol	24R-ethyl-5-en-cholest-3 $\beta$ -ol	83-46-5	Q q	396 484	255 394	10 10
13	5 $\alpha$ -Stigma(sito)stanol	24R-ethyl-5 $\alpha$ -cholestan-3 $\beta$ -ol	83-45-4	Q q	383 488	147 215	20 10

671 **98 Data availability**

672 All raw data will be available on the NOAA National Centers for Environmental Information  
673 (<https://www.ncei.noaa.gov/access/paleo-search/study/38503>).

674 The data will also be made available upon request.

675 **109 Author contributions**

676 GHM, ÁG and JS conceptualized research and obtained financial support for the NSF project ILLUME (Iceland landscape  
677 reconstruction using molecular proxies); GHM, ÁG, JHR, DJH, and NA participated in the field campaign to retrieve the  
678 sediment core; JS and GHM provided laboratory and analytical infrastructure; NA, DJH, and BRH processed all sediment  
679 samples; NA performed method development and sample analysis. TT and DJH performed the tephra analysis and developed  
680 the age model; NA performed the HYSPLIT analysis; NA wrote the manuscript draft, except for the age model paragraph  
681 (DJH); GHM, ÁG, JS, DJH, and JHR reviewed and edited the manuscript.

682 **110 Competing interests**

683 The authors declare that they have no conflict of interest.

684 **121 Acknowledgements**

685 We kindly thank Sveinbjörn Steinþórsson and Þór Blöndahl for lake coring assistance at Stóra Viðarvatn. We thank Dr. Jamie  
686 McFarlin (INSTAAR and University of Wyoming), Dr. Nadia Dildar (INSTAAR), Dr. Sebastian Kopf (INSTAAR), and  
687 Katelyn Eaman for their invaluable analytical support in the lab; Dr. Thomas Marchitto (INSTAAR) for providing access to  
688 the clean room used for sampling; Jeremy Caves Rugenstein (Colorado State University) for sharing his expertise on  
689 HYSPLIT; and Karl Painter and Isaiah Castro for helping with biogenic silica analyses.

690 **1312 Financial support**

691 This work was supported by the National Science Foundation grant ARC1836981 to GHM, ÁG, JS, and TT, and by a  
692 University of Iceland grant to ÁG.

- 694 Abas, M. R. B. and Mohamad, S.: Hazardous (Organic) Air Pollutants, *Encycl. Environ. Heal.*, 23–33,  
695 <https://doi.org/10.1016/B978-0-444-52272-6.00070-2>, 2011.
- 696 Aizenshtat, Z.: Perylene and its geochemical significance, *Geochim. Cosmoc. Acta*, 37, 559–567,  
697 [https://doi.org/10.1016/0016-7037\(73\)90218-4](https://doi.org/10.1016/0016-7037(73)90218-4), 1973.
- 698 Alkalaj, J., Hrafnisdottir, T., Ingimarsson, F., Smith, R. J., Kreiling, A. K., and Mischke, S.: Distribution of Recent non-marine  
699 ostracods in Icelandic lakes, springs, and cave pools, *J. Crustac. Biol.*, 39, 202–212, <https://doi.org/10.1093/jcbiol/ruz008>,  
700 2019.
- 701 Alsos, I. G., Lammers, Y., Kjellman, S. E., Merkel, M. K. F., Bender, E. M., Rouillard, A., Erlendsson, E., Guðmundsdóttir,  
702 E. R., Benediktsson, Í. Ö., Farnsworth, W. R., Brynjólfsson, S., Gísladóttir, G., Eddudóttir, S. D., and Schomacker, A.: Ancient  
703 sedimentary DNA shows rapid post-glacial colonisation of Iceland followed by relatively stable vegetation until the Norse  
704 settlement (Landnám) AD 870, *Quat. Sci. Rev.*, 259, <https://doi.org/10.1016/j.quascirev.2021.106903>, 2021.
- 705 Andersson, R. A. and Meyers, P. A.: Effect of climate change on delivery and degradation of lipid biomarkers in a Holocene  
706 peat sequence in the Eastern European Russian Arctic, *Org. Geochem.*, 53, 63–72,  
707 <https://doi.org/10.1016/j.orggeochem.2012.05.002>, 2012.
- 708 Ardenghi, N., Mulch, A., Koutsodendris, A., Pross, J., Kahmen, A., and Niedermeyer, E. M.: Temperature and moisture  
709 variability in the eastern Mediterranean region during Marine Isotope Stages 11–10 based on biomarker analysis of the Tenaghi  
710 Philippon peat deposit, *Quat. Sci. Rev.*, 225, 105977, <https://doi.org/10.1016/j.quascirev.2019.105977>, 2019.
- 711 Arellano, L., Fernández, P., Van Drooge, B. L., Rose, N. L., Nickus, U., Thies, H., Stuchlík, E., Camarero, L., Catalan, J., and  
712 Grimalt, J. O.: Drivers of atmospheric deposition of polycyclic aromatic hydrocarbons at European high-altitude sites, *Atmos.*  
713 *Chem. Phys.*, 18, 16081–16097, <https://doi.org/10.5194/acp-18-16081-2018>, 2018.
- 714 Argiriadis, E., Battistel, D., McWethy, D. B., Vecchiato, M., Kirchgorg, T., Kehrwald, N. M., Whitlock, C., Wilmshurst, J.  
715 M., and Barbante, C.: Lake sediment fecal and biomass burning biomarkers provide direct evidence for prehistoric human-lit  
716 fires in New Zealand, *Sci. Rep.*, 8, <https://doi.org/10.1038/s41598-018-30606-3>, 2018.
- 717 Axford, Y., Miller, G. H., Geirsdóttir, Á., and Langdon, P. G.: Holocene temperature history of northern Iceland inferred from  
718 subfossil midges, *Quat. Sci. Rev.*, 26, 3344–3358, <https://doi.org/10.1016/j.quascirev.2007.09.003>, 2007.
- 719 Ayris, P. M. and Delmelle, P.: The immediate environmental effects of tephra emission, *Bull. Volcanol.*, 74, 1905–1936,  
720 <https://doi.org/10.1007/s00445-012-0654-5>, 2012.
- 721 Bates, R., Erlendsson, E., Eddudóttir, S. D., Möckel, S. C., Tinganelli, L., and Gísladóttir, G.: Landnám , Land Use and  
722 Landscape Change at Kagaðarhóll in Northwest Iceland , *Environ. Archaeol.*, 0, 1–17,  
723 <https://doi.org/10.1080/14614103.2021.1949680>, 2021.
- 724 Battistel, D., Argiriadis, E., Kehrwald, N., Spigariol, M., Russell, J. M., and Barbante, C.: Fire and human record at Lake  
725 Victoria, East Africa, during the Early Iron Age: Did humans or climate cause massive ecosystem changes?, *Holocene*, 27,  
726 997–1007, <https://doi.org/10.1177/0959683616678466>, 2016.
- 727 Berger, A. and Loutre, M.-F.: Parameters of the Earths orbit for the last 5 Million years in 1 kyr resolution,  
728 <https://doi.org/10.1594/PANGAEA.56040>, 1999.
- 729 Berke, M. A., Sierra, A. C., Bush, R. T., Cheah, D., and O’Connor, K.: Controls on leaf wax fractionation and  $\delta^2\text{H}$  values in  
730 tundra vascular plants from western Greenland, *Geochim. Cosmoc. Acta*, 244, 565–583,  
731 <https://doi.org/10.1016/j.gca.2018.10.020>, 2019.
- 732 Bershaw, J., Penny, S. M., and Garzzone, C. N.: Stable isotopes of modern water across the Himalaya and eastern Tibetan  
733 Plateau: Implications for estimates of paleoelevation and paleoclimate, *J. Geophys. Res. Atmos.*, 117, 1–18,  
734 <https://doi.org/10.1029/2011JD016132>, 2012.
- 735 Birk, J. J., Dippold, M., Wiesenberg, G. L. B., and Glaser, B.: Combined quantification of faecal sterols, stanols, stanones and

736 bile acids in soils and terrestrial sediments by gas chromatography-mass spectrometry, *J. Chromatogr. A*, 1242, 1–10,  
737 <https://doi.org/10.1016/j.chroma.2012.04.027>, 2012.

738 Blaauw, M. and Christeny, J. A.: Flexible paleoclimate age-depth models using an autoregressive gamma process, *Bayesian*  
739 *Anal.*, 6, 457–474, <https://doi.org/10.1214/11-BA618>, 2011.

740 Bold, R.: Norse Utilisation of Archaeobotanical Resources within the Myvatnssveit locale, Northern Iceland, PhD thesis,  
741 Durham University, <http://etheses.dur.ac.uk/3440/>, 2012.

742 Bray, E. E. and Evans, E. D.: Distribution of *n*-paraffins as a clue to recognition of source beds, *Geochim. Cosmochim. Acta*, 22,  
743 2–15, [https://doi.org/10.1016/0016-7037\(61\)90069-2](https://doi.org/10.1016/0016-7037(61)90069-2), 1961.

744 Bronk Ramsey, C., Albert, P. G., Blockley, S. P. E., Hardiman, M., Housley, R. A., Lane, C. S., Lee, S., Matthews, I. P.,  
745 Smith, V. C., and Lowe, J. J.: Improved age estimates for key Late Quaternary European tephra horizons in the RESET lattice,  
746 *Quat. Sci. Rev.*, 118, 18–32, <https://doi.org/10.1016/j.quascirev.2014.11.007>, 2015.

747 Bull, I. D., Evershed, R. P., and Betancourt, P. P.: An organic geochemical investigation of the practice of manuring at a  
748 Minoan site on Pseira Island, Crete, *Geoarchaeology*, 16, 223–242, [https://doi.org/10.1002/1520-6548\(200102\)16:2<223::AID-GEA1002>3.0.CO;2-7](https://doi.org/10.1002/1520-6548(200102)16:2<223::AID-GEA1002>3.0.CO;2-7), 2001.

750 Bull, I. D., Lockheart, M. J., Elhmmali, M. M., Roberts, D. J., and Evershed, R. P.: The origin of faeces by means of biomarker  
751 detection, *Environ. Int.*, 27, 647–654, [https://doi.org/10.1016/S0160-4120\(01\)00124-6](https://doi.org/10.1016/S0160-4120(01)00124-6), 2002.

752 Bush, R. T., Berke, M. A., and Jacobson, A. D.: Plant Water  $\delta D$  and  $\delta^{18}O$  of Tundra Species from West Greenland, Arctic,  
753 *Antarct. Alp. Res.*, 49, 341–358, <https://doi.org/10.1657/AAAR0016-025>, 2017.

754 Callegaro, A., Battistel, D., Kehrwald, N. M., Matsubara Pereira, F., Kirchgorg, T., Del Carmen Villoslada Hidalgo, M., Bird,  
755 B. W., and Barbante, C.: Fire, vegetation, and Holocene climate in a southeastern Tibetan lake: A multi-biomarker  
756 reconstruction from Paru Co, *Clim. Past*, 14, 1543–1563, <https://doi.org/10.5194/cp-14-1543-2018>, 2018.

757 Canuel, E. A. and Martens, C. S.: Seasonal variations in the sources and alteration of organic matter associated with recently-  
758 deposited sediments, *Org. Geochem.*, 20, 563–577, [https://doi.org/10.1016/0146-6380\(93\)90024-6](https://doi.org/10.1016/0146-6380(93)90024-6), 1993.

759 Caves Rugenstein, J. K. and Chamberlain, C. P.: The evolution of hydroclimate in Asia over the Cenozoic: A stable-isotope  
760 perspective, *Earth-Science Rev.*, 185, 1129–1156, <https://doi.org/10.1016/j.earscirev.2018.09.003>, 2018.

761 Chandler, C., Cheney, P., Thomas, P., Trabaud, L., and Williams, D.: Fire in forestry. Volume 1. Forest fire behavior and  
762 effects. Volume 2. Forest fire management and organization., John Wiley & Sons, Inc., 1983.

763 Chen, A., Yang, L., Sun, L., Gao, Y., and Xie, Z.: Holocene changes in biomass burning in the boreal Northern Hemisphere,  
764 reconstructed from anhydrosugar fluxes in an Arctic sediment profile, *Sci. Total Environ.*, 867, 161460,  
765 <https://doi.org/10.1016/j.scitotenv.2023.161460>, 2023.

766 Colman, S. M., Peck, J. A., Karabanov, E. B., Carter, S. J., Bradbury, J. P., King, J. W., and Williams, D. F.: Continental  
767 climate response to orbital forcing from biogenic silica records in lake Baikal, *Nature*, 378, 769–771,  
768 <https://doi.org/10.1038/378769a0>, 1995.

769 Conley, D. J.: Biogenic silica as an estimate of siliceous microfossil abundance in Great Lakes sediments, *Biogeochemistry*,  
770 6, 161–179, <https://doi.org/10.1007/BF02182994>, 1988.

771 Conley, D. J. and Schelske, C. L.: Biogenic silica, in: Tracking environmental change using lake sediments, edited by: Last,  
772 W. M. and Smol, J. P., Springer Science & Business Media, 281–293, ISBN 1402006284, 2002.

773 Cordeiro, L. G. S. M., Carreira, R. S., and Wagener, A. L. R.: Geochemistry of fecal sterols in a contaminated estuary in  
774 southeastern Brazil, *Org. Geochem.*, 39, 1097–1103, <https://doi.org/10.1016/j.orggeochem.2008.02.022>, 2008.

775 Curtin, L., D’Andrea, W. J., Balascio, N. L., Shirazi, S., Shapiro, B., de Wet, G. A., Bradley, R. S., and Bakke, J.: Sedimentary  
776 DNA and molecular evidence for early human occupation of the Faroe Islands, *Commun. Earth Environ.*, 2,  
777 <https://doi.org/10.1038/s43247-021-00318-0>, 2021.

778 D’Anjou, R. M., Bradley, R. S., Balascio, N. L., and Finkelstein, D. B.: Climate impacts on human settlement and agricultural

779 activities in northern Norway revealed through sediment biogeochemistry, Proc. Natl. Acad. Sci. U. S. A., 109, 20332–20337,  
780 <https://doi.org/10.1073/pnas.1212730109>, 2012.

781 Dansgaard, W.: Stable isotopes in precipitation, Tellus, 16, 436–468, <https://doi.org/10.3402/tellusa.v16i4.8993>, 1964.

782 Davies, G. M. and Legg, C. J.: Fuel Moisture Thresholds in the Flammability of *Calluna vulgaris*, Fire Technol., 47, 421–436,  
783 <https://doi.org/10.1007/s10694-010-0162-0>, 2011.

784 Decrouy, L.: Biological and environmental controls on isotopes in ostracod shells, in: Developments in Quaternary Sciences,  
785 vol. 17, Elsevier, 165–181, 2012.

786 Denis, E. H.: Production and preservation of organic and fire-derived carbon across the Paleocene-Eocene Thermal Maximum,  
787 PhD thesis, Pennsylvania State University, [https://etda.libraries.psu.edu/files/final\\_submissions/12576](https://etda.libraries.psu.edu/files/final_submissions/12576), 2016.

788 Denis, E. H., Toney, J. L., Tarozo, R., Scott Anderson, R., Roach, L. D., and Huang, Y.: Polycyclic aromatic hydrocarbons  
789 (PAHs) in lake sediments record historic fire events: Validation using HPLC-fluorescence detection, Org. Geochem., 45, 7–  
790 17, <https://doi.org/10.1016/j.orggeochem.2012.01.005>, 2012.

791 Denis, E. H., Pedentchouk, N., Schouten, S., Pagani, M., and Freeman, K. H.: Fire and ecosystem change in the Arctic across  
792 the Paleocene–Eocene Thermal Maximum, Earth Planet. Sci. Lett., 467, 149–156, <https://doi.org/10.1016/j.epsl.2017.03.021>,  
793 2017.

794 Dion-Kirschner, H., McFarlin, J. M., Masterson, A. L., Axford, Y., and Osburn, M. R.: Modern constraints on the sources and  
795 climate signals recorded by sedimentary plant waxes in west Greenland, Geochim. Cosmoc. Acta, 286, 336–354,  
796 <https://doi.org/10.1016/j.gca.2020.07.027>, 2020.

797 Draxler, R. R., Hess, G. D., and Draxler R. R., and Hess G., D.: An overview of the HYSPLIT\_4 modelling system for  
798 trajectories, Aust. Meteorol. Mag., 47, 295–308, 1998.

799 Duan, Y., Wu, Y., Cao, X., Zhao, Y., and Ma, L.: Hydrogen isotope ratios of individual *n*-alkanes in plants from Gannan Gahai  
800 Lake (China) and surrounding area, Org. Geochem., 77, 96–105, <https://doi.org/10.1016/j.orggeochem.2014.10.005>, 2014.

801 Dugmore, A. J., Shore, J. S., Cook, G. T., Newton, A. J., Edwards, K. J., and Larsen, G.: The radiocarbon dating of tephra  
802 layers in Britain and Iceland, 15th Int. C Conf., 37, 379–388, 1995.

803 Eddudóttir, S. D., Erlendsson, E., Tinganelli, L., and Gísladóttir, G.: Climate change and human impact in a sensitive  
804 ecosystem: the Holocene environment of the Northwest Icelandic highland margin, Boreas, 45, 715–728,  
805 <https://doi.org/10.1111/bor.12184>, 2016.

806 Eddudóttir, S. D., Erlendsson, E., and Gísladóttir, G.: Effects of the Hekla 4 tephra on vegetation in Northwest Iceland, Veg.  
807 Hist. Archaeobot., 26, 389–402, <https://doi.org/10.1007/s00334-017-0603-5>, 2017.

808 Eddudóttir, S. D., Erlendsson, E., and Gísladóttir, G.: An Icelandic terrestrial record of North Atlantic cooling c. 8800–8100  
809 cal. yr BP, Quat. Sci. Rev., 197, 246–256, <https://doi.org/10.1016/j.quascirev.2018.07.017>, 2018.

810 Edvardsson, R.: The role of marine resources in the medieval economy of Vestfirðir, Iceland, PhD thesis, University of New  
811 York, UMI Number: 3396427, 2010.

812 Eglinton, G. and Hamilton, R. J.: Leaf epicuticular waxes, Science (80-. ), 156, 1322–1335,  
813 <https://doi.org/10.1126/science.156.3780.1322>, 1967.

814 Esri: ArcGIS Pro (Version 3.1.0.); Earthstar Geographic “World Imagery” map, accessed March 2023.,  
815 <https://doi.org/https://www.arcgis.com/home/item.html?id=10df2279f9684e4a9f6a7f08febac2a9>, 2023.

816 Evershed, R. P., Bethell, P. H., Reynolds, P. J., and Walsh, N. J.: 5 $\beta$ -Stigmastanol and related 5 $\beta$ -stanols as biomarkers of  
817 manuring: analysis of modern experimental material and assessment of the archaeological potential, J. Archaeol. Sci., 24, 485–  
818 495, <https://doi.org/10.1006/jasc.1996.0132>, 1997.

819 Feng, D., Liu, Y., Gao, Y., Zhou, J., Zheng, L., Qiao, G., Ma, L., Lin, Z., and Grathwohl, P.: Atmospheric bulk deposition of  
820 polycyclic aromatic hydrocarbons in Shanghai: Temporal and spatial variation, and global comparison, Environ. Pollut., 230,  
821 639–647, <https://doi.org/10.1016/j.envpol.2017.07.022>, 2017.

822 Fernandes, P. M. and Cruz, M. G.: Plant flammability experiments offer limited insight into vegetation-fire dynamics  
823 interactions, *New Phytol.*, 194, 606–609, <https://doi.org/10.1111/j.1469-8137.2012.04065.x>, 2012.

824 Fernández-Martínez, M., Preece, C., Corbera, J., Cano, O., Garcia-Porta, J., Sardans, J., Janssens, I. A., Sabater, F., and  
825 Peñuelas, J.: Bryophyte C: N: P stoichiometry, biogeochemical niches and elementome plasticity driven by environment and  
826 coexistence, *Ecol. Lett.*, 24, 1375–1386, 2021.

827 Ficken, K. J., Li, B., Swain, D. L., and Eglinton, G.: An *n*-alkane proxy for the sedimentary input of submerged/floating  
828 freshwater aquatic macrophytes, *Org. Geochem.*, 31, 745–749, [https://doi.org/10.1016/S0146-6380\(00\)00081-4](https://doi.org/10.1016/S0146-6380(00)00081-4), 2000.

829 Flowers, G. E., Björnsson, H., Geirsdóttir, Á., Miller, G. H., Black, J. L., and Clarke, G. K. C.: Holocene climate conditions  
830 and glacier variation in central Iceland from physical modelling and empirical evidence, *Quat. Sci. Rev.*, 27, 797–813,  
831 <https://doi.org/10.1016/j.quascirev.2007.12.004>, 2008.

832 Gagosian, R. B. and Peltzer, E. T.: The importance of atmospheric input of terrestrial organic material to deep sea sediments,  
833 *Org. Geochem.*, 10, 661–669, [https://doi.org/http://dx.doi.org/10.1016/S0146-6380\(86\)80002-X](https://doi.org/http://dx.doi.org/10.1016/S0146-6380(86)80002-X), 1986.

834 Geirsdóttir, Á., Miller, G. H., Thordarson, T., and Ólafsdóttir, K. B.: A 2000 year record of climate variations reconstructed  
835 from Haukadalsvatn, West Iceland, *J. Paleolimnol.*, 41, 95–115, <https://doi.org/10.1007/s10933-008-9253-z>, 2009a.

836 Geirsdóttir, Á., Miller, G. H., Axford, Y., and Ólafsdóttir, S.: Holocene and latest Pleistocene climate and glacier fluctuations  
837 in Iceland, *Quat. Sci. Rev.*, 28, 2107–2118, <https://doi.org/10.1016/j.quascirev.2009.03.013>, 2009b.

838 Geirsdóttir, Á., Miller, G. H., Larsen, D. J., and Ólafsdóttir, S.: Abrupt holocene climate transitions in the northern North  
839 Atlantic region recorded by synchronized lacustrine records in Iceland, *Quat. Sci. Rev.*, 70, 48–62,  
840 <https://doi.org/10.1016/j.quascirev.2013.03.010>, 2013.

841 Geirsdóttir, Á., Miller, G. H., Andrews, J. T., Harning, D. J., Anderson, L. S., Florian, C., Larsen, D. J., and Thordarson, T.:  
842 The onset of neoglaciation in Iceland and the 4.2 ka event, *Clim. Past*, 15, 25–40, <https://doi.org/10.5194/cp-15-25-2019>, 2019.

843 Geirsdóttir, Á., Harning, D. J., Miller, G. H., Andrews, J. T., Zhong, Y., and Caseldine, C.: Holocene history of landscape  
844 instability in Iceland: Can we deconvolve the impacts of climate, volcanism and human activity?, *Quat. Sci. Rev.*, 249,  
845 <https://doi.org/10.1016/j.quascirev.2020.106633>, 2020.

846 Geirsdóttir, Á., Miller, G. H., Harning, D. J., Hannesdóttir, H., Thordarson, T., and Jónsdóttir, I.: Recurrent outburst floods  
847 and explosive volcanism during the Younger Dryas–Early Holocene deglaciation in south Iceland: evidence from a lacustrine  
848 record, *J. Quat. Sci.*, 37, 1006–1023, <https://doi.org/10.1002/jqs.3344>, 2022.

849 George, I. J., Black, R. R., Geron, C. D., Aurell, J., Hays, M. D., Preston, W. T., and Gullett, B. K.: Volatile and semivolatile  
850 organic compounds in laboratory peat fire emissions, *Atmos. Environ.*, 132, 163–170,  
851 <https://doi.org/10.1016/j.atmosenv.2016.02.025>, 2016.

852 Gísladóttir, G., Woollett, J. M., Hébert, C. D., and Newton, A.: The Svalbarð project, *Archaeol. Islandica*, 10, 65–103, ISSN  
853 1560-8026, 2012.

854 Goad, L.: The Biosynthesis of Plant Sterols, 146–168, [https://doi.org/10.1007/978-3-642-66632-2\\_8](https://doi.org/10.1007/978-3-642-66632-2_8), 1977.

855 Goad, L. and Goodwin, T.: The biosynthesis of sterols in higher plants, *Biochem. J.*, 99, 735–746,  
856 <https://doi.org/10.1042/bj0990735>, 1966.

857 Goldammer, J. G. and Furyaev, V. V.: Fire in ecosystems of boreal Eurasia: Ecological impacts and links to the global system,  
858 *Fire Ecosyst. Boreal Eurasia*, 1–20, 1996.

859 Golomb, D., Barry, E., Fisher, G., Varanusupakul, P., Koleda, M., and Rooney, T.: Atmospheric deposition of polycyclic  
860 aromatic hydrocarbons near New England coastal waters, *Atmos. Environ.*, 35, 6245–6258, [https://doi.org/10.1016/S1352-2310\(01\)00456-3](https://doi.org/10.1016/S1352-2310(01)00456-3), 2001.

861

862 Grimalt, J. and Albaigés, J.: Source and occurrence of C<sub>12</sub>–C<sub>22</sub> *n*-alkane distributions with even carbon-number preference in  
863 sedimentary environments, *Geochim. Cosmoc. Acta*, 51, 1379–1384, [https://doi.org/10.1016/0016-7037\(87\)90322-X](https://doi.org/10.1016/0016-7037(87)90322-X), 1987.

864 Gross, M.: An investigation of paleo-wildfires during the Cretaceous-Paleogene (K-PG) boundary at El Kef, Tunisia,

865 Undergraduate Honors thesis, University of Colorado, Boulder, [https://scholar.colorado.edu/honr\\_theses/1351](https://scholar.colorado.edu/honr_theses/1351), 2017.

866 Guíñez, M., Escudero, L., Mandelli, A., Martínez, L. D., and Cerutti, S.: Volcanic ashes as a source for nitrated and oxygenated  
867 polycyclic aromatic hydrocarbon pollution, *Environ. Sci. Pollut. Res.*, *27*, 16972–16982, [https://doi.org/10.1007/s11356-020-](https://doi.org/10.1007/s11356-020-08130-7)  
868 08130-7, 2020.

869 Guo, J. and Liao, H.: In-situ formation of perylene in lacustrine sediments and its geochemical significance, *Acta Geochim.*,  
870 *39*, 587–594, <https://doi.org/10.1007/s11631-020-00400-y>, 2020.

871 Iceland Statistical Service: <https://www.hagstofa.is/>, last access: 13 March 2023.

872 Halsall, C. J., Sweetman, A. J., Barrie, L. A., and Jones, K. C.: Modelling the behaviour of PAHs during atmospheric transport  
873 from the UK to the Arctic, *Atmos. Environ.*, *35*, 255–267, [https://doi.org/10.1016/S1352-2310\(00\)00195-3](https://doi.org/10.1016/S1352-2310(00)00195-3), 2001.

874 Han, J. and Calvin, M.: Hydrocarbon distribution of algae and bacteria, and microbiological activity in sediments., *Proc. Natl.*  
875 *Acad. Sci. U. S. A.*, *64*, 436–443, <https://doi.org/10.1073/pnas.64.2.436>, 1969.

876 Hanke, U. M., Lima-Braun, A. L., Eglinton, T. I., Donnelly, J. P., Galy, V., Poussart, P., Hughen, K., McNichol, A. P., Xu,  
877 L., and Reddy, C. M.: Significance of perylene for source allocation of terrigenous organic matter in aquatic sediments,  
878 *Environ. Sci. Technol.*, *53*, 8244–8251, <https://doi.org/10.1021/acs.est.9b02344>, 2019.

879 Harning, D. J., Geirsdóttir, Á., Miller, G. H., and Zalzal, K.: Early Holocene deglaciation of Drangajökull, Vestfirðir, Iceland,  
880 *Quat. Sci. Rev.*, *153*, 192–198, <https://doi.org/10.1016/j.quascirev.2016.09.030>, 2016.

881 Harning, D. J., Thordarson, T., Geirsdóttir, Á., Zalzal, K., and Miller, G. H.: Provenance, stratigraphy and chronology of  
882 Holocene tephra from Vestfirðir, Iceland, *Quat. Geochronol.*, *46*, 59–76, <https://doi.org/10.1016/j.quageo.2018.03.007>, 2018a.

883 Harning, D. J., Geirsdóttir, Á., and Miller, G. H.: Punctuated Holocene climate of Vestfirðir, Iceland, linked to internal/external  
884 variables and oceanographic conditions, *Quat. Sci. Rev.*, *189*, 31–42, <https://doi.org/10.1016/j.quascirev.2018.04.009>, 2018b.

885 Harning, D. J., Curtin, L., Geirsdóttir, Á., D’Andrea, W. J., Miller, G. H., and Sepúlveda, J.: Lipid Biomarkers Quantify  
886 Holocene Summer Temperature and Ice Cap Sensitivity in Icelandic Lakes, *Geophys. Res. Lett.*, *47*,  
887 <https://doi.org/10.1029/2019GL085728>, 2020.

888 Harning, D. J., Jennings, A. E., Köseoglu, D., Belt, S. T., Geirsdóttir, Á., and Sepúlveda, J.: Response of biological productivity  
889 to North Atlantic marine front migration during the Holocene, *Clim. Past*, *17*, 379–396, [https://doi.org/10.5194/cp-17-379-](https://doi.org/10.5194/cp-17-379-2021)  
890 2021, 2021.

891 Harning, D. J., Sacco, S., Ananthawat, K., Ardenghi, N., Thordarson, T., Raberg, J. H., Sepúlveda, J., Geirsdóttir, Á., Shapiro,  
892 B., and Miller, G. H.: Delayed postglacial colonization of *Betula* in Iceland and the circum North Atlantic, *Elife*, *12*, 1–23,  
893 2023.

894 Hatcher, P. G. and McGillivray, P. A.: Sewage Contamination in the New York Bight. Coprostanol as an Indicator, *Environ.*  
895 *Sci. Technol.*, *13*, 1225–1229, <https://doi.org/10.1021/es60158a015>, 1979.

896 He, D., Zhang, K., Tang, J., Cui, X., and Sun, Y.: Using fecal sterols to assess dynamics of sewage input in sediments along a  
897 human-impacted river-estuary system in eastern China, *Sci. Total Environ.*, *636*, 787–797,  
898 <https://doi.org/10.1016/j.scitotenv.2018.04.314>, 2018.

899 Hernández, A., Bao, R., Giralt, S., Barker, P. A., Leng, M. J., Sloane, H. J., and Sáez, A.: Biogeochemical processes controlling  
900 oxygen and carbon isotopes of diatom silica in Late Glacial to Holocene lacustrine rhythmites, *Palaeogeogr. Palaeoclimatol.*  
901 *Palaeoecol.*, *299*, 413–425, <https://doi.org/10.1016/j.palaeo.2010.11.020>, 2011.

902 Hiles, W., Lawson, I. T., Roucoux, K. H., and Streeter, R. T.: Late survival of woodland contrasts with rapid limnological  
903 changes following settlement at Kalmanstjörn, Mývatnssveit, northeast Iceland, *Boreas*, *50*, 1209–1227,  
904 <https://doi.org/10.1111/bor.12529>, 2021.

905 Hjartarson, A. and Sæmundsson, K.: Geological map of Iceland, bedrock. 1: 600,000, Icel. GeoSurvey, Reykjavík, 2014.

906 Hoffmann, D. and Wynder, E. L.: Organic particulate pollutants: Chemical analysis and bioassays for carcinogenicity, in: *Air*  
907 *pollution*, vol. II, Academic Press New York, 67–95, ISBN 0-12-666602-4, 1977.

908 Hollister, K. V, Thomas, E. K., Raynolds, M. K., Bültmann, H., Raberg, J. H., Miller, G. H., and Sepúlveda, J.: Aquatic and  
909 terrestrial plant contributions to sedimentary plant waxes in a modern arctic lake setting, *J. Geophys. Res. Biogeosc.*, 127,  
910 <https://doi.org/https://doi.org/10.1029/2022JG006903>, 2022.

911 Hurrell, J. W.: Decadal trends in the North Atlantic Oscillation: Regional Temperatures and Precipitation, *Science*, 269, 676–  
912 679, <https://doi.org/10.1126/science.269.5224.676>, 1995.

913 Hurrell, J. W., Kushnir, Y., Otterson, G., and Visbeck, M.: An Overview of the North Atlantic Oscillation, *North Atl. Oscil.*  
914 *Clim. Significance Environ. Impact*, 134, 263, <https://doi.org/10.1029/GM134>, 2003.

915 Ifkirne, M., Beri, Q., Schaefer, A., Pham, Q. B., Acharki, S., and Farah, A.: Study of the impact of ash fallout from the Icelandic  
916 volcano Eyjafjöll (2010) on vegetation using MODIS data, *Nat. Hazards*, 1–21, <https://doi.org/10.1007/s11069-022-05544-z>,  
917 2022.

918 Iinuma, Y., Brüggemann, E., Gnauk, T., Müller, K., Andreae, M. O., Helas, G., Parmar, R., and Herrmann, H.: Source  
919 characterization of biomass burning particles: The combustion of selected European conifers, African hardwood, savanna  
920 grass, and German and Indonesian peat, *J. Geophys. Res. Atmos.*, 112, <https://doi.org/10.1029/2006JD007120>, 2007.

921 Ilyinskaya, E., Schmidt, A., Mather, T. A., Pope, F. D., Witham, C., Baxter, P., Jóhannsson, T., Pfeffer, M., Barsotti, S., Singh,  
922 A., Sanderson, P., Bergsson, B., McCormick Kilbride, B., Donovan, A., Peters, N., Oppenheimer, C., and Edmonds, M.:  
923 Understanding the environmental impacts of large fissure eruptions: Aerosol and gas emissions from the 2014–2015 Holuhraun  
924 eruption (Iceland), *Earth Planet. Sci. Lett.*, 472, 309–322, <https://doi.org/10.1016/j.epsl.2017.05.025>, 2017.

925 Jaffé, R., Cabrera, A., Hajje, N., and Carvajal-Chitty, H.: Organic biogeochemistry of a hypereutrophic tropical, freshwater  
926 lake - Part 1: particle associated and dissolved lipids, *Org. Geochem.*, 25, 227–240, [https://doi.org/10.1016/S0146-  
927 6380\(96\)00114-3](https://doi.org/10.1016/S0146-), 1996.

928 Jennings, A., Thordarson, T., Zalzal, K., Stoner, J., Hayward, C., Geirsdóttir, Á., and Miller, G. H.: Holocene tephra from  
929 Iceland and Alaska in SE Greenland shelf sediments, *Geol. Soc. London, Spec. Publ.*, 398, 157–193,  
930 <https://doi.org/10.1144/SP398.6>, 2014.

931 Jiang, C., Alexander, R., Kagi, R. I., and Murray, A. P.: Origin of perylene in ancient sediments and its geological significance,  
932 *Org. Geochem.*, 31, 1545–1559, [https://doi.org/10.1016/S0146-6380\(00\)00074-7](https://doi.org/10.1016/S0146-6380(00)00074-7), 2000.

933 Johnsen, A. R., Wick, L. Y., and Harms, H.: Principles of microbial PAH-degradation in soil, *Environ. Pollut.*, 133, 71–84,  
934 <https://doi.org/10.1016/j.envpol.2004.04.015>, 2005.

935 Jónsson, G. and Magnússon, M. S.: Hagskinna: Icelandic historical statistics, *Stat. Iceland, Reykjavík, Icel.*, 1997.

936 Junk, G. A. and Ford, C. S.: Review of organic emissions from selected combustion processes, Ames Lab., IA (USA), 1980.

937 Kardjilov, M. I., Gísladóttir, G., and Gíslason, S. R.: Land degradation in northeastern Iceland: present and past carbon fluxes,  
938 *L. Degrad. Dev.*, 17, 401–417, <https://doi.org/10.1002/ldr>, 2006.

939 Karlsdóttir, L., Hallsdóttir, M., Eggertsson, Ó., Thorssón, Æ. T., and Anamthawat-Jónsson, K.: Birch hybridization in  
940 Thistilfjörður, North-east Iceland during the Holocene, *Icelandic Agric. Sci.*, 27, 95–109, ISSN 1670-567X, 2014.

941 Karp, A. T., Holman, A. I., Hopper, P., Grice, K., and Freeman, K. H.: Fire distinguishers: Refined interpretations of polycyclic  
942 aromatic hydrocarbons for paleo-applications, *Geochim. Cosmoc. Acta*, 289, 93–113,  
943 <https://doi.org/10.1016/j.gca.2020.08.024>, 2020.

944 Kaushal, S. and Binford, M. W.: Relationship between C:N ratios of lake sediments, organic matter sources, and historical  
945 deforestation in Lake Pleasant, Massachusetts, USA, *J. Paleolimnol.*, 22, 439–442, <https://doi.org/10.1023/A:1008027028029>,  
946 1999.

947 Kilian, R., Biester, H., Behrmann, J., Baeza, O., Fesq-Martin, M., Hohner, M., Schimpf, D., Friedmann, A., and Mangini, A.:  
948 Millennium-scale volcanic impact on a superhumid and pristine ecosystem, *Geology*, 34, 609–612,  
949 <https://doi.org/10.1130/G22605.1>, 2006.

950 Kozak, K., Ruman, M., Kosek, K., Karasiński, G., Stachnik, Ł., and Polkowska, Z.: Impact of volcanic eruptions on the



951 occurrence of PAHs compounds in the aquatic ecosystem of the southern part of West Spitsbergen (Hornsund Fjord, Svalbard),  
952 Water (Switzerland), 9, <https://doi.org/10.3390/w9010042>, 2017.

953 Lake, S., Bullock, J. M., and Hartley, S.: Impacts of livestock grazing on lowland heathland in the UK, English Nat. Res.  
954 Reports, 422, 143, ISSN 0967-876X, 2001.

955 Lammel, G., Sehili, A. M., Bond, T. C., Feichter, J., and Grassl, H.: Gas/particle partitioning and global distribution of  
956 polycyclic aromatic hydrocarbons - A modelling approach, Chemosphere, 76, 98–106,  
957 <https://doi.org/10.1016/j.chemosphere.2009.02.017>, 2009.

958 Larsen, D. J., Miller, G. H., Geirsdóttir, Á., and Thordarson, T.: A 3000-year varved record of glacier activity and climate  
959 change from the proglacial lake Hvítárvatn, Iceland, Quat. Sci. Rev., 30, 2715–2731,  
960 <https://doi.org/10.1016/j.quascirev.2011.05.026>, 2011.

961 Larsen, D. J., Miller, G. H., Geirsdóttir, Á., and Ólafsdóttir, S.: Non-linear Holocene climate evolution in the North Atlantic:  
962 A high-resolution, multi-proxy record of glacier activity and environmental change from Hvítárvatn, central Iceland, Quat.  
963 Sci. Rev., 39, 14–25, <https://doi.org/10.1016/j.quascirev.2012.02.006>, 2012.

964 Larsen, G.: H4 and other acid Hekla tephra layers, Jokull, 27, 28–46, <https://timarit.is/gegnir/000527808>, 1977.

965 Larsen, G. and Eiríksson, J.: Late Quaternary terrestrial tephrochronology of Iceland—frequency of explosive eruptions, type  
966 and volume of tephra deposits, J. Quat. Sci. Publ. Quat. Res. Assoc., 23, 109–120, <https://doi.org/10.1002/jqs.1129>, 2008.

967 Larsen, G., Eiríksson, J., Knudsen, K. L., and Heinemeier, J.: Correlation of late Holocene terrestrial and marine tephra  
968 markers, north Iceland: Implications for reservoir age changes, Polar Res., 21, 283–290, <https://doi.org/10.1111/j.1751-8369.2002.tb00082.x>, 2002.

970 Lebrun, J., Bhiry, N., Woollett, J., and Sæmundsson, Þ.: Slope Dynamics in Relation to the Occupation and Abandonment of  
971 a Mountain Farm in Þistilfjörður, Northeast Iceland, Geosciences, 13, 30, <https://doi.org/10.3390/geosciences13020030>, 2023.

972 Lechler, A. R. and Galewsky, J.: Refining paleoaltimetry reconstructions of the Sierra Nevada: California, using air parcel  
973 trajectories, Geology, 41, 259–262, <https://doi.org/10.1130/G33553.1>, 2013.

974 Leeming, R., Ball, A., Ashbolt, N., and Nichols, P.: Using faecal sterols from humans and animals to distinguish faecal  
975 pollution in receiving waters, Water Res., 30, 2893–2900, [https://doi.org/10.1016/S0043-1354\(96\)00011-5](https://doi.org/10.1016/S0043-1354(96)00011-5), 1996.

976 Leeming, R. L., Ball, A., Ashbolt, N. J., Jones, G., and Nichols, P. D.: Distinguishing between human and animal sources of  
977 faecal pollution., 61, <http://hdl.handle.net/102.100.100/237154?index=1>, 1994.

978 Lerch, M., Bromm, T., Geitner, C., Haas, J. N., Schäfer, D., Glaser, B., and Zech, M.: Human and livestock faecal biomarkers  
979 at the prehistorical encampment site of Ullafelsen in the Fotsch Valley , Stubai Alps , Austria - potential and limitations, 1–  
980 24, <https://doi.org/10.5194/bg-2021-186>, 2021.

981 Li, C., Ma, S., Xia, Y., He, X., Gao, W., and Zhang, G.: Assessment of the relationship between ACL/CPI values of long chain  
982 *n*-alkanes and climate for the application of paleoclimate over the Tibetan Plateau, Quat. Int., 544, 76–87,  
983 <https://doi.org/10.1016/j.quaint.2020.02.028>, 2020.

984 Lima, A. L. C., Farrington, J. W., and Reddy, C. M.: Combustion-Derived Polycyclic Aromatic Hydrocarbons in the  
985 Environment—A Review, Environ. Forensics, 6, 109–131, <https://doi.org/10.1080/15275920590952739>, 2005.

986 Mack, R. N.: Initial Effects of Ashfall from Mount St. Helens on Vegetation in Eastern Washington and Adjacent Idaho,  
987 Science, 213, 537–539, <https://doi.org/10.1126/science.213.4507.537>, 1981.

988 Magi, E., Bianco, R., Ianni, C., and Di Carro, M.: Distribution of polycyclic aromatic hydrocarbons in the sediments of the  
989 Adriatic Sea, Environ. Pollut., 119, 91–98, [https://doi.org/10.1016/S0269-7491\(01\)00321-9](https://doi.org/10.1016/S0269-7491(01)00321-9), 2002.

990 Mankasingh, U. and Gísladóttir, G.: Early indicators of soil formation in the Icelandic sub-arctic highlands, Geoderma, 337,  
991 152–163, <https://doi.org/10.1016/j.geoderma.2018.09.002>, 2019.

992 Marino, E., Madrigal, J., Guijarro, M., Hernando, C., Dez, C., and Fernandez, C.: Flammability descriptors of fine dead fuels  
993 resulting from two mechanical treatments in shrubland: A comparative laboratory study, Int. J. Wildl. Fire, 19, 314–324,

994 <https://doi.org/10.1071/WF08123>, 2010.

995 Marlon, J. R.: The geography of fire: A paleo perspective, PhD thesis, University of Oregon, <http://hdl.handle.net/1794/10334>,

996 2009.

997 Marlon, J. R., Bartlein, P. J., Walsh, M. K., Harrison, S. P., Brown, K. J., Edwards, M. E., Higuera, P. E., Power, M. J.,

998 Anderson, R. S., Briles, C., Brunelle, A., Carcaillet, C., Daniels, M., Hu, F. S., Lavoie, M., Long, C., Minckley, T., Richard,

999 P. J. H., Scott, A. C., Shafer, D. S., Tinner, W., Umbanhowar, C. E., and Whitlock, C.: Wildfire responses to abrupt climate

1000 change in North America, *Proc. Natl. Acad. Sci. U. S. A.*, 106, 2519–2524, <https://doi.org/10.1073/pnas.0808212106>, 2009.

1001 Marlon, J. R., Bartlein, P. J., Daniiau, A. L., Harrison, S. P., Maezumi, S. Y., Power, M. J., Tinner, W., and Vanni re, B.:

1002 Global biomass burning: A synthesis and review of Holocene paleofire records and their controls, *Quat. Sci. Rev.*, 65, 5–25,

1003 <https://doi.org/10.1016/j.quascirev.2012.11.029>, 2013.

1004 Marzi, R., Torkelson, B. E., and Olson, R. K.: A revised carbon preference index, *Org. Geochem.*, 20, 1303–1306,

1005 [https://doi.org/10.1016/0146-6380\(93\)90016-5](https://doi.org/10.1016/0146-6380(93)90016-5), 1993.

1006 May, W. E., Wasik, S. P., and Freeman, D. H.: Determination of the solubility behavior of some polycyclic aromatic

1007 hydrocarbons in water, *Anal. Chem.*, 23, 877–884, <https://doi.org/10.1021/ac50029a042>, 1978.

1008 McCalley, D. V., Cooke, M., and Nickless, G.: Effect of sewage treatment on faecal sterols, *Water Res.*, 15, 1019–1025,

1009 [https://doi.org/10.1016/0043-1354\(81\)90211-6](https://doi.org/10.1016/0043-1354(81)90211-6), 1981.

1010 Mccarty, J. L., Aalto, J., Paunu, V. V., Arnold, S. R., Eckhardt, S., Klimont, Z., Fain, J. J., Evangeliou, N., Ven l inen, A.,

1011 Tchebakova, N. M., Parfenova, E. I., Kupiainen, K., Soja, A. J., Huang, L., and Wilson, S.: Reviews and syntheses: Arctic fire

1012 regimes and emissions in the 21st century, *Biogeosciences*, 18, 5053–5083, <https://doi.org/10.5194/bg-18-5053-2021>, 2021.

1013 McFarlin, J. M., Axford, Y., Masterson, A. L., and Osburn, M. R.: Calibration of modern sedimentary  $\delta^2\text{H}$  plant wax-water

1014 relationships in Greenland lakes, *Quat. Sci. Rev.*, 225, 105978, <https://doi.org/10.1016/j.quascirev.2019.105978>, 2019.

1015 McGovern, T. H., V steinsson, O., Fri riksoon, A., Church, M., Lawson, I., Simpson, I. A., Einarsson, A., Dugmore, A., Cook,

1016 G., Perdikaris, S., Edwards, K. J., Thomson, A. M., Adderley, W. P., Newton, A., Lucas, G., Edvardsson, R., Aldred, O., and

1017 Dunbar, E.: Landscapes of Settlement in Northern Iceland: Historical Ecology of Human Impact and Climate Fluctuation on

1018 the Millennial Scale, *Am. Anthropol.*, 109, 27–51, <https://doi.org/10.1525/aa.2007.109.1.27>, 2007.

1019 McGrath, T. E., Chan, W. G., and Hajajigol, R.: Low temperature mechanism for the formation of polycyclic aromatic

1020 hydrocarbons from the pyrolysis of cellulose. *Journal of Analytical and Applied Pyrolysis*, v. 66, p. 51-70, 2003., *J. Anal.*

1021 *Appl. Pyrolysis*, 66, 51–70, 2003.

1022 McKay, N. P., Kaufman, D. S., and Michelutti, N.: Biogenic silica concentration as a high-resolution, quantitative temperature

1023 proxy at Hallet Lake, south-central Alaska, *Geophys. Res. Lett.*, 35, 4–9, <https://doi.org/10.1029/2007GL032876>, 2008.

1024 Meyers, P. A.: Preservation of elemental and isotopic source identification of sedimentary organic matter, *Chem. Geol.*, 114,

1025 289–302, [https://doi.org/10.1016/0009-2541\(94\)90059-0](https://doi.org/10.1016/0009-2541(94)90059-0), 1994.

1026 Meyers, P. A.: Organic geochemical proxies of paleoceanographic, paleolimnologic, and paleoclimatic processes, *Org.*

1027 *Geochem.*, 27, 213–250, [https://doi.org/10.1016/S0146-6380\(97\)00049-1](https://doi.org/10.1016/S0146-6380(97)00049-1), 1997.

1028 Meyers, P. A. and Ishiwatari, R.: Lacustrine organic geochemistry-an overview of indicators of organic matter sources and

1029 diagenesis in lake sediments, *Org. Geochem.*, 20, 867–900, [https://doi.org/10.1016/0146-6380\(93\)90100-P](https://doi.org/10.1016/0146-6380(93)90100-P), 1993.

1030 Meyers, P. A. and Teranes, J. L.: Sediment Organic Matter, in: *Tracking Environmental Change Using Lake Sediments:*

1031 *Physical and Geochemical Methods*, edited by: Last, W. M. and Smol, J. P., Springer Netherlands, Dordrecht, 239–269,

1032 [https://doi.org/10.1007/0-306-47670-3\\_9](https://doi.org/10.1007/0-306-47670-3_9), 2001.

1033 Mjell, T. L., Ninnemann, U. S., Kleiven, H. F., and Hall, I. R.: Multidecadal changes in Iceland Scotland Overflow Water

1034 vigor over the last 600 years and its relationship to climate, *Geophys. Res. Lett.*, 43, 2111–2117,

1035 <https://doi.org/10.1002/2016GL068227>, 2016.

1036 Mooney, D. E.: Examining Possible Driftwood Use in Viking Age Icelandic Boats, *Nor. Archaeol. Rev.*, 49, 156–176,

1037 <https://doi.org/10.1080/00293652.2016.1211734>, 2016.

1038 Moossen, H., Bendle, J., Seki, O., Quillmann, U., and Kawamura, K.: North Atlantic Holocene climate evolution recorded by  
1039 high-resolution terrestrial and marine biomarker records, *Quat. Sci. Rev.*, 129, 111–127,  
1040 <https://doi.org/10.1016/j.quascirev.2015.10.013>, 2015.

1041 Murchison, D. G. and Raymond, A. C.: Igneous activity and organic maturation in the Midland Valley of Scotland, *Int. J. Coal*  
1042 *Geol.*, 14, 47–82, [https://doi.org/10.1016/0166-5162\(89\)90078-5](https://doi.org/10.1016/0166-5162(89)90078-5), 1989.

1043 Murtaugh, J. J. and Bunch, R. L.: Sterols as a measure of fecal pollution., *J. Water Pollut. Control Fed.*, 39, 404–409,  
1044 <https://www.jstor.org/stable/25035758>, 1967.

1045 NOAA: <https://www.ncei.noaa.gov/access/monitoring/nao/>, last access: 1 March 2023.

1046 Niedermeyer, E. M., Forrest, M., Beckmann, B., Sessions, A. L., Mulch, A., and Schefuß, E.: The stable hydrogen isotopic  
1047 composition of sedimentary plant waxes as quantitative proxy for rainfall in the West African Sahel, *Geochim. Cosmoc. Acta*,  
1048 184, 55–70, <https://doi.org/10.1016/j.gca.2016.03.034>, 2016.

1049 Norðdahl, H. and Pétursson, H. G.: Relative sea-level changes in Iceland: new aspects of the Weichselian deglaciation of  
1050 Iceland, *Dev. Quat. Sci. Elsevier*, 25–78, ISBN 0-444-50652-7, 2005.

1051 Óladóttir, B. A., Larsen, G., and Sigmarsson, O.: Holocene volcanic activity at Grímsvötn, Bárðarbunga and Kverkfjöll  
1052 subglacial centres beneath Vatnajökull, Iceland, *Bull. Volcanol.*, 73, 1187–1208, <https://doi.org/10.1007/s00445-011-0461-4>,  
1053 2011.

1054 Óladóttir, B. A., Thordarson, T., Geirsdóttir, Á., Jóhannsdóttir, G. E., and Mangerud, J.: The Saksunarvatn Ash and the G10ka  
1055 series tephra. Review and current state of knowledge, *Quat. Geochronol.*, 56, <https://doi.org/10.1016/j.quageo.2019.101041>,  
1056 2020.

1057 Ólafsdóttir, R., Schlyter, P., and Haraldsson, H. V.: Simulating icelandic vegetation cover during the holocene implications  
1058 for long-term land degradation, *Geogr. Ann. Ser. A, Phys. Geogr.*, 83, 203–215, [https://doi.org/10.1111/j.0435-](https://doi.org/10.1111/j.0435-3676.2001.00155.x)  
1059 [3676.2001.00155.x](https://doi.org/10.1111/j.0435-3676.2001.00155.x), 2001.

1060 Page, D. S., Boehm, P. D., Douglas, G. S., Bence, A. E., Burns, W. A., and Mankiewicz, P. J.: Pyrogenic polycyclic aromatic  
1061 hydrocarbons in sediments record past human activity: A case study in Prince William Sound, Alaska, *Mar. Pollut. Bull.*, 38,  
1062 247–260, [https://doi.org/10.1016/S0025-326X\(98\)00142-8](https://doi.org/10.1016/S0025-326X(98)00142-8), 1999.

1063 Pancost, R. D., Baas, M., Van Geel, B., and Sinninghe Damsté, J. S.: Biomarkers as proxies for plant inputs to peats: An  
1064 example from a sub-boreal ombrotrophic bog, *Org. Geochem.*, 33, 675–690, [https://doi.org/10.1016/S0146-6380\(02\)00048-7](https://doi.org/10.1016/S0146-6380(02)00048-7),  
1065 2002.

1066 Patterson, G. W.: Relation between Structure and Retention Time of Sterols in Gas Chromatography, *Anal. Chem.*, 43, 1165–  
1067 1170, <https://doi.org/10.1021/ac60304a015>, 1971.

1068 Petit, T., Lozier, M. S., Josey, S. A., and Cunningham, S. A.: Atlantic Deep Water Formation Occurs Primarily in the Iceland  
1069 Basin and Irminger Sea by Local Buoyancy Forcing, *Geophys. Res. Lett.*, 47, 1–9, <https://doi.org/10.1029/2020GL091028>,  
1070 2020.

1071 Pickarski, N., Kwiecien, O., and Litt, T.: Volcanic impact on terrestrial and aquatic ecosystems in the Eastern Mediterranean,  
1072 *Commun. Earth Environ.*, 4, 1–12, <https://doi.org/10.1038/s43247-023-00827-0>, 2023.

1073 Pinta, E.: Norse Management of Wooden Resources across the North Atlantic: Highlights from the Norse Greenlandic  
1074 Settlements, *Environ. Archaeol.*, 26, 209–221, <https://doi.org/10.1080/14614103.2018.1547510>, 2021.

1075 Plucinski, M. P., Anderson, W. R., Bradstock, R. A., and Gill, A. M.: The initiation of fire spread in shrubland fuels recreated  
1076 in the laboratory, *Int. J. Wildl. Fire*, 19, 512–520, <https://doi.org/10.1071/WF09038>, 2010.

1077 Power, M. J., Marlon, J., Ortiz, N., Bartlein, P. J., Harrison, S. P., Mayle, F. E., Ballouche, A., Bradshaw, R. H. W., Carcaillet,  
1078 C., Cordova, C., Mooney, S., Moreno, P. I., Prentice, I. C., Thonicke, K., Tinner, W., Whitlock, C., Zhang, Y., Zhao, Y., Ali,  
1079 A. A., Anderson, R. S., Beer, R., Behling, H., Briles, C., Brown, K. J., Brunelle, A., Bush, M., Camill, P., Chu, G. Q., Clark,

1080 J., Colombaroli, D., Connor, S., Daniau, A. L., Daniels, M., Dodson, J., Doughty, E., Edwards, M. E., Finsinger, W., Foster,  
1081 D., Frechette, J., Gaillard, M. J., Gavin, D. G., Gobet, E., Haberle, S., Hallett, D. J., Higuera, P., Hope, G., Horn, S., Inoue, J.,  
1082 Kaltenrieder, P., Kennedy, L., Kong, Z. C., Larsen, C., Long, C. J., Lynch, J., Lynch, E. A., McGlone, M., Meeks, S., Mensing,  
1083 S., Meyer, G., Minckley, T., Mohr, J., Nelson, D. M., New, J., Newnham, R., Noti, R., Oswald, W., Pierce, J., Richard, P. J.  
1084 H., Rowe, C., Sanchez Goñi, M. F., Shuman, B. N., Takahara, H., Toney, J., Turney, C., Urrego-Sanchez, D. H., Umbanhowar,  
1085 C., Vandergoes, M., Vanniere, B., Vescovi, E., Walsh, M., Wang, X., Williams, N., Wilmshurst, J., and Zhang, J. H.: Changes  
1086 in fire regimes since the last glacial maximum: An assessment based on a global synthesis and analysis of charcoal data, *Clim.*  
1087 *Dyn.*, 30, 887–907, <https://doi.org/10.1007/s00382-007-0334-x>, 2008.

1088 Prokopenko, A., Williams, D. F., Kavel, P., and Karabanov, E.: The organic indexes in the surface sediments of Lake Baikal  
1089 water system and the processes controlling their variation, *IPCCCE Newslett*, 7, 49–55, 1993.

1090 Purushothama, S., Pan, W. P., Riley, J. T., and Lloyd, W. G.: Analysis of polynuclear aromatic hydrocarbons from coal fly  
1091 ash, *Fuel Process. Technol.*, 53, 235–242, [https://doi.org/10.1016/S0378-3820\(97\)00056-8](https://doi.org/10.1016/S0378-3820(97)00056-8), 1998.

1092 Quirk, M. M., Wardroper, A. M. K., Brooks, P. W., Wheatley, A. E., and Maxwell, J. R.: Transformations of acyclic and cyclic  
1093 isoprenoids in recent sedimentary environments, in: *Biogeochimie de la matiere organique a l'interface eau-sediment marin*.  
1094 Centre National de la Recherche Scientifique. Colloque international. 293/1979/Marseille; France; Paris: Ed. du CNRS; DA.,  
1095 225–232, PASCALGEODEBRGM8120323455, 1980.

1096 R Core Team: R: A Language and Environment for Statistical Computing. R Foundation for Statistical Computing, Vienna,  
1097 Austria., <https://www.r-project.org/>, 2020.

1098 Raposeiro, P. M., Hernández, A., Pla-rabes, S., Gonçalves, V., and Bao, R.: Climate change facilitated the early colonization  
1099 of the Azores Archipelago during medieval times, *Proc. Natl. Acad. Sci.*, 118, [https://doi.org/10.1073/pnas.2108236118/-](https://doi.org/10.1073/pnas.2108236118/-/DCSupplemental.Published)  
1100 [/DCSupplemental.Published](https://doi.org/10.1073/pnas.2108236118/-/DCSupplemental.Published), 2021.

1101 Rein, G., Cleaver, N., Ashton, C., Pironi, P., and Torero, J. L.: The severity of smouldering peat fires and damage to the forest  
1102 soil, *Catena*, 74, 304–309, <https://doi.org/10.1016/j.catena.2008.05.008>, 2008.

1103 Richter, N., Russell, J. M., Garfinkel, J., and Huang, Y.: Impacts of Norse settlement on terrestrial and aquatic ecosystems in  
1104 Southwest Iceland, *J. Paleolimnol.*, 65, 255–269, <https://doi.org/10.1007/s10933-020-00169-3>, 2021.

1105 Rieger, S., Schoepfhorster, D. B., and Furbush, C. E.: Exploratory soil survey of Alaska, US Department of Agriculture, Soil  
1106 Conservation Service, 1979.

1107 Routh, J., Hugelius, G., Kuhry, P., Filley, T., Tillman, P. K., Becher, M., and Crill, P.: Multi-proxy study of soil organic matter  
1108 dynamics in permafrost peat deposits reveal vulnerability to climate change in the European Russian Arctic, *Chem. Geol.*, 368,  
1109 104–117, <https://doi.org/10.1016/j.chemgeo.2013.12.022>, 2014.

1110 Roy, N., Bhiry, N., Woollett, J., and Fréchette, B.: Vegetation History since the Mid-Holocene in Northeastern Iceland,  
1111 *Ecoscience*, 25, 109–123, <https://doi.org/10.1080/11956860.2018.1443419>, 2018.

1112 Rundel, P. W., Stichler, W., Zander, R. H., and Ziegler, H.: Carbon and hydrogen isotope ratios of bryophytes from arid and  
1113 humid regions, *Oecologia*, 44, 91–94, 1979.

1114 Sachse, D., Billault, I., Bowen, G. J., Chikaraishi, Y., Dawson, T. E., Feakins, S. J., Freeman, K. H., Magill, C. R., McInerney,  
1115 F. A., van der Meer, M. T. J., Polissar, P., Robins, R. J., Sachs, J. P., Schmidt, H., Sessions, A. L., White, J. W. C. C., West,  
1116 J. B., Kahmen, A., and Meer, M. T. J. Van Der: Molecular Paleohydrology: Interpreting the Hydrogen-Isotopic Composition  
1117 of Lipid Biomarkers from Photosynthesizing Organisms, *Annu. Rev. Earth Planet. Sci.*, 40, 221–249,  
1118 <https://doi.org/10.1146/annurev-earth-042711-105535>, 2012.

1119 Santana, V. M. and Marrs, R. H.: Flammability properties of British heathland and moorland vegetation: Models for predicting  
1120 fire ignition, *J. Environ. Manage.*, 139, 88–96, <https://doi.org/10.1016/j.jenvman.2014.02.027>, 2014.

1121 Santana, V. M., Baeza, M. J., and Vallejo, V. R.: Fuel structural traits modulating soil temperatures in different species patches  
1122 of Mediterranean Basin shrublands, *Int. J. Wildl. Fire*, 20, 668–677, <https://doi.org/10.1071/WF10083>, 2011.

1123 Scarff, F. R. and Westoby, M.: Leaf litter flammability in some semi-arid Australian woodlands, *Funct. Ecol.*, 20, 745–752,  
1124 <https://doi.org/10.1111/j.1365-2435.2006.01174.x>, 2006.

1125 De Schutter, A., Kervyn, M., Canters, F., Bosshard-Stadlin, S. A., Songo, M. A. M., and Mattsson, H. B.: Ash fall impact on  
1126 vegetation: a remote sensing approach of the Oldoinyo Lengai 2007–08 eruption, *J. Appl. Volcanol.*, 4, 1–18, 2015.

1127 Sear, D. A., Allen, M. S., Hassall, J. D., Maloney, A. E., Langdon, P. G., Morrison, A. E., Henderson, A. C. G., Mackay, H.,  
1128 Croudace, I. W., Clarke, C., Sachs, J. P., Macdonald, G., Chiverrell, R. C., Leng, M. J., Cisneros-Dozal, L. M., and Fonville,  
1129 T.: Human settlement of East Polynesia earlier, incremental, and coincident with prolonged South Pacific drought, *Proc. Natl.*  
1130 *Acad. Sci.*, 201920975, <https://doi.org/10.1073/pnas.1920975117>, 2020.

1131 Segato, D., Villoslada Hidalgo, M. D. C., Edwards, R., Barbaro, E., Vallenga, P., Kjær, H. A., Simonsen, M., Vinther, B.,  
1132 Maffezzoli, N., Zangrando, R., Turetta, C., Battistel, D., Vésteinsson, O., Barbante, C., and Spolaor, A.: Five thousand years  
1133 of fire history in the high North Atlantic region: Natural variability and ancient human forcing, *Clim. Past*, 17, 1533–1545,  
1134 <https://doi.org/10.5194/cp-17-1533-2021>, 2021.

1135 Shillito, L.-M., Whelton, H. L., Blong, J. C., Jenkins, D. L., Connolly, T. J., and Bull, I. D.: Pre-Clovis occupation of the  
1136 Americas identified by human faecal biomarkers in coprolites from Paisley Caves, Oregon, *Sci. Adv.*, 1–9,  
1137 <https://doi.org/10.1126/sciadv.aba6404>, 2020.

1138 Siao, W. S., Balasubramanian, R., Rianawati, E., Karthikeyan, S., and Streets, D. G.: Characterization and source  
1139 apportionment of particulate matter  $\leq 2.5 \mu\text{m}$  in Sumatra, Indonesia, during a recent peat fire episode, *Environ. Sci. Technol.*,  
1140 41, 3488–3494, <https://doi.org/10.1021/es061943k>, 2007.

1141 Simpson, I. A., Van Bergen, P. F., Perret, V., Elhmmali, M. M., Roberts, D. J., and Evershed, R. P.: Lipid biomarkers of  
1142 manuring practice in relict anthropogenic soils, Holocene, 9, 223–229, <https://doi.org/10.1191/09596839966898333>, 1999.

1143 Sistiaga, A., Berna, F., Laursen, R., and Goldberg, P.: Steroidal biomarker analysis of a 14,000 years old putative human  
1144 coprolite from Paisley Cave, Oregon, *J. Archaeol. Sci.*, 41, 813–817, <https://doi.org/10.1016/j.jas.2013.10.016>, 2014.

1145 Slater, G. F., Benson, A. A., Marvin, C., and Muir, D.: PAH fluxes to Siskiwit revisited: Trends in fluxes and sources of  
1146 pyrogenic PAH and perylene constrained via radiocarbon analysis, *Environ. Sci. Technol.*, 47, 5066–5073,  
1147 <https://doi.org/10.1021/es400272z>, 2013.

1148 Smith, B. N. and Epstein, S.: Two Categories of  $^{13}\text{C}/^{12}\text{C}$  ratios for Higher Plants, *Plant Physiol.*, 47, 380–384,  
1149 <https://doi.org/10.1104/pp.47.3.380>, 1971.

1150 Smith, K. P.: Landnám: the settlement of Iceland in archaeological and historical perspective, *World Archaeol.*, 26, 319–347,  
1151 <https://doi.org/10.1080/00438243.1995.9980280>, 1995.

1152 Stein, A. F., Draxler, R. R., Rolph, G. D., Stunder, B. J. B., Cohen, M. D., and Ngan, F.: NOAA’s HYSPLIT atmospheric  
1153 transport and dispersion modeling system, *Bull. Am. Meteorol. Soc.*, 96, 2059–2077, <https://doi.org/10.1175/BAMS-D-14-00110.1>, 2015.

1154 Stogiannidis, E., Laane, R., and Broderick, G.: Source characterization of polycyclic aromatic hydrocarbons by using their  
1155 molecular indices: an overview of possibilities, *Rev. Environ. Contam. Toxicol.*, 234, 49–133, <https://doi.org/10.1007/978-3-319-10638-0>, 2015.

1156 Sugiyama, S., Minowa, M., Fukamachi, Y., Hata, S., Yamamoto, Y., Sauter, T., Schneider, C., and Schaefer, M.: Subglacial  
1157 discharge controls seasonal variations in the thermal structure of a glacial lake in Patagonia, *Nat. Commun.*, 12, 1–9,  
1158 <https://doi.org/10.1038/s41467-021-26578-0>, 2021.

1159 Sveinbjarnardóttir, G., Erlendsson, E., Vickers, K., McGovern, T. H., Milek, K. B., Edwards, K. J., Simpson, I. A., and Cook,  
1160 G.: The palaeoecology of a high status Icelandic farm, *Environ. Archaeol.*, 12, 187–206,  
1161 <https://doi.org/10.1179/174963107x226453>, 2007.

1162 Sveinbjörnsdóttir, Á. E., Stefánsson, A., Heinemeier, J., Arnórsson, S., Eiríksdóttir, E. S., and Ólafsdóttir, R.: Assessing the  
1163 sources of inorganic carbon in surface-, soil- and non-thermal groundwater in Iceland by  $\delta^{13}\text{C}$  and  $^{14}\text{C}$ , *Geochim. Cosmochim. Acta*,  
1164 174, 1035–1045, <https://doi.org/10.1016/j.gca.2021.02.042>, 2021.

1166 Acta, 279, 165–188, 2020.

1167 Thomas, E. K., Briner, J. P., Ryan-Henry, J. J., and Huang, Y.: A major increase in winter snowfall during the middle Holocene  
1168 on western Greenland caused by reduced sea ice in Baffin Bay and the Labrador Sea, *Geophys. Res. Lett.*, 43, 5302–5308,  
1169 <https://doi.org/10.1002/2016GL068513>. Received, 2016.

1170 Thorarinsson, S.: The eruptions of Hekla in historical times. In: Einarsson, T., Kjartansson, G., Thorarinsson, S. (Eds.), *The  
1171 eruption of Hekla 1947–1948 I*, Soc. Sci. Isl., Reykjavik, 1–177, 1967.

1172 Thorarinsson, S.: *Vötnin stríð, Saga Skeidarárhlaupa og Grímsvatnagosa* [The swift Flow. rivers Hist. Grímsvötn jökulhlaups  
1173 eruptions. Icelandic]. Menn. Reykjavík, 1974.

1174 Thordarson, T. and Höskuldsson, Á.: Postglacial volcanism in Iceland, *Jökull*, 58, 197–228,  
1175 <https://doi.org/10.33799/jokull2008.58.197>, 2008.

1176 Tierney, J. E., Pausata, F. S. R., and DeMenocal, P. B.: Rainfall regimes of the Green Sahara, *Sci. Adv.*, 3,  
1177 <https://doi.org/10.1126/sciadv.1601503>, 2017.

1178 Trouet, V., Esper, J., Graham, N. E., Baker, A., Scourse, J. D., and Frank, D. C.: Persistent Positive North Atlantic Oscillation  
1179 Mode Dominated the Medieval Climate Anomaly, *Science*, 324, 78–80, <https://doi.org/10.1126/science.1166349>, 2009.

1180 Tyagi, P., Edwards, D. R., and Coyne, M. S.: Fecal sterol and bile acid biomarkers: Runoff concentrations in animal waste-  
1181 amended pastures, *Water. Air. Soil Pollut.*, 198, 45–54, <https://doi.org/10.1007/s11270-008-9824-7>, 2009.

1182 Vachula, R. S., Huang, Y., Longo, W. M., Dee, S. G., Daniels, W. C., and Russell, J. M.: Evidence of Ice Age humans in  
1183 eastern Beringia suggests early migration to North America, *Quat. Sci. Rev.*, 205, 35–44,  
1184 <https://doi.org/10.1016/j.quascirev.2018.12.003>, 2019.

1185 Vachula, R. S., Huang, Y., Russell, J. M., Abbott, M. B., Finkenbinder, M. S., and O'Donnell, J. A.: Sedimentary biomarkers  
1186 reaffirm human impacts on northern Beringian ecosystems during the Last Glacial period, *Boreas*,  
1187 <https://doi.org/10.1111/bor.12449>, 2020.

1188 Varga, G., Dagsson-Walhausserová, P., Gresina, F., and Helgadottir, A.: Saharan dust and giant quartz particle transport  
1189 towards Iceland, *Sci. Rep.*, 11, 1–12, <https://doi.org/10.1038/s41598-021-91481-z>, 2021.

1190 Vázquez, C., Vallejo, A., Vergès, J. M., and Barrio, R. J.: Livestock activity biomarkers: Estimating domestication and diet of  
1191 livestock in ancient samples, *J. Archaeol. Sci. Reports*, 40, 103220, <https://doi.org/10.1016/j.jasrep.2021.103220>, 2021.

1192 Wallace, J. M. and Hobbs, P. V.: *Atmospheric science: an introductory survey*, Academic Press, ISBN 0-12-732951-X, 2006.

1193 Wang, Q. and Huang, H.: Perylene preservation in an oxidizing paleoenvironment and its limitation as a redox proxy,  
1194 *Palaeogeogr. Palaeoclimatol. Palaeoecol.*, 562, <https://doi.org/10.1016/j.palaeo.2020.110104>, 2021.

1195 Wardroper, A. M. K., Maxwell, J. R., and Morris, R. J.: Sterols of a diatomaceous ooze from walvis bay, *Steroids*, 32, 203–  
1196 221, [https://doi.org/10.1016/0039-128X\(78\)90006-5](https://doi.org/10.1016/0039-128X(78)90006-5), 1978.

1197 Wilkie, K. M. K., Chaplignin, B., Meyer, H., Burns, S., Petsch, S., and Brigham-Grette, J.: Modern isotope hydrology and  
1198 controls on  $\delta D$  of plant leaf waxes at Lake El'gygytgyn, NE Russia, *Clim. Past*, 9, 335–352, [https://doi.org/10.5194/cp-9-335-](https://doi.org/10.5194/cp-9-335-2013)  
1199 2013, 2013.

1200 Wooller, M., Wang, Y., and Axford, Y.: A multiple stable isotope record of Late Quaternary limnological changes and  
1201 chironomid paleoecology from northeastern Iceland, *J. Paleolimnol.*, 40, 63–77, <https://doi.org/10.1007/s10933-007-9144-8>,  
1202 2008.

1203 Landmælingar Íslands: <https://www.lmi.is/is/moya/page/licence-for-national-land-survey-of-iceland-free-data>, last access: 1  
1204 March 2023.

1205 Icelandic Meteorological Office: [www.vedur.is](http://www.vedur.is), last access: 1 January 2022.

1206 Yunker, M. B., Macdonald, R. W., Vingarzan, R., Mitchell, H., Goyette, D., and Sylvestre, S.: PAHs in the Fraser River basin:  
1207 a critical appraisal of PAH ratios as indicators of PAH source and composition, *Org. Geochem.*, 33, 489–515,  
1208 [https://doi.org/10.1016/S0146-6380\(02\)00002-5](https://doi.org/10.1016/S0146-6380(02)00002-5), 2002.

1209 Zennaro, P., Kehrwald, N., McConnell, J. R., Schüpbach, S., Maselli, O. J., Marlon, J., Vallelonga, P., Leuenberger, D.,  
1210 Zangrando, R., Spolaor, A., Borrotti, M., Barbaro, E., Gambaro, A., and Barbante, C.: Fire in ice: Two millennia of boreal  
1211 forest fire history from the Greenland NEEM ice core, *Clim. Past*, 10, 1905–1924, <https://doi.org/10.5194/cp-10-1905-2014>,  
1212 2014.

1213 Zennaro, P., Kehrwald, N., Marlon, J., Ruddiman, W. F., Brücher, T., Agostinelli, C., Dahl-Jensen, D., Zangrando, R.,  
1214 Gambaro, A., and Barbante, C.: Europe on fire three thousand years ago: Arson or climate?, *Geophys. Res. Lett.*, 42, 5023–  
1215 2033, <https://doi.org/10.1002/2015GL064259>, 2015.

1216